Diploma Thesis

Age-related changes in uptake and release of trace elements in marine microplastics

Submitted in satisfaction of the requirements for the degree of
Diplom-Ingenieurin
of the TU Wien, Faculty of Technical Chemistry

---

ausgeführt zum Zwecke der Erlangung des akademischen Grades einer
Diplom-Ingenieurin
eingereicht an der Technischen Universität Wien, Fakultät für Technische Chemie

von

Michaela Porkert
Matr.Nr.: 01535375

Supervised by

Univ.Prof. Dipl.-Ing. Dr.techn. Andreas Limbeck

and

Projektass. Dipl.-Ing. Dr.techn. Lukas Brunnbauer

(E164-01-2 - Forschungsgruppe Oberflächen-, Spurenanalytik und Chemometrie)

eingereicht an der Technischen Universität Wien

Fakultät für Technische Chemie

von

Wien, im November 2022

_____

Vorname Nachname

Eidesstattliche Erklärung

Ich erkläre an Eid statt, dass die vorliegende Arbeit nach den anerkannten Grundsätzen für wissenschaftliche Abhandlungen von mir selbstständig erstellt wurde. Alle verwendeten Hilfsmittel, insbesondere die zugrunde gelegte Literatur, sind in dieser Arbeit genannt und aufgelistet. Die aus den Quellen wörtlich entnommenen Stellen, sind als solche kenntlich gemacht.

Das Thema dieser Arbeit wurde von mir bisher weder im In- noch Ausland einer Beurteilerin/einem Beurteiler zur Begutachtung in irgendeiner Form als Prüfungsarbeit vorgelegt. Diese Arbeit stimmt mit der von den Begutachterinnen/Begutachtern beurteilten Arbeit überein.

Wien, Datum Unterschrift _____

Zusammenfassung

Aufgrund des wachsenden Bedarfs an Kunststoffen wird auch die Entsorgung immer bedeutsamer. Eine größere Menge des entsorgten Kunststoffabfalls endet in den Ozeanen. Dort erfahren die Kunststoffe Degradationsprozesse und bilden Mikroplastikpartikel (MP). Die Partikel werden von Mikroorganismen überwachsen, von Meereslebewesen aufgenommen und gelangen schließlich in die menschliche Nahrungskette. MPs stehen im Verdacht enthaltene Additive wie Zn und Al freizusetzen und Spurenelemente wie Pb und Cd aus dem Ozean zu adsorbieren.

In dieser Arbeit wurden vier häufig in der Verpackungsindustrie eingesetzte Polymere untersucht: Polystyrol (PS), Polyamid (PA), Polyethylentherepthalat (PET) und Polyvinylidenchlorid (PVDC). Diese Proben wurden künstlich mittels UV-Bestrahlung und oxidierenden Reagenzien gealtert. Änderungen, welche durch die Alterung verursacht wurden, wurden mit gängigen Methoden wie Raman und FTIR-Spektroskopie untersucht. Die nativen und gealterten Polymere wurden mit künstlichem Meerwasser behandelt, das mit ausgewählten Schwermetallen wie Pb und Cd versetzt war.
Um quantitative Masseninformationen über die altersbedingten Veränderungen in der Aufnahme und Freisetzung von anorganischen Spezies zu erhalten, wurde ein mikrowellenunterstützter Aufschluss gefolgt von einer flüssig induktiv gekoppelter Plasma Massen Spektrometrie Analyse (ICP-MS) durchgeführt. Laserablations-ICP-MS (LA-ICP-MS) und Laser-induced breakdown spectroscopy (LIBS) wurden zur qualitativen ortsaufgelösten Analyse in festen MPs verwendet. Untersucht wurde sowohl die Verteilung von Spurenelementen als auch von Sauerstoff als Marker für Oxidation/Degradation innerhalb einzelner Partikel.

Im Vergleich zu nativen Proben zeigen gealterten PS Proben eine deutlich erhöhte Aufnahme von Schwermetallen wie Pb und eine höhere Freisetzung von Additiven wie Zn. PA zeigte Auswaschen von Additiven ohne merkliche Änderung der Molekül Struktur durch die Alterung und zeigte keine erhöhte Aufnahme für eines der untersuchten Elemente. PET zeigte vor allem bei den Tiefenprofilen das Auswaschen von Sb in den Randbereichen der Partikel. Darüber hinaus zeigte es eine erhöhte Absorption einiger zugesetzter Spurenelemente wie Nd und Th. PVDC zeigte größere Änderungen durch die künstliche Alterung, welche sich auch hier in einer erhöhten Abgabe von Spurenelementen zeigte, die besonders gut in den Tiefenprofilen zu beobachten war. Die Adsorption einiger Elemente in PVDC scheint unabhängig von der Alterung zu sein.
Das Aufnahmeverhalten ist für jedes zugesetzte Spurenelement und die Abgabe jedes Additivs unterschiedlich. Die gemessenen Tiefenprofile und Images der einzelnen MP Partikel zeigen eine Vielfalt an Ergebnissen welche abhängig vom jeweiligen Polymer und des untersuchten Elementes sind. Die größten Änderungen zeigten sich, im oberflächennahen Bereich, wo auch die größte Material Veränderung durch Degradationsprozesse stattfand. Bei manchen Polymertypen wurde auch eine Veränderung der Bulk-Zusammensetzung beobachtet. Molekulare Änderungen der Struktur durch die Alterung, wurden nur in den ersten 200 nm von der Oberfläche durch die Änderung des Sauerstoffgehalts festgestellt. Es zeigte sich das besonders die Kombination der Ergebnisse von Bulk-Analyse und Ortsaufgelösten Informationen besonders wertvoll ist, um die Situation besser beurteilen zu können.

Abstract

Due to the growing demand and use of plastics, the disposal and waste of plastic products is getting more important. A greater amount of the discarded plastic ends up in the oceans. There it undergoes degradation processes, resulting in the formation of microplastics (MP). The particles get overgrown by microorganisms, ingested by marine life, and further enter the human food chain. MPs are under suspicion to release contained additives and adsorb trace elements from the ocean.

In this thesis four different commonly used polymers were investigated. Polystyrene (PS), Polyamide (PA), Polyethylenterepthalate (PET) and Polyvinylidenchloride (PVDC). These samples were artificially aged by UV irradiation and oxidizing reagents. The changes caused by degradation were investigated with common methods, such as Raman and FTIR spectroscopy. Further the native and degraded polymers were treated with artificial seawater spiked with selected heavy metals such as Pb and Cd. To obtain quantitative bulk information of the age-related changes in uptake and release of inorganic species, microwave assisted digestion followed by liquid inductively coupled plasma mass spectrometry (ICP-MS) analysis was carried out. Laser ablation ICP-MS (LA-ICP-MS) and laser induced breakdown spectroscopy (LIBS) were used for qualitative spatially resolved analysis in solid MPs. Investigated were both the distribution of trace elements, and O as a marker for oxidation/degradation within individual particles.

The aged PS samples clearly show an increased uptake of heavy metals such as Pb and increased release of additives containing Zn. PA showed leaching of additives with no noticeable change in molecular structure with ageing and did not show increased uptake for any of the elements examined. Especially in the depth profiles, PET showed the washing out of Sb in the edge areas of the particles. Further it showed an increased absorption of some added trace elements like Nd and Th. PVDC showed major changes due to artificial ageing, which was also reflected in an increased release of trace elements, which was particularly evident in the depth profiles whereas the increased adsorption of some elements seemed to be independent from ageing. The uptake and leaching behaviour is different for each trace element and each additive respectively. The measured depth profiles and images of the single MP particles showed various results depending on the polymer type and elements. Biggest changes were observed in surface near regions, whereas for others also the bulk composition was affected. Degradation was noticed only in the first 200 nm from surface by the change of oxygen content.

It turned out that the combination of the results of bulk analysis and spatially resolved information is particularly valuable to be able to better assess the situation.

Acknowledgment

First of all, I would like to express my gratitude to Andreas Limbeck, who gave me the opportunity to work on this exciting research question and to be part of this amazing working group. He always had creative input for improvement and an open ear for suggestions and questions.

Lukas Brunnbauer was a great tutor, who gave support whenever needed. He was at least as excited as I was about the project on this topic, which provided a lot of motivation to work on it.

I further want to express my gratefullness to the whole work group, which created a pleasant atmosphere, and made work joyful every day.

Jakob Willner and Birgit Achleitner supported me with my IR and Raman measurements.

Birgit Achleitner and Lukas Brunnbauer also joined me on a trip to the Czech academy of sciences in Berno, which was enabled by Andreas Limbeck and Pavel Porizka. There further Raman measurements of my samples were processed by Martin Kizovsky.

Thomas Konegger enabled me the density measurements the polymers and gave always helpful advice.

I also want to mention Peter Spieß-Knafl who not only read this work once, to improve it constantly as well as Lukas Brunnbauer.

I want to thank my family and friends which supported and accompanied me during this exciting times.

I learned a lot from the mentioned people, and I am very grateful to work with all of them, for all their help and patience. I don't want to miss this great experience.

Thank you all.

Table of Content

Abbreviations

ATR	Attenuated total reflection
CRM	Certified reference material
DCI	Dual concentric injection
H_2O_2	Hydrogen peroxide
HNO_3	Nitric acid
ICCD	Intensified charge-coupled device
ICP	Inductively coupled plasma
IR	Infrared
LA	Laser ablation
LD	Low density
LDPE	Low density polyethylene terephthalate
LIBS	Laser induced breakdown spectrometry
LM	Light microscopy
LOD	Limit of detection
LOQ	Limit of quantification
m	Mass
M	Mol weight
m/z	Mass to charge ratio
MP	Micro plastic
MS	Mass spectrometry
Nd-YAG	neodymium-doped yttrium aluminium garnet
OES	Optical emission spectrometry
p.a.	Pro analysis
PA	Polyamide
PCA	Principal component analysis
PET	Polyethylene terephthalate
PFA	Perfluoralkoxy alkane
ppb	Parts per billion
ppm	Parts per million
ppt	Parts per trillion
PS	Polystyrene
PVDC	Polyvinylidene chloride
QC	Quality control
SEM	Secondary electron microscopy
T	Temperature
UV	Ultraviolet
V	Volume
z	Charge

1 Introduction

Due to the growing consumption and usage of plastics, the disposal and waste of plastic products is becoming more important. Unfortunately, a greater amount of the discarded plastic ends up in the sea. It is estimated that each year up to 10 Mt of waste enters the oceans. About 70 % of the waste is sinking to the ground, ~15% is flushed to the beaches and the remaining 15% stay in the water column (Deutschland, 2017). Another source are small particles which uncouple from textiles during the washing processes and enter the ecosystem through the sewage system. The plastic waste undergoes degradation processes, accompanied by changes in chemical properties. These surface modifications supported by formed biofilms change the reactivity of the previous inert polymers. This weakens the structures of the polymers and makes it more suitable for adsorption, leaching and complex formation which in the end also leads to the formation of microplastic (MP). These microplastics may adsorb chemical compounds for example heavy metals while additives are leached out as seen in Figure 1.1 (Neves, et al., 2015) (Wang, et al., 2020). The washed-out components of the polymers are often found to bioaccumulate and have toxic effects to marine life.

Due to biodegradation and porosity, the particles serve as a habitat for microorganism. Various algae and bacillus bacteria are the most common representatives. The appearance of this species is accompanied by an interplay of attachment, growth, respiration, and mortality. A consequence of clinging is the increase of the density. Depending on the seawater salinity, temperature, sun hours and irradiation the biofouling process on the particles is faster therefore, also the increase of the density. Thereby the particles tend to settle down and may be mistaken by the sea creatures with their food and ingested by them (Kooi, et al., 2017). Hence, small particles enter through the water into the food chain of various marine organisms, and later also into that of humans. The adsorbed compounds may have an effect on the health of humans and animals.

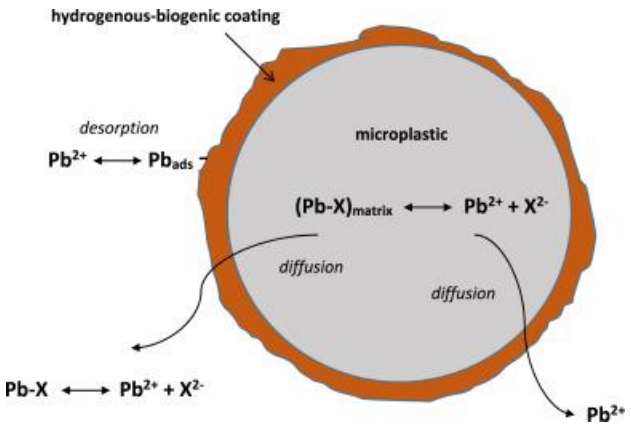

Figure 1.1: Leaching and adsorption of Pb in MP with hydrogenous-biogenic coating (Turner, et al., 2020)

Per definition microplastics are particles smaller than 5 mm in diameter with a wide variation of the polymer type, composition, size, and shape. Due to this wide range of physical and chemical properties various analytical tools are necessary for a full characterization. Fourier transformation infrared (FTIR) and Raman spectroscopy are typical methods to characterize changes in functional groups of the polymer chains and were also supportive in this thesis (Affolter, 2001) (Noda, et al., 2007). Due to the macroscopic change in properties after degradation (sink-swim behaviour and colour) helium

pycnometry measurements for density determination is commonly reported in the literature. Light microscopy is used to investigate the particle structure and size (Frick & Stern, 2017). State of the art is also the use of ICP-MS to determine the concentrations of hazardous and today restricted additives like Br, Cd or Pb. These additives were commonly used to enhance polymers durability and for colouring (Bart, 2005). For ICP-MS measurements liquid samples are required which were obtained either by microwave digestion or by leaching the MPs in various aqueous media (Massos & Turner, 2017) (Turner & Holmes, 2014).

These sample preparation steps always come with the problem of possible contamination, analyte loss in case of digestion, or incomplete results (Pereira, et al., 2011). Summarizing, the conventional analytical tools used to investigate MPs enable a partial material characterisation only. For example, sample leaching/digestion provides in combination with ICP-MS analysis only bulk information about the prevailing metal contents, whereas techniques applied for determination of changes in the molecular structure such as IR- or Raman-spectroscopy are limited to the analysis of the sample surface.

Therefore, the application of novel analytical tools may enable a more comprehensive characterization of MPs. So, solid sampling techniques were carried out to gain information about the distribution of the metals present in the individual particles.

In this work, four different polymer types were investigated: Polystyrene (PS), Polyamide (PA), Polyethylene terephthalate (PET) and Polyvinylidene chloride (PVDC). They were artificially altered by UV irradiation, treated with oxidizing agents (HNO_3 and H_2O_2) or a combination of both. Subsequently. they were exposed to artificially seawater spiked with a selection of heavy metals for various times. In a first step, conventional characterisation of the MPs was carried out. Therefore, microwave assisted digestion of the treated and untreated polymers was carried out followed by a quantitative determination of trace metals by inductively coupled plasma mass spectrometry (ICP-MS). The degradation of aged MPs was assessed by FT-IR- and Raman-spectroscopy and the density was determined using He pycnometry.

As novel tools, Laser ablation inductively coupled plasma spectroscopy (LA-ICP-MS) and laser induced breakdown spectroscopy (LIBS) were applied for the comprehensive characterization of MPs degradation and the investigation of uptake and release of inorganic constituents. This should enable the simultaneous detection of both the distribution and content of heavier elements like Pb and Zn and lighter elements like H, C, and O which are relevant species for polymer chemistry.

The main goal of this work was to evaluate the release of additives and the uptake of trace elements from seawater in native and degraded polymers. The quantification of metal contents was possible by digestion of the polymer samples and subsequent ICP-MS analysis of the derived solutions. Additionally, to assess the distribution of the individual elements in polymer particles, LA-ICP-MS and LIBS were combined and used. The information obtained should help to assess the situation and behaviour of microplastics in the sea.

2 Theory

2.1 Polymer Samples

PS, PA, PET and PVDC are frequently used for fibers, and packaging materials. According to the manufacturer the selected plastics have in common, that they are all thermoplastic and unstable to UV irradiation. Thermoplastics can be deformed in a certain temperature range and are the only plastic type that can be recycled mechanically. Their properties are summarized in Table 2.1.. Microscope pictures of the untreated samples are shown in Figure 2.1 and the monomer of each polymer in Figure 2.2.

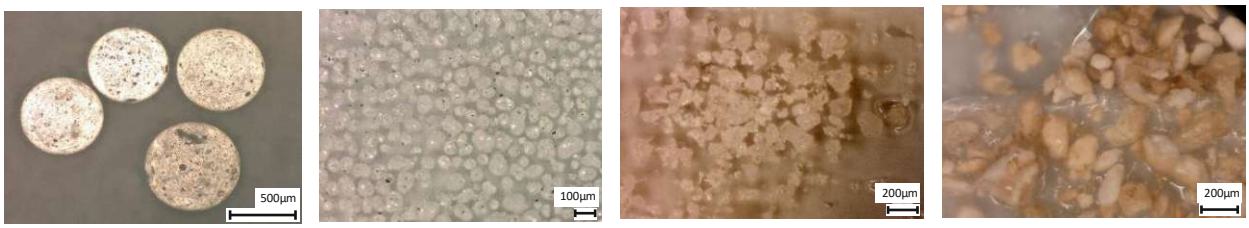

Figure 2.1: Microscope pictures of native MP samples; f.l.t.r.: PS, PA, PET, PVDC

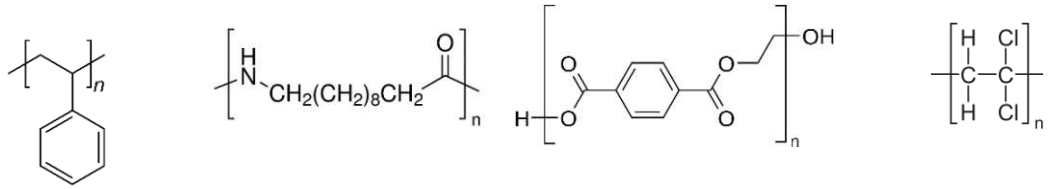

Figure 2.2: Monomers f.l.t.r. PS, PA, PET and PVDC (Wikipedia.org, 2021)

Polystyrene is a colourless, amorph, hard and brittle rigid which is usable in a broad field from household, containers, packaging material and for glazing and as foam. Its chemical and UV resistance is poor (GoodFellow, 2021) (Elias, 2001).

Polyamide is a semi crystalline white thermoplastic polymer. In this case nylon 12 was provided. More common derivates are nylon 6 or 6,6. Nylon normally has a high-water absorbance. The used modification however has the lowest water absorbance of all, but the highest heat resistance and strength. It is often used for fillings and fibers (GoodFellow, 2021) (Elias, 2001).

Polyethylene terephthalate is a transparent, colourless, thermoplastic, which is produced at large scale in different modifications. They differ from amorph to crystalline. The density gives a good measure for its crystallinity. PET is resistant to most chemicals but tends to build stress cracks. It has bad barrier properties except for water. The main usage is packaging materials also for groceries or insulators for electronic applications (GoodFellow, 2021) (Elias, 2001).

Polyvinylidene chloride is a transparent colourless thermoplastic, which has a low permeability for gases. It is often used in barrier films in multilayers and mainly for packaging. Stabilizers are often required (GoodFellow, 2021) (Elias, 2001).

Polymers durability and properties are enhanced by the addition of additives. A broad variety of additive is known to modify the polymers to the corresponding application. An additive is per definition an adjuvant or supplement which are added in small amounts to reach or improve specific properties.

These properties can be colour, structure, UV- or temperature resistance, elasticity, E-module an many more (Maier & Schiller, 2016).

Table 2.1: Investigated polymers and their properties (GoodFellow, 2021)

Property	PS	PA	PET	PVDC
Particle size range (µm)	600-900	30-250	100-300	50-500
Density (g cm^{-3})	0.6	1.020	0.920	1.630
Water absorption (over 24 h) (%)	<0.400	1.60	<0.015	0.100
Product form	Expandable bead	Particle	Particle	Particle
Colour	White	Silver grey	Colourless	White

2.2 Characterization of material changes after degradation

Degradation means changes in the original structure of the polymers, mainly the cleavage of polymer chains into oligomers and monomers. These changes are dependent on the type of polymer so the polymer chain itself and the degradation conditions. There are different types of degradation. Photo-, thermal-, chemical- and mechanical degradation are some of these types. Since these are plastic particles that are no longer intended for use, the latter is not important. All polymers show degradation by influence of UV- or γ-radiation. Polymers contain often hydrolysable bonds. Hydrolysation caused by chemical processes and enzyme-catalysed hydrolysis are important mechanisms. The change in pH has a catalytic effect on hydrolysis. Whether an increase or decrease in the pH value accelerates the degradation depends on the functional groups in the polymer chain. Also, the water uptake shows an influence of the degradation speed. Polymers with a greater water uptake seem to degrade faster, because the water leads to swelling and weakens the structure. It also effects the pH inside the pores, so there could also be catalytic effect due to pH change in the inner of the particles. Beside the chemical bond, water uptake and pH also the presence of copolymers has an effect on the degradation speed (Göpferich, 1994).

Next to degradation, erosion is another important process at altering materials. Degradation favours erosion. Erosion means the loss of material, so monomers and oligomers leaving the polymer structure. It is divided in to two types: Heterogeneous and homogeneous erosion. Heterogeneous erosion takes place on the surface of the material, so the form and shape are changing. Homogenous erosion, which takes place in the inner of the material, so geometric shape stays the same. The principle is illustrated in Figure 2.3 (Göpferich, 1994).

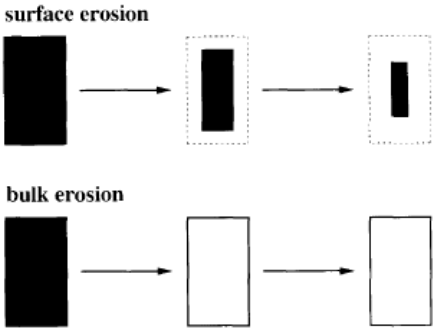

Figure 2.3: Schematic illustration of surface erosion and bulk erosion (Göpferich, 1994)

Further important aspects according to the longevity of polymers are the resistance against chemicals especially eroding ones like acids and bases, resistance against autooxidation (thermo oxidative and photo oxidative), mechanical stress and biological altering. Figure 2.4 summarizes the strains of plastics and the possible consequences according to that.

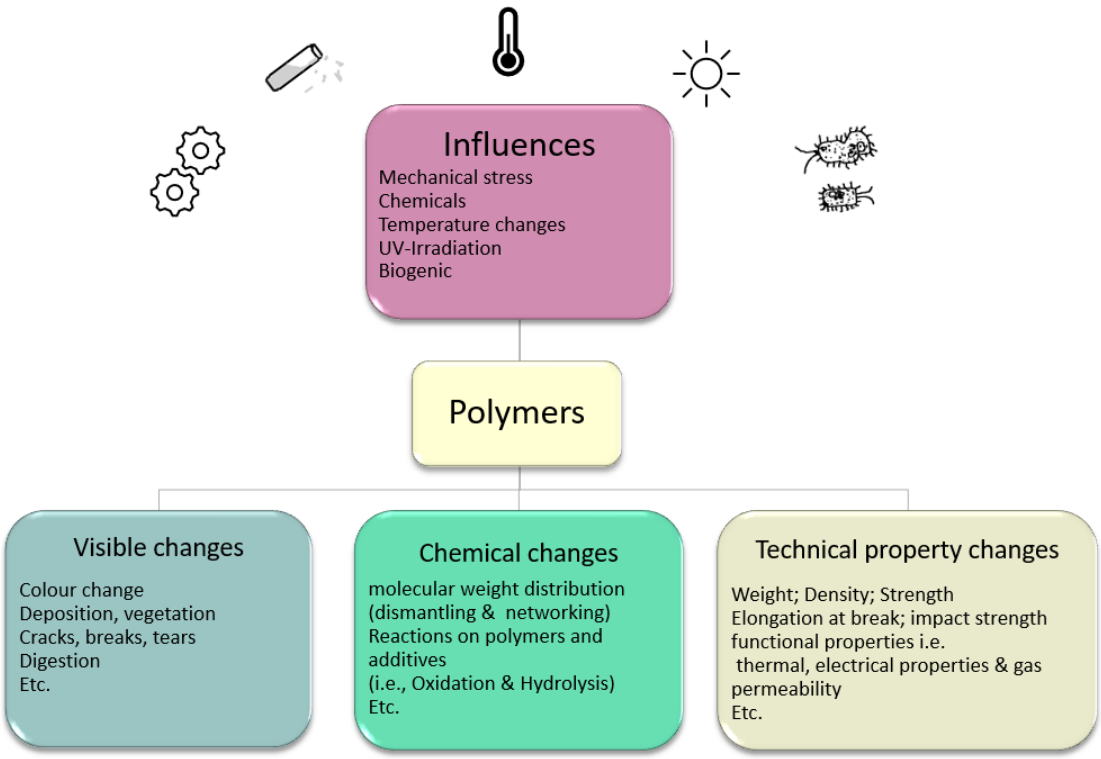

Figure 2.4: Overview of Influences in degradation and erosion in polymers

The stressing methods that were mainly observed in this work were chemical stress by addition of oxidizing agents such as HNO_3 and H_2O_2 or UV irradiation. Both methods favour oxidation reactions and the uptake from O or forming functional groups containing O such as carbonyls.

The main reaction therefore is the autooxidation reaction. It is a heterogenous reaction between gaseous or dissolved O and solid polymer surface. The reaction starts with the formation of radicals R• which is formed by strains such as shown in Figure 2.4. It is favoured by redox active metal ions which are contained in the ocean as well as in the polymers themselves as additives. The alkyl radical reacts

fast with O forming peroxy radicals ROO•. This species further reacts with RH to hydroxyradical and is the speed determining step. After this step it forms a cycle of autooxidation as seen in Figure 2.5 (Affolter, 2001). Metal ions can catalyse this reaction.

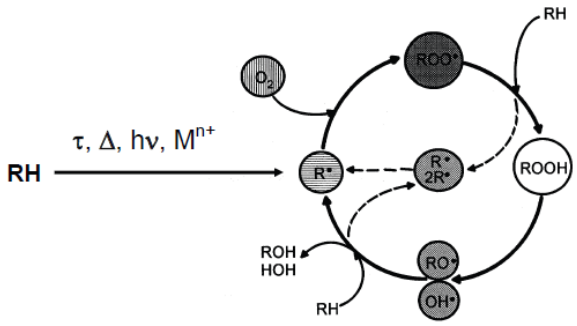

Figure 2.5: Autooxidation cycle (Affolter, 2001)

The uptake of O and type of polymer influence the reaction speed. Different polymers show different resistance to these procedures. Also, the combination of different treatment methods shows an influence of the occurring material changes. An important effect is also the vegetation of microorganism, which might influence the uptake of trace elements, caused by the bioaccumulation on the particle´s surface. Due to the variety in changes, the characterization of the changes regarding degradation is important but challenging (Shim, et al., 2016).

2.2.1 Molecular Analysis

2.2.1.1 FTIR-Spectrometry

Infrared spectroscopy is a complementary method to Raman spectroscopy. This technic normally uses polychromatic light of wavenumbers from 4000 cm^{-1} to 625 cm^{-1}. Commonly used light sources include Nernst glower, laser, or black radiators. Thermal detectors or else pyroelectric detectors are often used for detection. Every bond in a molecule that undergoes a dipole change during excitation of the specific vibrational states of these bonds is IR active. The required energy for this excitation is measured and specific for different functional groups and bonds. The degrees of freedom, 3n-5 for linear and 3n-6 for angled molecules, where n is the number of atoms in the molecule, give the possible bands per bond (Thompson, 2018). The stronger the bond, the shorter is the wavelength associated with its vibration and the greater is the vibrational frequency.

Attenuated total reflection (ATR) is suitable for direct measurements of solid and liquid samples and a reliable IR method. The sample is brought directly on the surface of an ATR crystal and pressed down close to the surface. The infrared radiation is totally internally reflected when passing a material with higher refractive index such as the ATR crystal (e.g. Diamond, ZnSe or Ge). In addition, an evanescent wave is created due to the reflectance and extends slightly beyond the surface. Finally, it penetrates the sample which is in direct contact with the ATR crystal. The penetration depth is very small but is compensated by reflection of multiple times. So, a bigger amount of sample volume is investigated. The spectrum is influenced by many aspects such as the effective pathway, the efficiency of the sample

contact, the angle of incidence, material of the crystal and its refractive index. As well as from the sample and the penetration depth of the evanescent light (Thompson, 2018).

Main advantages are fast and reliable measurements and the simple setup. For spatially resolved analysis resolution is limited to the wavelength (several 100 nm to 1 mm). Another disadvantage is that only surface information is obtained.

2.2.1.2 Raman Spectrometry

Raman spectrometry is based on the inelastic scattering of monochromatic photons on electron shells. Due to the incoming energy, electrons are raised in higher virtual states and fall back in lower energy states. For excitation a monochromatic laser is used, normally in the VIS region of light. A distinction is made between three cases. Excited electrons fall back in a lower energy level (Stokes Scattering), in the original energy level (Rayleigh Scattering) and in a higher energy level than the original (Antistokes Scattering). The energy difference after excitation is measured as Raman shift and is specific for different functional groups and chemical bonds. Substances that get easily polarized show a higher Raman activity. The selection rules of this method state that the polarizability of the bond must change to be detected as a Raman band according to the Raman Shift. Spectral Raman bands are weak and can be easily superimposed by stronger emission such as from fluorescence. Therefore, it can be challenging to find the right excitation energy. It is always a compromise between an intense signal and the fluorescence background (McCreery & Winefordner, 2000). The detection is normally carried out by semi-conductor detector or charge coupled devices.

This technique provides reliable information about the molecule structure and is well established for polymer analysis. The spatially resolution is a bit higher than for IR-Spectroscopy but gives also only surface information. Due to its weak intensity Raman scattering gets easily overlapped by fluorescence, so that weak bands are presumably overseen. Also, cosmic radiation can be found in spectra and lead to miss interpretation. Dark samples are more difficult to measure, because of the high light absorption. As simple and robust the technique itself is, the more know how is required to obtain promising results.

2.2.2 Elemental Analysis

2.2.2.1 Laser Induced Breakdown Spectrometry – LIBS

LIBS uses a laser -generated plasma to gain information about the elemental composition of solid samples. The principle is based on the application of a pulsed laser with sufficient energy on the surface of a solid sample forming a local plasma directly on the sample (Figure 2.6). A complex chain of processes is following, which can be divided into three major steps: plasma ignition, plasma expansion and plasma decay. These processes are influenced by some factors, like the initial laser energy (flux), the pulse duration, the pressure and the surrounding atmosphere.

The plasma is formed by vaporizing of an opaque target surface followed by absorption of laser light in the vaporized material. Beside vaporization, atomization, ionization and excitation are the major reactions.

To produce a plasma, laser intensities from about 10^9 W cm^{-2} are required. The plasma is accompanied by the absorption of laser light, vaporization, the formation of charged particle (ionization), atomization, excitation, and the emittance of characteristic light from relaxation of the excited species. The developing plasma plume contains molecules and atoms of the solid target, which were ablated by the laser beam. Due the recombination of free electrons with ions and the relaxation of excited ions, atoms and molecules characteristic light is emitted. The expected reactions are shown in (1) to Equation(3). These reactions happen at about 10 ns to 100 µs after the laser pulse. Ionic emission happens first and is overlapped by emission of atoms which is further overlapped by molecular emission. The gate delay sets the actual time frame for the measurement, to only detect relevant signals and reduce noise. The emitted light of the excited analytes is collected via an optic and fragmented with a polychromator and finally detected by and CCD or ICCD. A spectrum of a specific wavelength region can be recorded. Qualitative information is given by detecting the position of the emission lines and the quantitative information by the varying intensities (Miziolek, et al., 2009) (Brunnbauer, et al., 2020) (Singh & Thakur, 2007).

Recombination	$M^+ + e^- \rightarrow M + hv$	(1)
Relaxation of ions	$M^{+*} \rightarrow M + hv$	(2)
Relaxation of atoms	$M^{+*} \rightarrow M + hv$	(3)

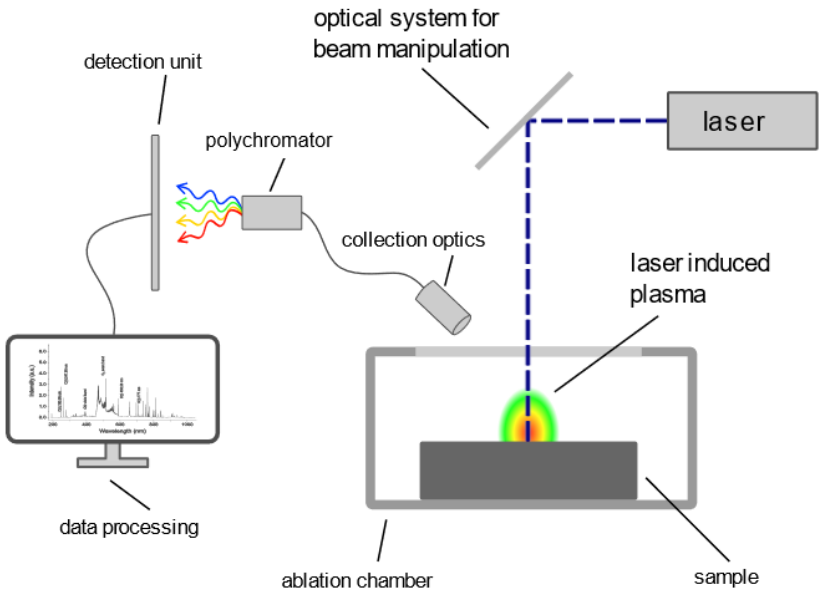

Figure 2.6: LIBS Setup (L. Brunnbauer)

A main advantage of the laser-based technique is the possibility to apply it on solid samples without any sample preparation. It is a reliable method for spatially resolved elemental analysis. For this thesis the most important advantage, was the possibility to detect lighter elements such as C, H and O, further molecular emissions such as C2 or CN-bands can be investigated. These are relevant species for polymer degradation. To obtain high intensities, high laser energies and larger beam diameters are required, which leads to limitation in resolution for spatially resolved analysis. Additionally, focusing on uneven surfaces is hard to realize.

2.3 ICP-MS (liquid sampling)

Inductively coupled plasma mass spectrometry (ICP-MS) is a technique used routinely for inorganic trace analysis. A basic setup is shown in Figure 2.7. A liquid sample is transported by a tube by a peristaltic pump or through a six-ways-valve into the system. The sample is nebulized in fine aerosol and bigger droplets are removed in the spray chamber. Only about 1% of the injected liquid sample are introduced into the plasma torch. The plasma is usually generated by argon gas and an inductive coil and reaches 6 000 to 10 000 K. The plasma conditions could be influenced by bigger drops, because more energy would be necessary to evaporate the liquid sample, this could lead to extinguishing the plasma. The plasma vaporizes the aerosol and triggers atomization and ionization. The possible reactions are seen bellow in equation (4) - (9) (Becker, 2007). For ICP-MS the ionization reactions are more favourable, whereas for inductively coupled plasma optical emission spectrometry (ICP-OES) the atomization reactions are favoured (Thomas, 2013).

Electron Ionization	$M + e^- \rightarrow M^+ + 2e^-$	(4)
Charge Transfer Ionization	$M + Ar^+ \rightarrow M^+ + Ar$	(5)
Electron Excitation of atoms	$M + e^- \rightarrow M^* + e^-$	(6)
Electron Excitation of argon	$M + e^- \rightarrow Ar^* + e^-$	(7)
Ion- electron radiative recombination	$M^+ + e^- \rightarrow M^* + hv$	(8)
Penning Ionization	$M + Ar^{m*} \rightarrow M^+ + Ar + e^-$	(9)

Via an interface of two cones, sampling cone and skimmer cone, ions, photons, and neutral particles are transferred into the high vacuum of the mass spectrometer. In order to separate photons and neutral particles, different geometric setups are used. An option is to create a 90 ° angle in the path through the ion optics to the mass analyser. The photons and neutral particles cannot follow the angle and are separated from the ions. The resulting ion beam is focused by an ion optic, which leads the beam further to the mass analyser. Usual mass analyser systems for ICP-MS applications are time of flight, sector field and quadrupole mass spectrometer. A mass analyser is basically a mass filter. A quadrupole mass analyser, which was provided in the used system, consists of two cathodes and two anodes in diagonal position to the same pole. The four electrodes generate an oscillating magnetic field. According to the frequency only a specific mass to charge ratio (m/z) can pass through the field and finally reach the electron multiplier detector. This follows Equation (10) (Wiley Information Services GmbH, 2021) (Linge & Jarvis, 2009). The detector records the sample concentration as current. An external calibration curve can be used to calculate the concentration.

$$\frac{m}{z} = \frac{2 * U}{A * (r_0^2 * f^2)} \qquad (10)$$

m/z .....mass to charge ratio ($g*mol^{-1}*C^{-1}$)
r.....radius (m)
f.....frequency (s^{-1})
U.....voltage (V)
A..... amplitude (V)

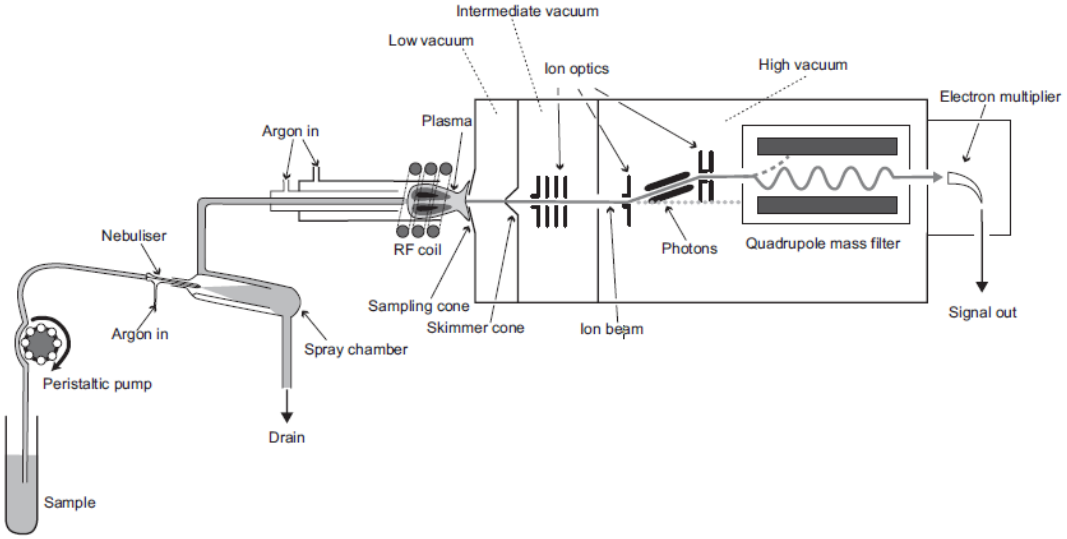

Figure 2.7: Schematic diagram of the major components of an ICP-MS instrument (Linge & Jarvis, 2009)

A problem with ICP-MS is that lighter elements get easily interfered by polyatomic molecules with the same nominal m/z ratio. This is a result of the high temperature in the plasma which enables reactions and the emergence of molecules which would not exist under normal conditions. To minder the occurrence of polyatomic molecules, a collision cell with kinetic energy discriminant mode can be introduced between the ion optic and the mass analyser. This is a chamber filled with a collision gas, for example a mixture of He and H. The idea behind the so-called kinetic energy discriminant mode (KED) is that polyatomic molecules have a higher effective cross section and are more likely to collide with the helium atoms which goes along with the loss of kinetic energy. At the end of the chamber is a voltage barrier, which means that only ions with a sufficient kinetic energy can go further (Figure 2.8). The effect of the collision cell can be regulated by the gas flow of the KED gas and the energy barrier. So, the polyatomic species can be separated, and mass interferences can be reduced. It is worth mentioning that the overall intensities generally decrease when using a collision cell.

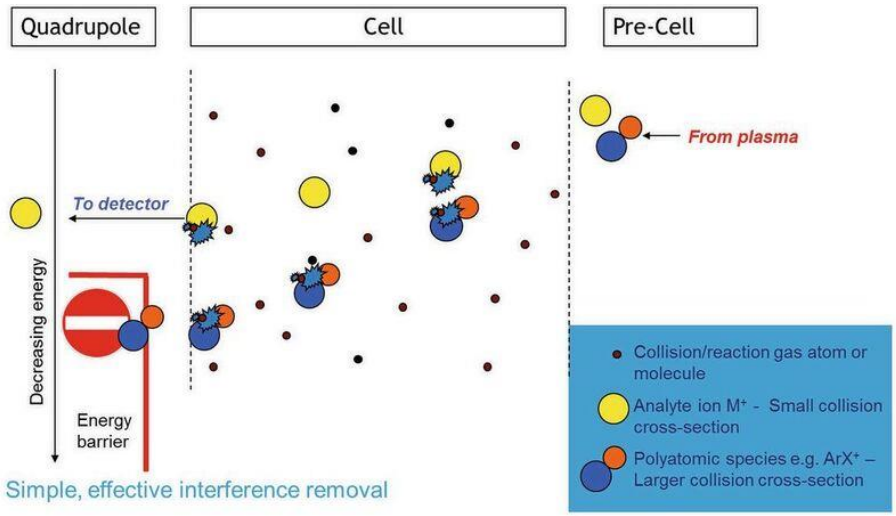

Figure 2.8: How collision cell technology with KED for ICP-MS works (Thermo Fisher Scientific)

ICP-MS is a reliable, well-established method for trace analytics. It enables fast qualitative and quantitative information and is easy to quantify with external calibration curves. Typical limits of detection for trace elements such as Pb or Cd in aqueous sample solutions are at 0,01 µg/L.
The requirement of liquid samples comes in case of solid samples, with elaborate sample preparation due to the necessary microwave assisted digestion. The fact that only bulk information is obtained warrants the need of combination with other methods to receive spatial information. To reach results with similar limits of detections, methods such as LA-ICP-MS and a combination of LIBS and LA-ICP-MS were used for spatially resolved analysis.

2.4 LA-ICP-MS (solid sampling)

The principle of LA-ICP-MS is similar to ICP-MS. A difference is that solid samples can be measured directly by focusing a laser on the sample surface like LIBS. The same reaction mechanisms take place as with LIBS, but with LA-ICP-MS the emitted light is not of interest, only the particles generated in the ablation process. The ablated small particles were transported by a helium gas flow due to a dual concentric injection system (DCI) to the plasma torch and excited, ionized, separated, and analysed as already described in 2.3. The setup of this technique is shown in Figure 2.9.

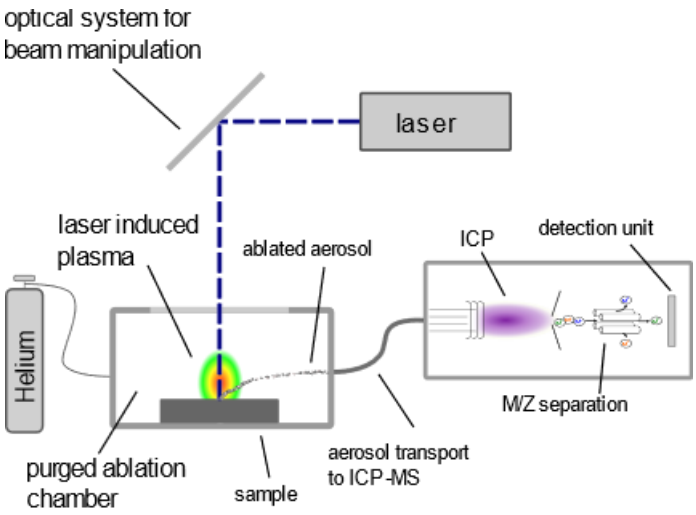

Figure 2.9: Setup Laser ablation inductively coupled plasma mass spectrometry for solid samples (L. Brunnbauer)

The use of a lasers for ablating sample provides spatially information and enables images and depth profiles of distribution of analytes in the investigated samples. The small beam diameter enables good lateral resolution of 5 to 150 µm. No elaborate sample preparation is required.
The quantification is more difficult than for liquid samples, because solid standards with the same matrix as the actual samples are required since the ablation process as well as particle transport highly dependents on the sample matrix. Additionally, analysis of non-flat samples (e.g., spherical samples) is challenging.

2.5 LA-ICP-MS and LIBS Tandem (solid sampling)

To obtain spatially resolved analysis depth profiles and images could be measured in a tandem setup of the two laser-based methods (Brunnbauer, et al., 2020). The combination of LA-ICP-MS and LIBS enables improved sample characterization and the information about the distribution from lighter elements such as H,C and O (LIBS) and less abundant trace elements (LA-ICP-MS) at the same time. A laser is applied directly on the solid sample. Small particles are ablated, whilst a local plasma is formed on the sample surface which leads to excitation and further emittance of characteristic light due to the relaxation of the excited species as described in 2.2.2.1. The spectral lines are collected with an optic and separated with a polychromator and finally detected with an ICCD. The particles produced after breakdown of the plasma were introduced in the argon plasma torch and analysed like described earlier (2.4) (LA-ICP-MS). The principal setup of such a Tandem system is shown in Figure 2.10.

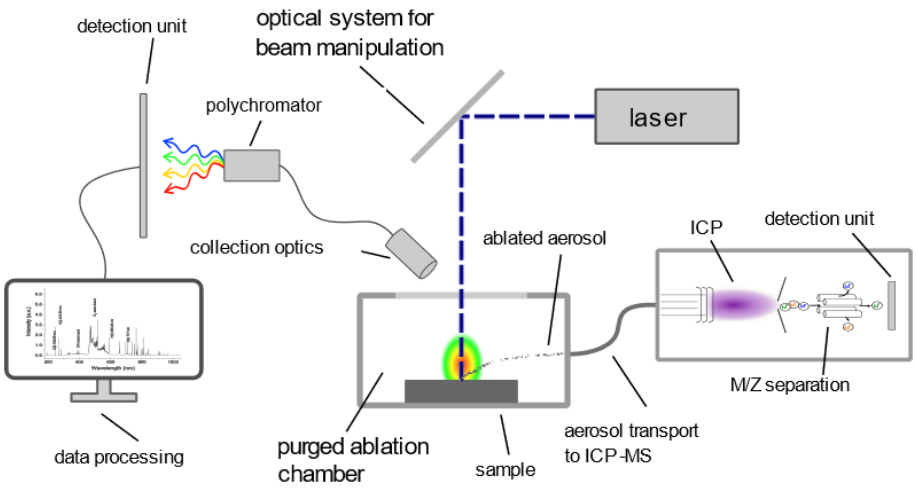

Figure 2.10: Setup Tandem LIBS and LA-ICP-MS for solid samples (L. Brunnbauer)

This setup enables the simultaneous detection of both, the trace elements like Pb and Zn and light elements like H, C, and O as a marker for degradation. This reveals depth profiles and images which visualize the distribution of contained additives, the uptake of trace elements and marker for degradation.

The combination of the two laser-based methods requires some compromises in the setup. To gain high signal intensities in LIBS spectra bigger beam diameters and high laser energies are necessary. This comes along with a decrease in resolution. LIBS systems work better in argon atmosphere because of the needed plasma, whereas LA systems show good performance in helium atmosphere. Also, the requested laser systems are different, as LIBS prefers lasers in IR region and for LA higher resolution is enabled with lasers with shorter wavelength.

3 Experimental

3.1 Reagents and consumables

The used ultrapure water (18 MΩ cm) was prepared by a Barnsted Easypure II (Thermo Scientific, USA) and is further also named MilliQ.

In this thesis four different polymers which are commonly used for industrial applications were investigated in representation of the variety of different polymer types and are listed in Table 3.1.

Table 3.1: List of used samples

Name	Abbreviation	Supplier	Product Nr.
Polystyrene	PS	GoodFellow	ST31-PD-000103
Polyamide	PA	GoodFellow	AM37-PD-000145
Polyethylene terephthalate	PET	GoodFellow	ET31-PD-000131
Polyvinylidene chloride	PVDC	GoodFellow	CV30-PD-000110

For the spiking procedure and the measuring with ICP-MS liquid ICP Standard solutions were provided and are shown in Table 3.2.

Table 3.2: List of used ICP Standard solutions

Name	Element	Concentration (mg/kg)	Supplier
Aluminium	Al	985	Certipur Merck KGaA
Cadmium	Cd	967.7	p.a. 99% Art.2011 Merck
Neodymium	Nd	1000	Aristar BDH laboratory supplies Pool
Nickel	Ni	988	Certipur Merck
Lead	Pb	1000	Certipur Merck
Antimony	Sb	1000	Certipur Merck
Thorium	Th	1000	Cl6-162 Thy Merck
Titan	Ti	999	Certipur Merck
Zinc	Zn	982	Certipur Merck
Indium	In	1000	Certipur Merck

Table 3.3 contains a list of the used chemicals and their quality for the preparation of the artificial seawater, as digestion reagents for microwave assisted digestion, artificial ageing with oxidizing reagents and the provided gases for supplying ICP-MS, LA-ICP-MS and LIBS.

Table 3.3: List of used chemicals

Name	Formular	Supplier and Quality
Sodium chloride	NaCl	p.a. Emsure Merck
Sodium sulphate	Na_2SO_4	p.a. waterfree ACS ISO Merck
Potassium chloride	KCl	p.a. Merck
Sodium hydrogen carbonate	$NaHCO_3$	p.a. Merck
Potassium bromide	KBr	p.a. Merck
Boric acid	H_3BO_3	p.a. Art.165 Merck
Sodium fluoride	NaF	p.a. Art.6449 Merck
Magnesium chloride hexahydrate	$MgCl_2*6H_2O$	p.a. Merck
Calcium chloride	$CaCl_2$	p.a. Merck
Strontium chloride hexahydrate	$SrCl_2*6H_2O$	p.a. Art.7865 Merck
Nitric acid	HNO_3	65% p.a. EMSURE Reg, Supelco Merck
Hydrogen peroxide	H_2O_2	30%, Suprapur Merck
Nitrogen (gaseous)	N_2	99,999 Vol% UN1066 Messner
Helium (gaseous)	He	≥99.999 Vol% UN1046 Messner
Argon (gaseous)	Ar	99,999% UN1006 Messner

A list of the used consumables for spiking experiments, handling liquid samples and solid sample preparation like polishing and embedding is shown in Table 3.4.

Table 3.4: List of consumables

Name	Supplier
Blue cap 50 mL	Centrifuge tubes w. cap 50 mL, Brand GmbH + Co KG
Centrifuge tube 15 mL	Centrifuge tubes w. screwcap VWR
Microscope slide	631-1552 VWR European Article
SiC Sandpaper	Silicon Carbide Paper FEPA, Struers
Pipette tips 10-100 µL	epT.I.P.S Eppendorf AG
Pipette tips 100-1000 µL	epT.I.P.S Eppendorf AG
Pipette tips 0.1-5 mL	epT.I.P.S Eppendorf AG
Pipette tips 1-10 mL	epT.I.P.S Eppendorf AG
Epoxy resin components	EpoFix Kit UN3082, UN2259, Struers
Acryl resin components	ClaroCit Kit UN1866, Struers

3.2 Sample Preparation

3.2.1 Artificial Degradation

The degradation procedure was performed to simulate the erosive and harsh conditions that plastics are exposed to in nature. The aim was to cause damage to the material. The different procedures are described in the following section. Because of the variety of the polymers different changes in the material were expected after degradation processes. The four investigated polymers were Polystyrene (PS), Polyamide (PA; Nylon 12), Polyethylene terephthalate (PET) and Polyvinylidene chloride (PVDC) (GoodFellow, 2021).

The polymers were artificially degraded by different methods. The preliminary tests were performed with PS and four different ageing procedures. A summary of the various treatments is found in Table 3.5. The first treatment was exposure to UV radiation for a certain time. Therefore, the polymers were placed in a 1,5 L beaker and filled with ultrapure water. This beaker was cooled in an ice bath and continuously stirred. An UV Lamp (Hg medium pressure lamp; 500 W; 200-600 nm; TQ-150 Heraeus, Hanau Germany) was dipped in and the aperture was covered by a box to protect from the UV radiation. A picture of this setting is shown in Figure 3.1.

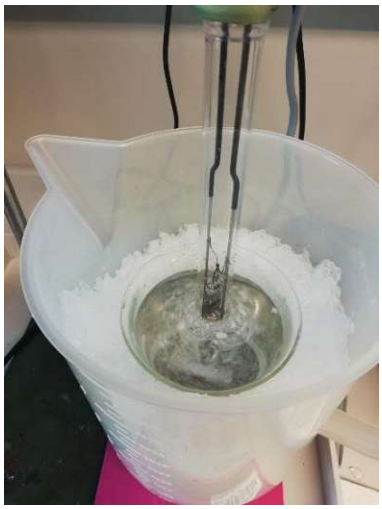

Figure 3.1: Setup artificial ageing procedure of polymer samples with dipped in UV Lamp in an ice bath cooled beaker

A second treatment procedure was performed by soaking the polymer particles in concentrated HNO_3 and H_2O_2. Therefore, different mixtures from 40 to 80 Vol% HNO_3 with 5 Vol% H_2O_2 were prepared and used for treatment. This should lead to oxidation in the polymer structure.

These experiments were also performed with HNO_3 only as a third method.

A fourth method was to mix the first and the second procedure by combine UV irradiation and up to 20 Vol% HNO_3 and 5 Vol% H_2O_2. An overview of applied aging procedures is provided in Table 3.5.

Table 3.5: Overview of different artificial treatment methods

Method	Treatment	Duration
1	UV irradiation	1-20 h
2	HNO_3 and H_2O_2	1 to 2 weeks
3	HNO_3	1 to 2 weeks
4	UV irradiation, HNO_3 and H_2O_2	20 h

3.2.2 Adding trace elements in artificial seawater

At first artificial seawater was prepared as described by (Kester, et al., 1967). Therefore, all reagents in Table 3.6 were weighed and dissolved in 1 L ultrapure water.

Table 3.6: Recipe for 1 L artificial seawater (Kester, et al., 1967)

Reagent	Mol mass (g mol^{-1})	Portion (g kg^{-1})	Mass (g)
NaCl	58.44	23.926	47.852
Na_2SO_4	142.04	4.008	8.016
KCl	74.56	0.677	1.354
$NaHCO_3$	84	0.196	0.392
KBr	119.01	0.098	0.196
H_3BO_3	61.83	0.026	0.052
NaF	41.99	0.003	0.006
$MgCl_2*6H_2O$	203.33	10.831	21.663
$CaCl_2$	110.98	1.519	1.146
$SrCl_2*6H_2O$	266.64	0.024	0.048

The elements which were chosen for the spiking process were dependent on the already contained elements in the individual polymer. They are summarized in Table 3.7. Each of these elements should be present in the artificial seawater in a concentration of about 100 µg/L. For this purpose, each of the original standard solutions was diluted to 50 mg/L. For each selected element 90 µL of these dilutions were pipetted in 50 mL vessels and filled up with artificial seawater.

Table 3.7: Summary of elements used for spiking polymers

Polymer	Element additive/contamination	Element spiked
PS	Al, Ti, Rb, Sb, Cs, Zn, Cu	Ni, Sb, Cd, Pb, Th, Nd
PA	Al, Zn, Pb, Al	Ni, Sb, Cd, Th, Nd
PET	Al, Sb	Ni, Pb, Cd, Th, Nd
PVDC	Al, Zn, Sb	Ni, Zn, Pb, Cd, Th, Nd

Then for PS 0.25 g Sample was weighed in, in small beakers and 10 mL of the spiked seawater was added. For PA, PET and PVDC 3.5 g and 25 mL of spiked seawater were filled in 50 mL vessels (Blue caps). A magnetic stirrer was added in each vessel, and they were stirred from 5 h to 28 d. For PS, each sample was prepared separately in a vessel. While for the other plastics a certain amount of solid was removed after 5 h, 15 h, 24 h, 4 d, 7 d, 14 d, 21 d and 28 d.

After removing the MPs, the supernatant was removed, and 3 mL ultrapure water was added. The particles were mixed by means of a vortex (Vortex Genie 2, Scientific Industries) for 30 s and then centrifuged (EBA20, Hettich Zentrifugen, Tuttlingen Germany) for 10 min at 3000 rpm. Then the supernatant was again withdrawn, and the process repeated three times.

At last, the particles were dried under vacuum in a desiccator.

Washing was necessary to prevent metals from sticking on the surface of the remaining solution. Only residual metals that are attached to the plastic or have diffused into the interior should be analysed. To determine the correct number of washing steps, experiments were carried out in which a fraction was washed 10 times. The washing water of each step was measured using liquid ICP-MS.

3.2.3 Sample preparation for measurement

In dependence on the further measurement method, different sample preparation procedures were performed. The three main sample types were liquid samples for ICP-MS measurements, embedded particles for imaging and single particles for depth profile analysis using LIBS/LA-ICP-MS.

3.2.3.1 Liquid Bulk samples by microwave assisted digestion

To enable liquid measurements microwave assisted digestion was performed with a Multiwave 5000 (Anton Paar) (Figure 3.2). The aim was to mineralize the polymer matrix to CO_2 and H_2O, resulting in a quantitative dissolution of the inorganic sample constituents.

About 0.025 g of solid and dry polymer sample were weighed and placed in teflon vials as seen in Figure 3.2. 8 mL HNO_3 (65%) and 2 mL H_2O_2 (30%) was added. The temperature program is shown in Table 3.8. The whole temperature program took about 80 min per run. Between every sample run a cleaning run with only the digestion reagents was performed at the same parameters as the digestion runs to clean the teflon vessels.

Figure 3.2: Microwave Multiwave 5000 for microwave assisted digestion Anton Paar and teflon vials as digestion vessels

Table 3.8: Temperature program "polymer middle" for microwave assisted digestion

	Program steps	Power
1.Step	Heating 15 min up to 200 °C	1200 W
2.Step	Hold 40 min 200 °C (T_{max}=210 °C)	250 W
3.Step	Cooling down to 60 °C	-

To find the optimum digestion conditions for the four polymers, various tests were carried out in which both the composition of the digestion reagents and the temperature program were varied. The method described above showed the best compromise between workload and digestion success.

In the case of higher weights or smaller amounts of effluent, precipitation formed after dilution of the samples.
After digestion the samples were diluted 1: 20 for the liquid measurements with 4% HNO_3.

3.2.3.2 Solid samples- embedded particles

At first a small piece of double-sided tape was placed on a Si Wafer. For each polymer sample, some of the particles were spread on a separate double-sided tape. Then the embedding resin used was prepared according to the manufacturer, and a small amount was filled in the forms. Then the prepared Si Wafer pieces were put upside down, with tweezers in the resin in cylindric forms (diameter 3,5 cm). Finally, the rest of the resin was filled in the forms. The pieces were pressed down to make sure they are laying on the ground.
The first attempts were made with epoxy resin and the later ones with acrylic resin.

After hardening (for epoxy 12 h, for acryl 20 min) the samples were polished dry per hand with SiC sandpaper. The goal was to expose cross-sections of the particles to image them with LA-ICP-MS and LIBS. According to the FEPA standard, sandpaper was used graded in coarseness from P320, P400, P600, P1200, P2000, P2400 and P4000.

The degree and the quality of the cut were evaluated using a light microscope (Olympus BX41M). After polishing, the sections were suitable for the measurements (Figure 3.3 and Figure 3.4).

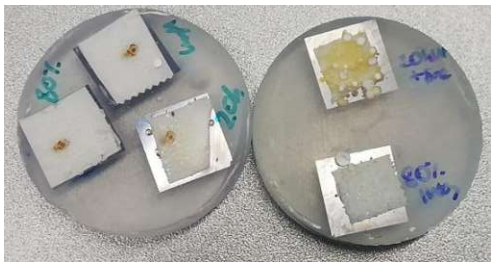

Figure 3.3: Cuts of embedded PS particles in acryl resin on a double-sided tape (white) on a Si Wafer (grey)

Figure 3.4: Microscope (VHX Digital Microscope) picture 200x magnitude of embedded polished PS particles

3.2.3.3 *Solid samples- Single particles*

To enable depth profile analysis on individual particles, double-sided tape was placed on a microscope slide. The polymer particles were spread over the tape pieces. The prepared samples (Figure 3.5 and Figure 3.6) were ready for depth profile analysis with LA-ICP-MS and LIBS.

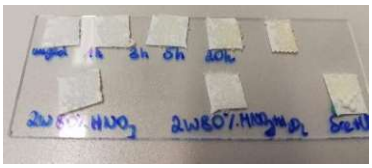

Figure 3.5: Microscope slide with singe particles for depth profile analysis with PS Particles

Figure 3.6: Single PS particles for depth profile analysis on a microscope slide

3.3 Characterization of material changes after degradation

There were many different methods to investigate the degradation in the material. For polymers, infrared spectroscopy (IR), Raman spectroscopy and laser induced breakdown spectrometry (LIBS) are well proved methods to observe changes by uptake of O and changes of functional groups of the polymers.

3.3.1 FT- ATR-Spectroscopy

3.3.1.1 *Instrumentation and Data Treatment*

For the experimental part a thermostated FTIR-Spectrometer (Specac Thermostat 25°C; Perkin Elmer Spectra 65 FTIR-Spectrometer) with ATR crystal was used. The data processing was performed by measuring adsorption spectra using Spectrum (Perkin Elmer Spectrum 10.4.1.262; 2013). The performed settings are found in Table 3.9. For background correction air was measured.

The single spectra of the samples were all normalized to a peak that was not changed by the ageing process and gains the highest signal. This is necessary because of the occurring differences in the measured spectra by different applied pressure and contact area with the ATR crystal.

Table 3.9: Parameter settings for FTIR-ATR spectroscopy

Parameter	Setting
Wavenumber range (cm^{-1})	550-4000
Resolution (cm^{-1})	4
Crystal	Diamond/ KRS-S
Accumulation scans	6

3.3.2 Raman Spectroscopy

3.3.2.1 Instrumentation and Data Treatment

The native and the degraded polymer samples were sent to Central European Institute of Technology, Brno University of Technology and measured at the Institute of Scientific Instruments, Czech Academy of Sciences with a Raman spectrometer (RENISHAW Raman micro spectrometer). The used parameters are summarized in Table 3.10.

Table 3.10: Settings Raman spectroscopy at 532 nm (Brno Czech Academy of Science)

Parameter	Setting
Integration time (s)	1.000
Accumulation scans	15
Laser energy (mW)	3.8
Laser wavelength (nm)	532
Objective (Leica N PLAN EPI)	20x/0.40

3.3.3 LIBS

3.3.3.1 Instrumentation and Data Treatment

The measurements were performed by a laser induced breakdown spectrometer (J200 Tandem, Applied Spectra) equipped with an Nd-YAG-Laser with a wavelength of 266 nm in combination with an ICCD detector (PI-MAX 4, Teledyne Princeton instruments). The spectrometer provided was a Czerny-Turner spectrometer (Spectra Pro HRS-750, 750 mm Triple Grating Imaging Spectrograph). The parameters were controlled by Axiom 2.0 (2004-2200 Applied Spectra Inc.) and the ICCD parameters by LightField V.6.13.1.2008 (2010-2020 Teledyne Princeton Instruments). This experimental setup was used to perform the analysis of changes in the polymer after degradation and in combination with LA-ICP-MS to image cross sections and analyse profiles of the polymers.

The measurement settings for the detection of changes after degradation are shown in Table 3.11. These measurements were preliminary and only done with the different aged polystyrene samples.

Table 3.11: Settings for LIBS measurements to detect changes in material after degradation with a broadband spectrometer and an ICCD

	Parameter	Setting
LIBS	**Gate delay (s)**	0.1
	Laser energy (%)	80
	Number of shots	10
	Rep. rate (Hz)	10
	Warm up energy (%)	100
	Warm up shots ()	150
	Spot size (µm)	80
	Gas flow Ar (L min^{-1})	1
	Min experiment delay (s)	1
	Number of experiment passes ()	1
ICCD	**Grid density ICCD (g mm^{-1})**	1800
	Entrance port slith wide (µm)	300
	Blaze (nm)	500
	ICCD center wavelength (nm)	780
	Frames per scan	10
	Gain ()	100
	Accumulations	10

The obtained spectra from the broadband spectrometer were evaluated with the software Aurora V18.212 (Applied Spectra Inc.). The O signal detected with the ICCD was obtained by integration with a phyton script with integration limits from 776.312 to 777.257 nm. The intensity of the elements detected with the broadband spectrometer and the O signal were then normalized to the C band at 193 nm because it was the most intensive that didn't change (Guezenoc, et al., 2019). A statistical evaluation was following operated by OriginPro 2016G (1991-2015 OriginLab Coorp, USA).

For the spatially resolved analysis like images and depth profile analysis a different setup and different settings were used. These are described in 3.4.2 and in 3.4.3.

3.3.4 Density measurements with He-Pycnometry

3.3.4.1 Instrumentation and Data Treatment

Helium Pycnometry was performed to determine the skeletal density of the provided polymer samples. Skeletal density means the ratio of the mass to the volume of the solid material and its closed pores within the material (ASTM D3766) (Pennsylvania State University, 2022). The principle is using the relationship between volume and pressure of an expanding gas according to Boyle-Marotte´s law.

The weighted sample is filled in a sealed cup of known volume and placed in the thermostated (20 °C) sample chamber. He is introduced into the chamber and then expand to a second empty chamber of known volume. The pressure of helium in both chambers is measured, and then used to calculate the volume repressed by the porous sample. The density is determined by dividing the sample weight by the volume measured. Closed pores are included in the total density, whereas open pores are not. Each sample was measured three times and for each measurement 3 to 10 runs were performed depending on the deviation between the single runs. The standard deviation and mean values were calculated from the sum of the single runs.

3.4 Determination of uptake and release of trace elements metals

3.4.1 Liquid Bulk Samples

For the quantitative analysis of the liquid microwave digested samples an external calibration was required. At first a multielement standard (Al, Cd, Nd, Ni, Pb, Sb, Th, Ti and Zn) with a concentration of 1 mg/L was prepared by pipetting the 10 µL of every 1000 mg/L standard solution listed in (3.1) in a 10 mL vial and filled up with 3% HNO_3. This solution was diluted 1:200 to 5 µg/L. From the 5 µg/L multielement stock solution 10 standards from 0 to 5 µg/L were prepared by gravimetric weighing the pipetted volume of each added solution. All standards were filled up with 3% HNO_3 up to 10 mL. To compensate for instrumental drifts during ICP-MS analysis, an internal standard of 1 µg/L In was added. To control whether there are drifts between the measurements a quality control standard (QC) was measured repeatedly after ten samples. The actual concentrations were calculated by dividing the pipetted volume multiplied with the concentration of the pipetted solution by the mass of the matrix.

The microwave digested samples were diluted 1:20, and 1 µg/L internal In standard was added and the vial were filled with HNO_3 (3%). The vials were placed in the ESI SC2DX (Elemental Scientific, Mainz, Germany) autosampler and then measured like described below.
Additionally, a survey run with ICP-MS was carried out, to detect the contained additives in the polymers. Therefore, all polymer samples were digested by microwave and then diluted 1:50 with 3% HNO_3 and then analysed. The results are relevant information for the spiking procedure.

3.4.1.1 Instrumentation and Data Treatment

For the liquid bulk analysis, a Thermo Scientific iCAP-Q (Thermo Fisher Scientific, USA), quadrupole ICP-MS, equipped with a linear range detector was used. A Peltier-cooled cyclone chamber was used in combination with a concentric PFA nebulizer. The measurement settings are shown in Table 3.12. Table 3.13 contains a list of the possible interferences for the detected isotopes. The selection of the measured isotopes was chosen based on the relative abundance of the isotopes as well as the possible interferences.

To reduce interferences from multiatomic molecules the collision cell with a He & H mix gas flow of 4.5 mL min^{-1} kinetic energy discrimination mode (KED mode) was used. This should provide more reliable results especially for the isotopes ^{27}Al and ^{48}Ti.

Table 3.12: ICP-MS parameters for liquid bulk measurements

Parameter	Setting
RF-Power (W)	1550
Cool gas flow Ar (L min^{-1})	14
Nebulizer gas flow Ar (L min^{-1})	0.9964
Auxiliary gas flow Ar (L min^{-1})	0.8000
Sample flow rate (µL min^{-1})	400
Dwell Time (s)	0.01

Table 3.13: Possible relevant interferences of measured isotopes

Isotope	Relevant Interferences
^{27}Al	$^{14}N^{13}C$, $^{15}N^{12}C$, $^{16}O^{11}B$, $^{16}O^{1}H^{10}B$, $^{1}H^{26}Mg$
^{48}Ti	^{48}Ca, $^{36}Ar^{12}C$, $^{13}C^{35}Cl$
^{60}Ni	-
^{68}Zn	-
^{112}Cd	-
^{121}Sb	-
^{142}Nd	-
^{208}Pb	-
^{232}Th	-

The quality of the measurements was controlled by measuring a "tune A" solution containing the elements Li, U, Ba, Bi, Ce, Co, Pb and In with a concentration of 1 µg L^{-1} to cover the whole element region. The system was tuned by automatically optimizing the gas flow and torch position for maximizing intensities while measuring tune A solution. The sample loop was flushed by a HNO_3 (3%) solution "FAST Carrier Solution" (Elemental Scientific Inc., Mainz, Germany). The Autosampler System was flushed also by a 3% HNO_3 "autosampler rinse" (Elemental Scientific Inc., Mainz, Germany).

3.4.2 Solid Samples Images

3.4.2.1 Instrumentation and Data Treatment

For the spatially resolved analysis, a Thermo Scientific iCAP-Q (Thermo Fisher Scientific, USA), quadrupole ICP-MS equipped with a linear range detector was used. The measurement settings are shown in Table 3.14.

Table 3.14: ICP-MS parameters for solid sampling Imaging

Parameter	Setting
RF-Power (W)	1550
Cool gas flow Ar (L min^{-1})	14
Make-up gas flow Ar (L min^{-1})	0.8500
Auxiliary gas flow Ar (L min^{-1})	0.8000
Dwell time (s)	0.012

The coupled laser system was an ESI NWR 193 (Elemental Scientific Industries, Inc Portland, USA) with a ArF Excimer laser at 193 nm wavelength. The ablation was performed under He atmosphere with a gas flow of 800 mL min^{-1} (carrier gas). The ablation chamber was coupled to the ICP-MS with a teflon tube with an inner diameter of 2 mm. The helium gas flow was mixed with argon as make up gas before entering the plasma torch. The samples were placed in the sample chamber, taking care that all samples have the same height as the edge of the sample holder.
The Instrument was tuned daily for maximum ^{115}In intensity by ablating NIST612. Additionally, the laser energy was checked daily at 100% laser energy and a beam diameter of 150 µm.

The here described settings for imaging particle cross sections was improved and varied in many trials. The final settings are shown in Table 3.15. The injection of the ablated samples was performed by an DCI (dual concentric injection System, ESI, USA) to achieve better wash out times in the chamber. Because of the polishing the resin was fading with the polymer. To minder this effect all measured cross sections were pre-ablated before the actual measurement.

Table 3.15: Parameters for solid sampling imaging with LA-ICP-MS

Parameter	Setting
Chamber He (carrier gas) (mL min^{-1})	800
Repetition rate (Hz)	100
Laser energy (%)	30
Beam size (µm)	7x7
Overlap (µm)	6,03
Scan speed (µm s^{-1})	97
Injection system	Analytical Cup; DCI
Polymer	**Isotopes**
PS	^{13}C, ^{27}Al, ^{64}Zn, ^{112}Cd, ^{121}Sb, ^{208}Pb
PA	^{13}C, ^{27}Al, ^{64}Zn, ^{112}Cd, ^{121}Sb, ^{208}Pb
PET	^{13}C, ^{27}Al, ^{112}Cd, ^{121}Sb, ^{208}Pb
PVDC	^{13}C, ^{27}Al, ^{64}Zn, ^{112}Cd, ^{121}Sb, ^{208}Pb

The imaging measurements of PS were also carried out in combination with LIBS in a tandem setup. The used parameters are shown in Table 3.16.

Table 3.16: Parameters for solid sampling imaging with LA-ICP-MS and LIBS as Tandem

	Parameter	Setting
LA-ICP-MS	**Chamber He (carrier gas) (mL min^{-1})**	800
	Repetition rate (Hz)	1
	Laser energy (%)	40
	Beam size (µm)	40x40
	Overlap (µm)	No overlap
	Injection system	Analytical Cup; DCI
ICCD	**Grid density ICCD (g mm^{-1})**	1800
	Entrance port slith wide (µm)	300
	Blaze (nm)	500
	ICCD center wavelength (nm)	780
	Frames per scan	10
	Gain ()	70
	Accumulations	10

The measured intensities of the isotopes were then exported as CSV files, as well as the laser logfiles. Both files of each measurement were then imported in Iolite (2022 Iolite Software, Elemental Scientific Laser) and background correction was carried out. Then Iolite was used to generate images.
To generate tandem images the detected LIBS signals were imported in ImageLab (Epina Image Lab, Epina GmBH) and merged with the in Iolite generated images.

3.4.3 Solid Sampling depth profiles Tandem

For analysing depth profiles, the same ICP-MS, and laser System as in 3.2.3.2 described was used. As samples the single particles prepared as described in 3.2.3.3 were used. The used parameters for analysis are shown in Table 3.17 and Table 3.18. The detected isotopes depend on the analysed polymer and are summarized in Table 3.19.

The instrument was tuned daily for maximum ^{115}In intensity by ablating NIST612.

PS was measured by ablating three patterns with three shots each line and 10 passes per shot. For PET and PA, three patterns of three shots each were measured, with each position being ablated 10 times with the laser. Investigated PVDC particles were larger, so 6 patterns of 20 shots each could be measured. The measured isotopes were the same as for the images shown in Table 3.15.

Table 3.17: ICP-MS parameters for solid sampling depth profiles measurements

Parameter	Setting
RF-Power (W)	1550
Cool gas flow Ar (L min^{-1})	14
Make-up gas flow Ar (L min^{-1})	0.8500
Auxiliary gas flow Ar (L min^{-1})	0.8000
Dwell time (s)	0.005

For depth profile analysis different settings were tried, the settings for the final measurements for all four polymer samples are shown in Table 3.18. To enable the detection of K and Ca the grid was set to 600g mm^{-1} for the analysis of PET, PVDC and PA.

Table 3.18: Settings for LIBS in combination with LA-ICP-MS as Tandem for depth profile analysis

	Parameter	Setting
LA	**Chamber He (carrier gas) (mL min^{-1})**	800
	Repetition rate (Hz)	20
	Laser energy (%)	40
	Beam size (µm)	40x40
	Overlap (µm)	No overlap
ICCD	**Grid density ICCD (g mm^{-1})**	600
	Entrance port slit wide (µm)	300
	Blaze (nm)	500
	ICCD Center wavelength (nm)	540
	Frames per scan	10
	Gain ()	100
	Accumulations	10

Table 3.19: Detected Elements and Isotopes for PS, PA, PET and PVDC

Polymer	Element with ICCD	Isotope with LA-ICP-MS
PS	O	^{13}C, ^{27}Al, ^{66}Zn, ^{108}Pb
PA	Ca, K, O, C	^{13}C, ^{27}Al, ^{64}Zn, ^{108}Pb, ^{112}Cd, ^{121}Sb
PET	Ca, K, O, C	^{13}C, ^{27}Al, ^{64}Zn, ^{108}Pb, ^{112}Cd, ^{121}Sb
PVDC	Ca, K, O, C	^{13}C, ^{27}Al, ^{64}Zn, ^{108}Pb, ^{112}Cd, ^{121}Sb

The emission lines of the elements of interest which were detected with LIBS were integrated using a python script. The integration limits are shown in Table 3.20.

The data analysed with ICP-MS was exported as csv file and baseline corrected with Iolight (2022 Iolight Software, Elemental Scientific Laser). The edited data was merged and statistically evaluated and plotted with OriginPro.

Table 3.20: Integration Limits of element bands for phyton script

Element Band	Integration range
O at 777.19 nm	775.9-779.0
K at 766.49 nm	765.8-767.2
K at 769.89 nm	769.05-770.35
Ca at 757.58 nm	753.95-755.95

4 Results and discussion

4.1 Initial Samples

4.1.1 Survey Run

To investigate the contained additives in the native polymers a survey run was carried out. The digested sample solution was quickly scanned several times from ^{3}Li to ^{238}U. Elements that are present in large quantities can be easily found in this way. Due to the high measurement speed, it is possible to overlook elements in lower concentrations. The results of the survey run from the investigated polymers are summarized in Table 4.1. After the survey run it is not definite which detected element is an additive and which might be contamination. As already mentioned, there is a variety of possible additives to improve properties and increase lifetime of plastics. In this project only inorganic species were observed and discussed in the following section. Some of the detected elements are recorded as common additives, even though, it is not clear which of these possible additives was really added. Some suggestions are discussed further.

TiO_2 is often added as white pigment in PET and PS especially when they are in contact with food. Other common inorganic pigments are Pb(Cr, Mo, S)O_4 (orange or red), Fe-, Zn-, Cd-, Cr- salts and carbon black (CB). Al or Zn are often added to create a metallic shining. In PA this was visible by the small sparkling parts on the polymer surface and in PET which seemed a bit shiny.
Metallic salts, based on combinations of Ba, Cd, Zn, Ca or Pb, are often used as heat stabilizers in PVC, PVDC and PS. As flame retardants metal hydrates like $Al(OH)_3$ and $Mg_2(OH)_4$ and Sb salts are commonly used especially in thermoplastics. For Light and UV stabilization mixed metals and TiO_2 are common supplements. Zn metal organic compounds are typically used for the synthesis of polystyrene via addition polymerization. Ag and Cu are added because of their biocide properties and to inhibit the growth of microorganisms. Rb an Cs are rare, but are recently used in the electronic industry, for thin films or solar cells. However, there was no explanation why Rb and Cs should be added in the native bought polymers (Ambrogie, et al., 2017) (Bart, 2005) (Pfaender, 2013) (Marturano, et al., 2017).

Table 4.1: Results survey run ICP- MS of PA, PS, PVDC and PET

Polymer	Element detected Survey Run
PS	Al, Ti, Rb, Sb, Cs, Zn, Cu
PA	Al, Zn, Pb
PVDC	Sb
PET	Al, Sb

4.1.2 Washing attempts

After the spiking procedure of the samples, the polymer particles were removed from the solution. To remove the residual droplets of artificial sea water present on the polymer particles, which contain the metals of interest and might therefore affect the outcome of the adsorption experiments, washing steps with ultra-pour water were performed. To see if the washing causes only removal of remaining artificial sea water or also leaching of the adsorbed elements from the inside of the particles different attempts were performed, to determine the correct number of washing steps. The aim was to find a compromise between the adsorption and leaching. Experiments were carried out in which a fraction was washed 10 times. The washing water of each step was measured using liquid ICP-MS. The results of these washing attempts are shown in Figure 4.1 and Figure 4.2. The two graphs differ only in the scaling to make the small concentration in the right picture more visible.

The experiments were repeated several times and always came to a similar result. The results presented here were carried out with particles that had been placed in a seawater metal solution for 24 h. Both graphs show that between two and four washes there is only little difference in the concentration of metals in the wash solution. Therefore, three washing steps were defined for the further tests.

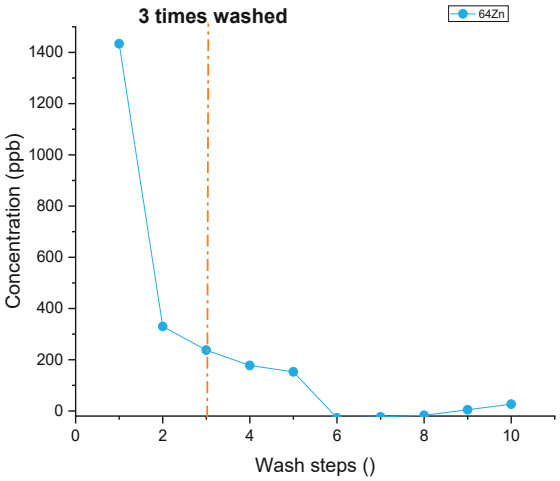

Figure 4.1: Washing attempts with Zn

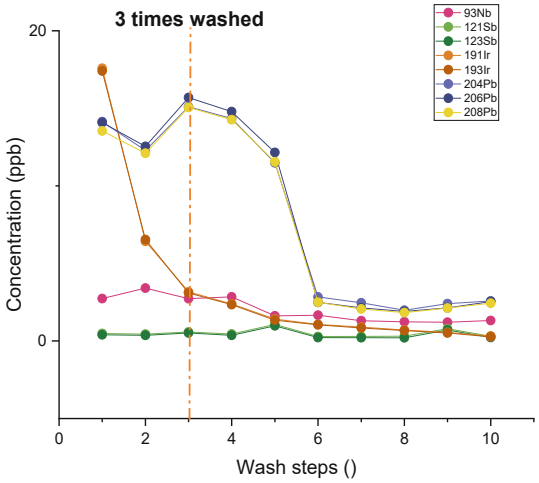

Figure 4.2: Washing attempts without Zn

4.1.3 Macroscopic Changes

After applying ageing treatment methods, different changes in the material occurred. Some are shown in the pictures below (Figure 4.3- Figure 4.6). Figure 4.4 shows a 20 h irradiated PS sample which turned yellowish due to the treatment. PS sample treated with oxidizing reagents shown in Figure 4.5 did not change significantly. Figure 4.6 contains a picture of a 20 h UV irradiated PS sample which was also treated with 20% $HNO_3$and 5% H_2O_2. This sample turned yellowish and some of the beads expanded (white beads) due to the heat of the UV lamp. Due to the HNO_3 the density of the medium during the UV irradiation was increased and the particles tend to float and therefore stayed near to the UV lamp and were exposed more to its heat.

Figure 4.3: untreated (native) PS ample

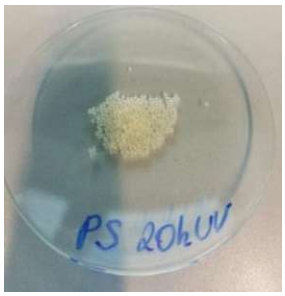

Figure 4.4: 20 h UV irradiated PS sample

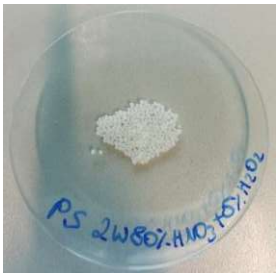

Figure 4.5: PS sample treated for 2 weeks with 80% HNO3 and 5% H2O2

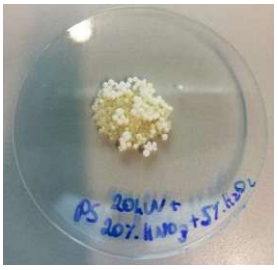

Figure 4.6: 20 h UV irradiated with 20% HNO_3 and 5% H_2O_2 treated PS sample

The longer the treatment with UV radiation was, the darker was the change in colour. The treated polymer samples were characterized as described in 3.3. Because of these insights the first treatment method (UV irradiation) was chosen for artificial ageing of the other polymers. The pictures of the native and UV irradiated PA, PET and PVDC samples are shown in Figure 4.7 to Figure 4.12. PET and PVDC turned also yellow, while PA seems to stay unchanged.

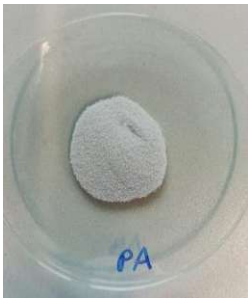

Figure 4.7: untreated (native) PA sample

Figure 4.8: untreated (native) PET sample

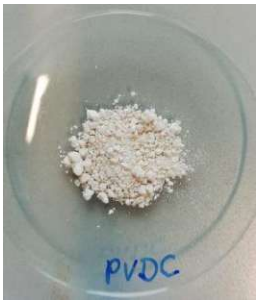

Figure 4.9: untreated (native) PVDC sample

Figure 4.10: 20 h UV irradiated PA sample

Figure 4.11: 20 h UV irradiated PET sample

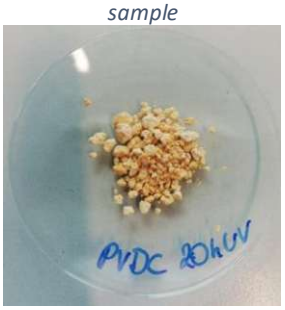

Figure 4.12: 20 h UV irradiated PVDC sample

4.1.4 FTIR-ATR Spectroscopy

As already indicated by the observed changes in the colour resulted ageing of the different polymers in alterations of the molecular structure, in the following sections the findings derived for the individual polymers measured with FTIR-ATR spectroscopy are presented and discussed.

4.1.4.1 PS

The following graphs show IR Spectra of different treated PS samples. An assignment of the according bands is found in Table 4.2. All measured PS spectra were normalized to the most intense peak at 695 cm^{-1}.

Figure 4.13 shows IR spectra for PS samples which were exposed to UV radiation for different durations. It is obvious that the UV irradiation influences the measured samples. At about 1736 cm^{-1} a new band is occurring which increases by treatment duration. This band could be a carbonyl band and would mean that oxidation happened at the polymer chain especially because there is no O in the untreated PS sample. The other bands nearly stay the same. The combination of the bands at 695 cm^{-1} and 755 cm^{-1} could also be an indicator for a mono or meta substitution of the benzene ring. Which of the two positions is present can be determined by comparison with spectra of substituted rings in the range from 1600 cm^{-1} to 2000 cm^{-1}. Depending on the type of substitution, there are more or less pronounced benzene fingers In this case the spectra is similar to Toluene and so it should be mono substituted (Thompson, 2018) (Noda, et al., 2007) (Yabagi, et al., 2017).

Figure 4.14 introduces samples treated with different mixtures of HNO_3 and water. These show a similar behaviour like the UV irradiated samples. Also, for these, a carbonyl band was obtained, but it is less intensive even under the harshest conditions.

In comparison, Figure 4.15 shows the spectra of PS samples that have been treated with both UV radiation and oxidizing reagents. Also here, a new band at about 1730 cm^{-1} is obtained.

Figure 4.16 shows a comparison of the harshest conditions of each treatment methods of the different PS samples. No matter which method was used, a new band which supposed to be a carbonyl band was occurring. The difference between the methods results in the intensity of the carbonyl band. Samples which treated only with UV radiation revealed the greatest difference compared with the unaged sample. It did not make any difference if there was added H_2O_2 or not when treated with HNO_3. The addition of oxidizing reagents if treated with UV irradiation seems to reduce the ageing effect of the irradiation but didn´t show a big impact at all.

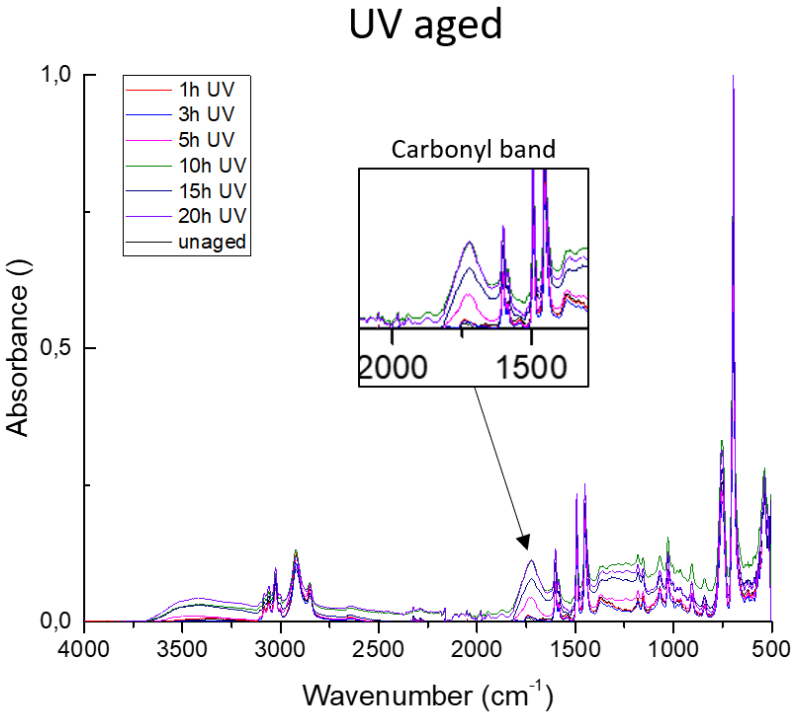

Figure 4.13: IR-Spectra of different UV irradiated PS Samples

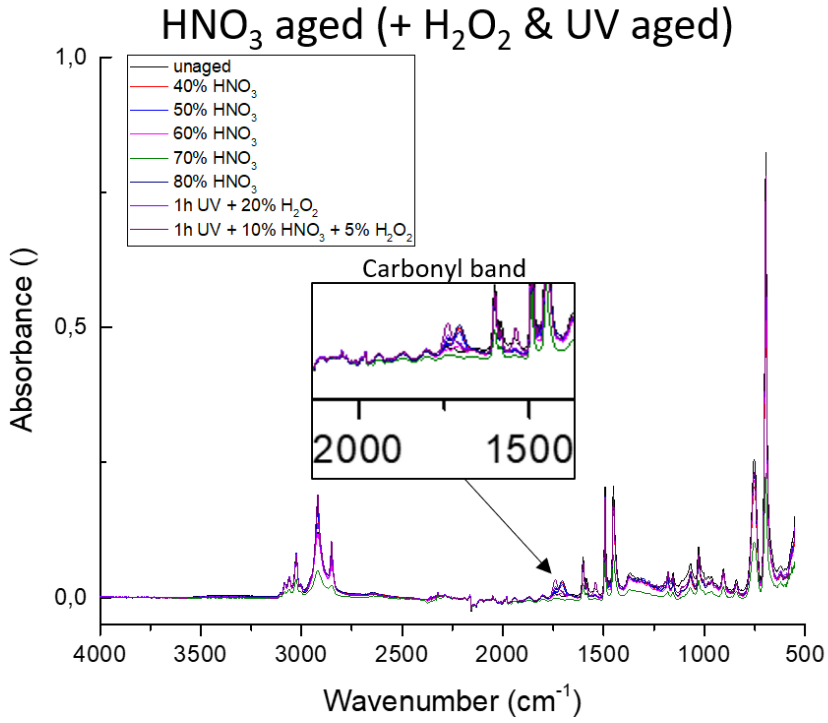

Figure 4.14: IR-Spectra of different with HNO_3 treated PS Samples

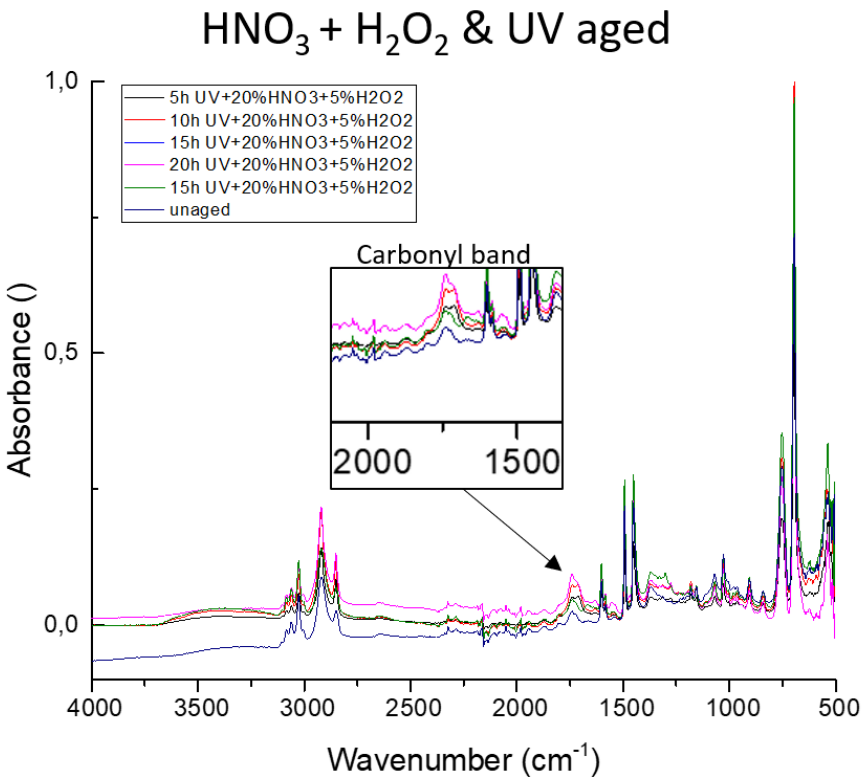

Figure 4.15: IR-Spectra of different with HNO_3 and H_2O_2 treated and UV irradiated PS Samples

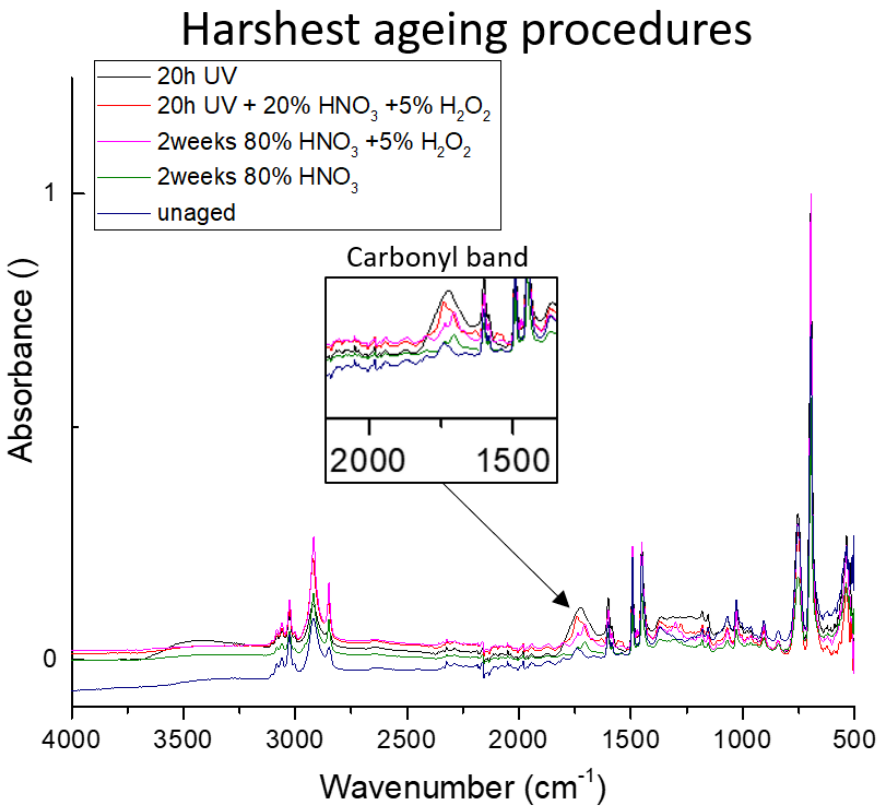

Figure 4.16: Comparison of IR-Spectra from different artificial aged PS Samples

Table 4.2: IR Band assignment of PS samples

Wavenumber (cm^{-1})	Band assignment
695	Aromatic ring band
754	Aromatic out of plane C-H band
904	C-H-band out of plane bending vibration
1028	C-O band
1452-1600	Stretching ring mode
1601	Stretching of C=C in benzene ring
1736	Carbonyl C=O stretching vibration
2853	Asymmetrical CH_2 stretching
2923	Symmetrical CH_2 stretching
3026	=C-H stretching

4.1.4.2 PA

Figure 4.17 shows PA samples that were irradiated with UV light for certain times. The band assignment is found in Table 4.3 (Thompson, 2018). The spectra were normalized to the band at 2919 cm^{-1} because it was the most intense that did not change. Compared to the unaged PA sample the intensity of peaks in two regions seems to decrease with advanced ageing. The first region is between 950 and 1200 cm^{-1} and the second is a peak at about 1544 cm^{-1} which belongs to CN and NH deformation vibrations.

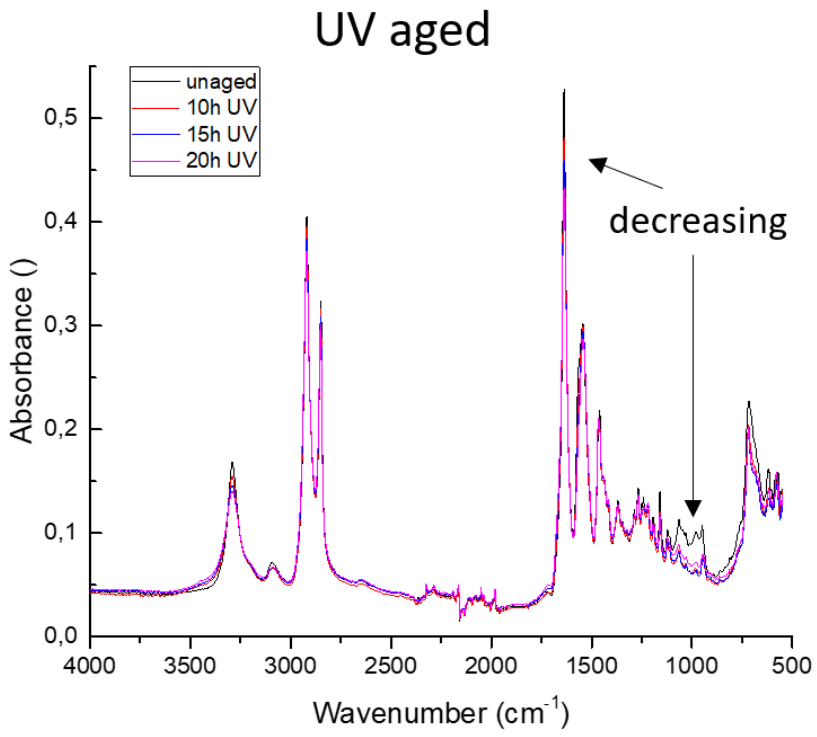

Figure 4.17: IR-Spectra of different UV irradiated PA samples

Table 4.3: IR Band assignment of PA samples

Wavenumber (cm^{-1})	Band assignment
716	NH
949	CH and NH rocking
1459	C-CO-NH_2
1544	-NH and –CN deformation
1638	-NH_2 bending vibration; Amide
2849	CH_2; CH_3 and NH
2919	CH_2; CH_3 and NH
3291	-NH_2 stretching vibration

4.1.4.3 PET

Figure 4.18 shows IR spectra of different UV irradiated PET samples, the according band assignment is found in Table 4.4 (Thompson, 2018). The spectra were normalized to the band at 1713 cm^{-1}.

The aged samples show a decrease in four bands at 722 cm^{-1} (Ring CH, CO out of plane bending), 1094 cm^{-1} (C-O stretching), 1243 cm^{-1} (O-C=O stretching) and 1713 cm^{-1} (C=O stretching). All those bands are vibrations of the carbonyl group in the polymer. Thus, the ageing procedure may influence the carbonyl C. The bands of the aromatic ring seem to stay unchanged.

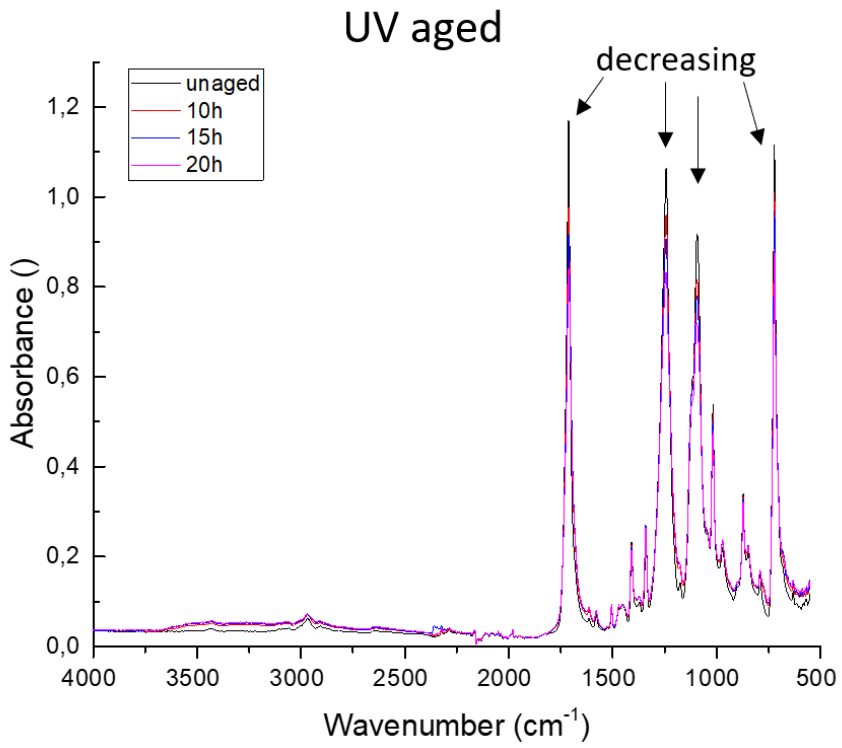

Figure 4.18: IR-Spectra of different UV irradiated PET samples

Table 4.4: IR Band assignment of PET samples

Wavenumber (cm^{-1})	Band assignment
722	Ring CH out of plane bending; CO out of plane bending
872	Vibrations of aromatic ring
972	trans C-O stretching and vibration of ester group
1018	Vibrations of aromatic ring
1094	C-O stretching of gauche conformer and trans conformer
1243	O-C=O stretching
1340	CH2 wagging vibration of trans conformation
1409	Vibrations of aromatic ring
1713	C=O stretching
2971	Vibrations of aromatic ring

4.1.4.4 PVDC

The spectra in Figure 4.19 show different UV irradiated PVDC spectra. These spectra were not normalized, because there was no band that was not changing. The band assignment is shown in Table 4.5 (Thompson, 2018). The bands at 609 cm^{-1} (C-Cl stretch vibration), 969 cm^{-1} (C-C stretch vibration), 1044 cm^{-1} (C-C stretch vibration) and 1424 cm^{-1} (CH_2 bending mode) show a lower intensity due to the ageing procedure. A new band emerges at 1722 cm^{-1}, which increases significantly with ageing, which leads to a carbonyl band. A possible explanation is chloride atom getting substituted by an O, due to the ageing procedure.

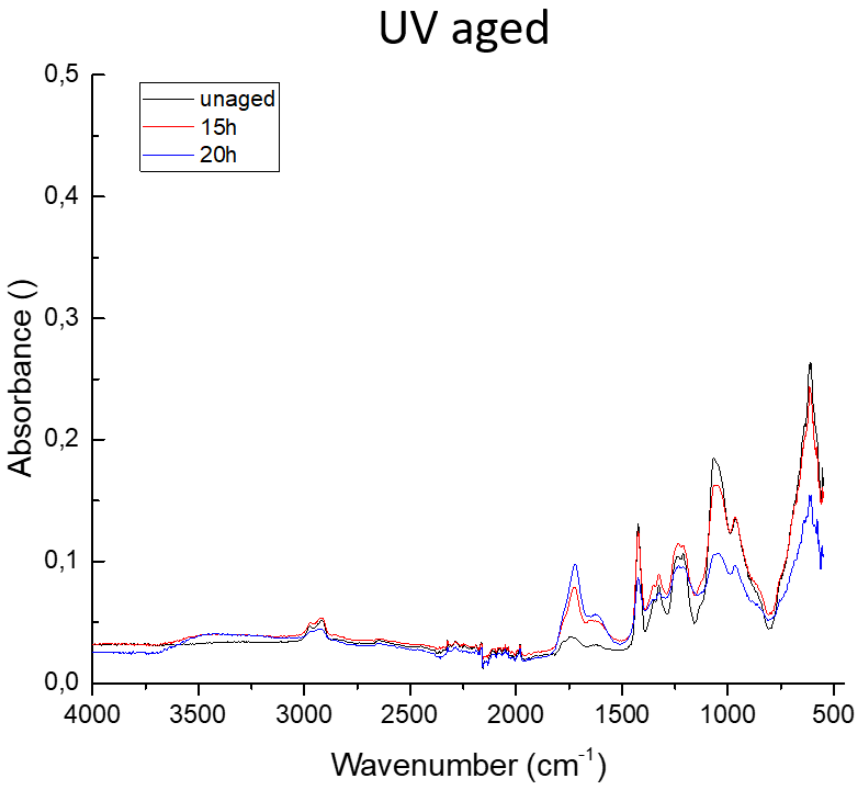

Figure 4.19: IR-Spectra of different UV irradiated PVDC samples

Table 4.5: IR Band assignment of PVDC samples

Wavenumber (cm^{-1})	Band assignment
609	C-Cl stretch vibration
969	C-C stretch vibration
1044	C-C stretch vibration
1211	-
1351	CH_2 stretching mode
1424	CH_2 bending mode
1722	C=O α, β-unsaturated acyclic carbonyl
2926	CH_2 stretching mode

4.1.5 Raman Spectroscopy

Raman measurements were also carried out to obtain further information about changes in the molecular structure between natural and aged polymer samples. Therefore, the samples were sent to the Czech Academy of Science Brno. For more detailed discussion statistical an evaluation of the data has been performed using chemometrics.

The chemometrics in evaluation revealed data which would not have been visible otherwise. In the following most of the discussion was taken from the provided report.

They were able to distinguish different types of treatment according to the changes in PS peak height (Figure 4.20 and Figure 4.21). It seems that the harsher the conditions, the smaller the peak is. Probably due to the higher degradation of the chemical structure within the molecule.

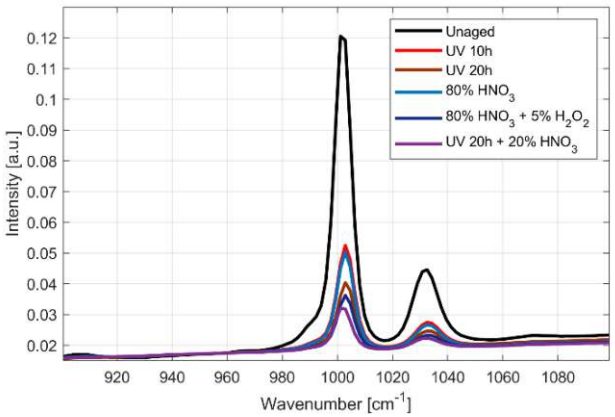

Figure 4.20: Groups-averaged spectra zoomed at the main polystyrene peak at 1003 cm^{-1} from report of Raman measurements Czech Academy of Science

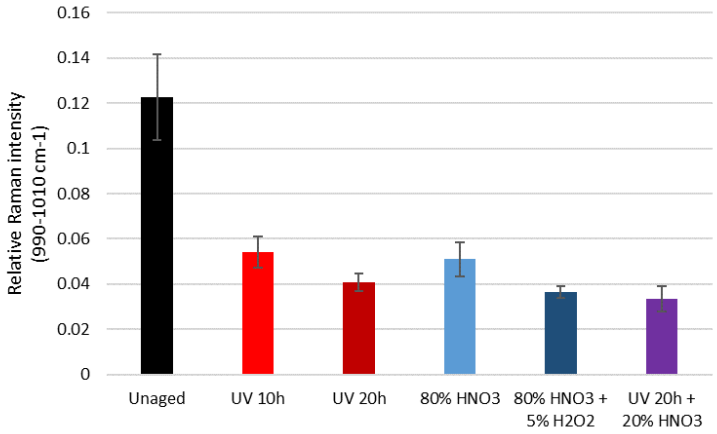

Figure 4.21: PS peak intensities among samples from report of Raman measurements Czech Academy of Science

Also, a principal component analysis (PCA) was performed with the data. The UV aged and the acid aged were observed separately (Figure 4.22 and Figure 4.23). The samples treated more harshly appear further from the unaged group. If combined, groups "UV 10 h" and "80% HNO_3" slightly overlay, such as groups "UV 20 h" and "80% HNO_3 + 5% H_2O_2" do. This suggests that the damage is comparable between those samples. Considering the results, using Raman spectroscopy for detection of different degrees of aging of polystyrene looks like a promising concept.

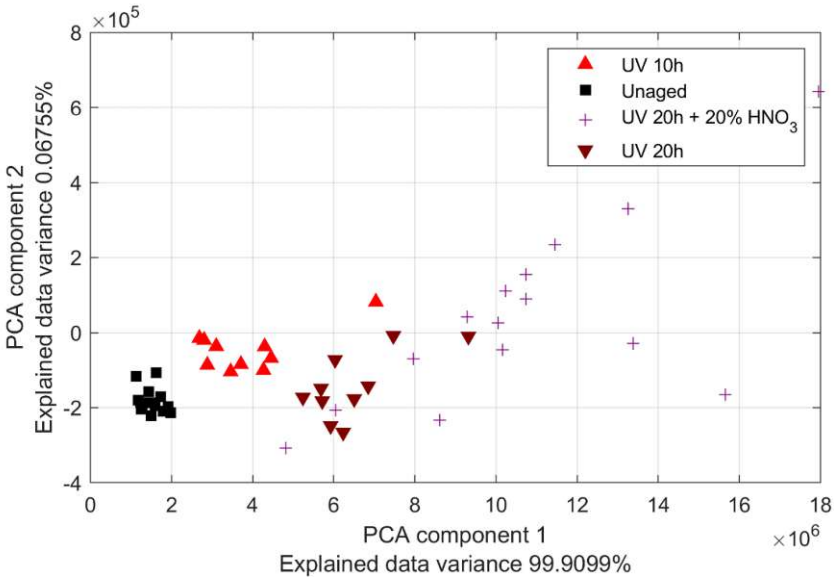

Figure 4.22: PCA: Differentiation of groups for UV-treated samples (including UV+HNO_3) from report of Raman measurements Czech Academy of Science

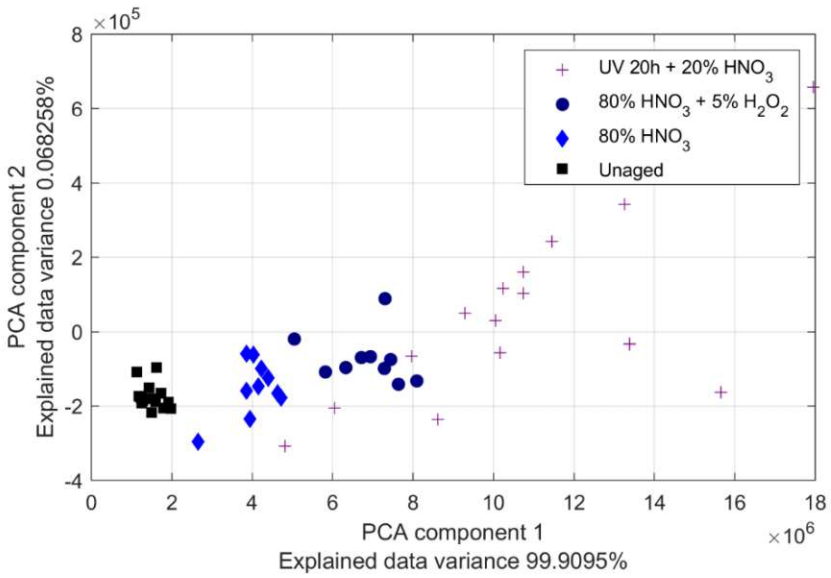

Figure 4.23: PCA: Differentiation of groups for HNO_3-treated samples (including UV+HNO_3) from report of Raman measurements Czech Academy of Science

The grouped and stacked spectra of native and 20 h UV aged PA and PET are shown in Figure 4.24. Similar to the previous measurements of PS, aging does not seem to influence the peaks distribution. However, changes in the background signal are visible (pristine samples have more "flat" background). To observe changes in peaks intensities, spectra of each polymer were normalized to their highest peak (1437 cm^{-1} for PA and 1615 cm^{-1} for PET) and aged spectra were subtracted from the pristine ones. That provided differential spectra of both polymers depicting spectral changes between aged and unaged samples.

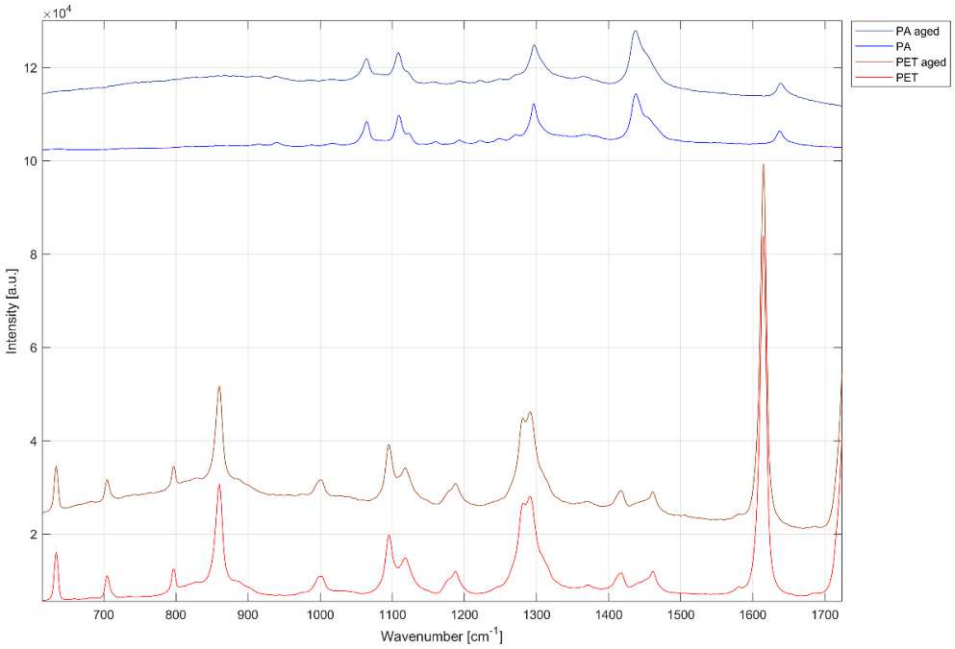

Figure 4.24: All spectra grouped, averaged, and stacked (PA, PET) from report of Raman measurements Czech Academy of Science

From the differential spectra (Figure 4.25) it looks like the PA sample degraded more as the resulting differences in peaks heights are much larger than with PET. This could be due to PETs larger hydrophobicity which could prevent it from damages caused by water.

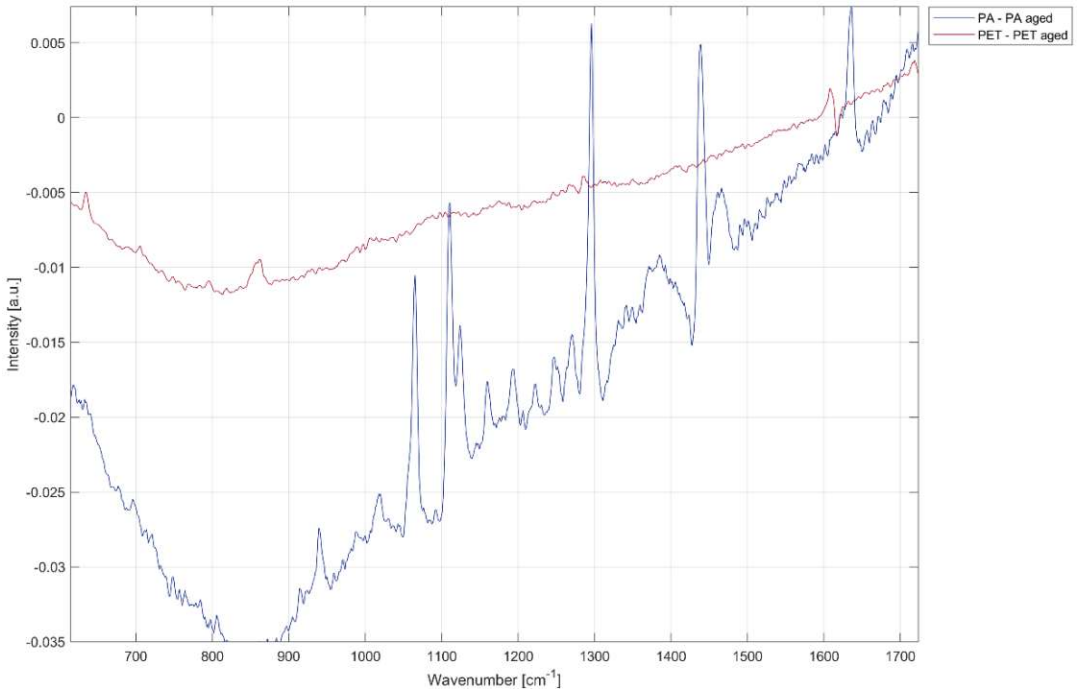

Figure 4.25: Differential spectra of PA and PET from report of Raman measurements Czech Academy of Science

Raman maps were used to show possible chemical changes (related to the degradation processes) within the particles. Line-scans were chosen to map the whole diameter of the particle (in case of PS it was only a part of the diameter because of their large size). All spectra for line-scans were smoothed and normalized at a significant peak of the polymer that the particles were fixed in (1453 cm-1 for PA and PET in acrylate, 824 cm-1 for PS in epoxy resin).

For PS there is reduced intensity of the main PS peak which corresponds to the results from the previous measurements.

For PA samples there is no visible difference in peaks progression through the particle except for different background levels inside and outside of the particle. Although, differential spectra from the middle area of the particles corresponded to the experiment with granules.

For PET particles, however, there seems to be a visible difference in the “steepness” in which the PET peaks appear and disappear when the line-scan enters or leaves the particle (Figure 4.26). This could either be from the damages of the particle being more severe towards the edges, or from the submerged part of the particle, if it is wider than the cross-section (this could lead to the polymer signal even behind the “edges” of the particle). The differential spectra of PET showed increased changes in peaks heights compared to the previous experiment.

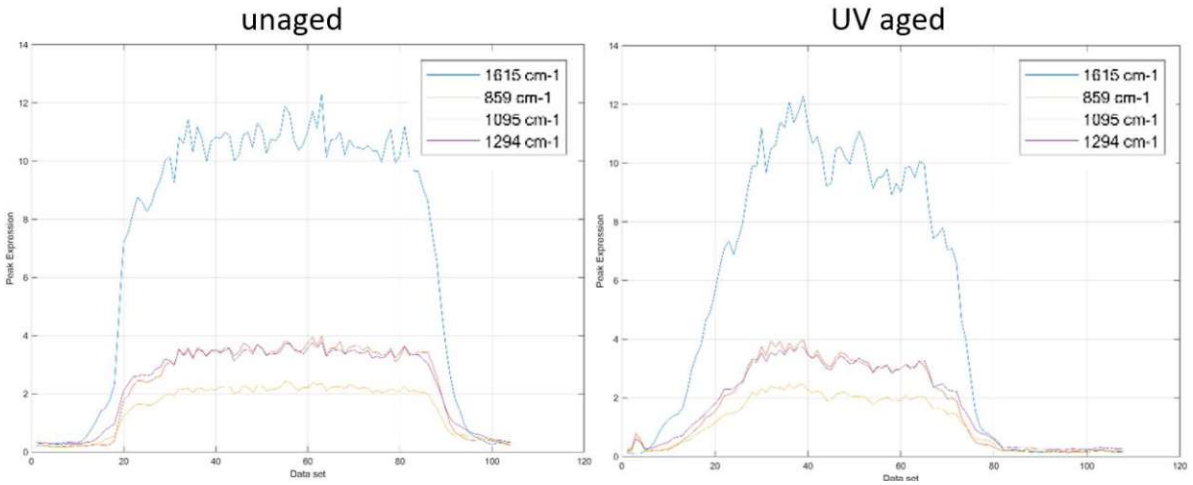

Figure 4.26: PET peaks intensities changes through the particle unaged and UV aged sample from report of Raman measurements Czech Academy of Science

For PVDC no report was provided, because of the high fluorescence in the spectra.

Using Raman spectroscopy for analysis of different aging processes on various polymers seems to be an interesting option with a lot of potential. The results suggest that chemically there are no obvious differences between pristine and aged samples (spectra show the same peaks), but the changes might be more physical (the peaks have decreased intensities). To clearly evaluate the possibilities of this method and establish the processes of the particles aging, more measurement is required.

4.1.6 LIBS

Because of the developing carbonyl band in PS, an increase of O in the polymer was expected and proved by measurements with LIBS. The following graphs show the results of the preliminary tests on aged PS samples. The aim was to explore if there are any detectable changes due to ageing procedures. Figure 4.27 shows three spectra of different PS samples measured with the broadband spectrometer. Only the section in which the H line and the O line can be found is shown, since the remaining area remained unchanged for the different samples and is therefore not relevant for the assessment. The emission line of H at 656 nm is visible, whereas the O emission line at 777 nm was not. Because of that, the O signal was detected with the more sensitive ICCD detector with a gain of 70, the obtained spectra are shown in Figure 4.28. The emission line for H decreases in the aged samples compared to the native.

The LIBS measurements were performed with 5 particles of each sample. The average and standard deviation were calculated out of these 5 particles and are shown in Figure 4.29 for the measurements of 0 h to 20 h UV irradiated PS samples. Figure 4.30 contains the results for the measurements of samples treated for two weeks with HNO_3 and H_2O_2. Both graphs contain the measured H signal at 655 nm and the with the ICCD monitored O signal at 777 nm, both were normalized to C at 193 nm. Originally the signals were given in cps. Later the signals were normalized to the laser energy. The high standard deviation is up to 35 % of the averages derives from the different sizes and the difficulties in focusing on the surface of the round particles. Also, other C bands especially the C2 fragment at 515 nm and C at 247 nm were monitored but did not show any change in the signal intensity so they were not used for discussion of the results.

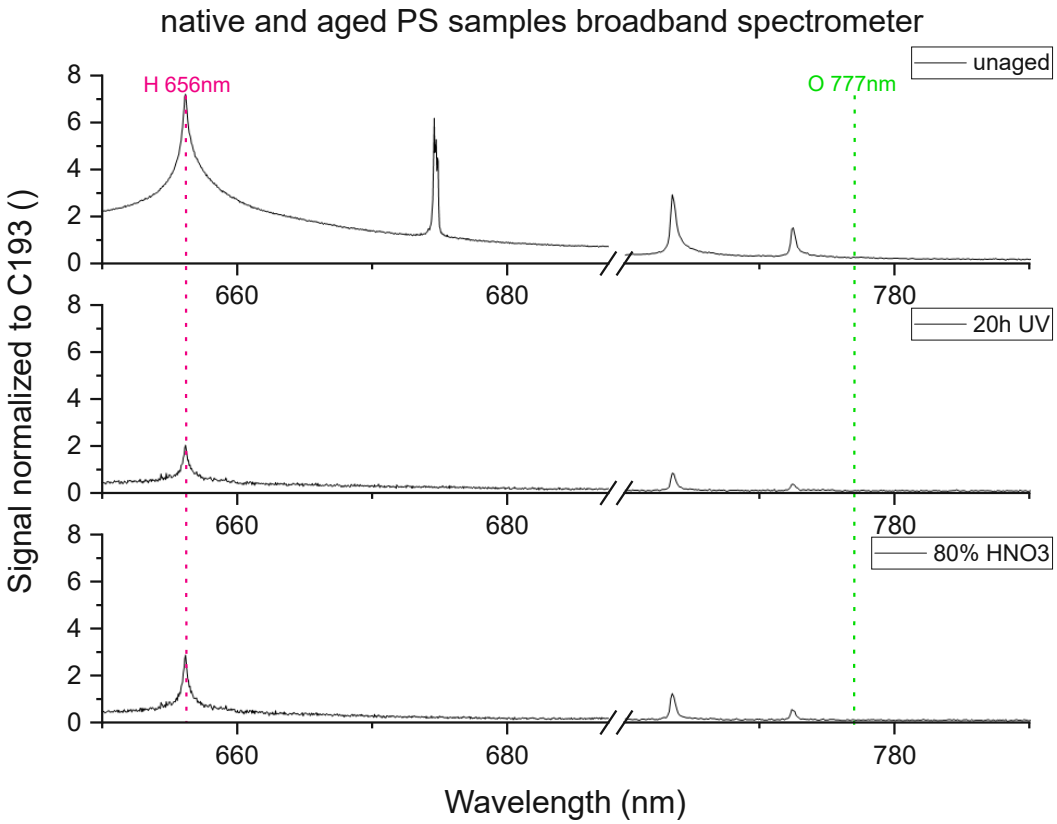

Figure 4.27: LIBS Spectra of a native, a 20 h UV aged and a two weeks in 80 Vol% HNO3 aged PS Sample, normalized to C193 measured with broadband spectrometer; H at 656 nm (pink) and O at 777 nm (green)

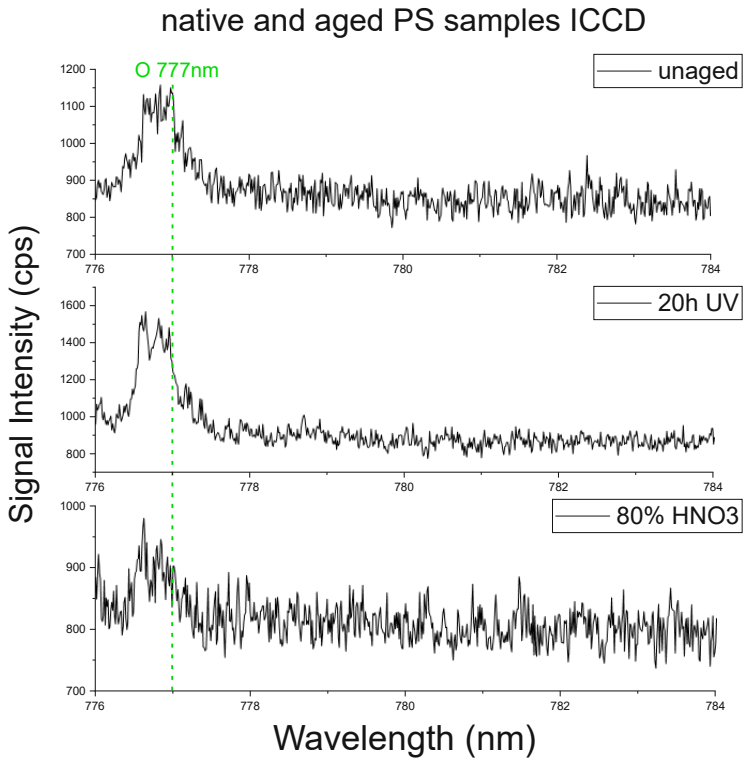

Figure 4.28: LIBS Spectra of a native, a 20 h UV aged and a two weeks in 80 Vol% HNO3 aged PS Sample normalized to laser energy measured with ICCD; O at 777 nm (green)

The H signal decreases, while the O signal increases with further ageing time (Figure 4.29). It becomes clear that changes are only noticeable after a certain irradiation time, as here from about 10 h. This knowledge was of great importance for further work.

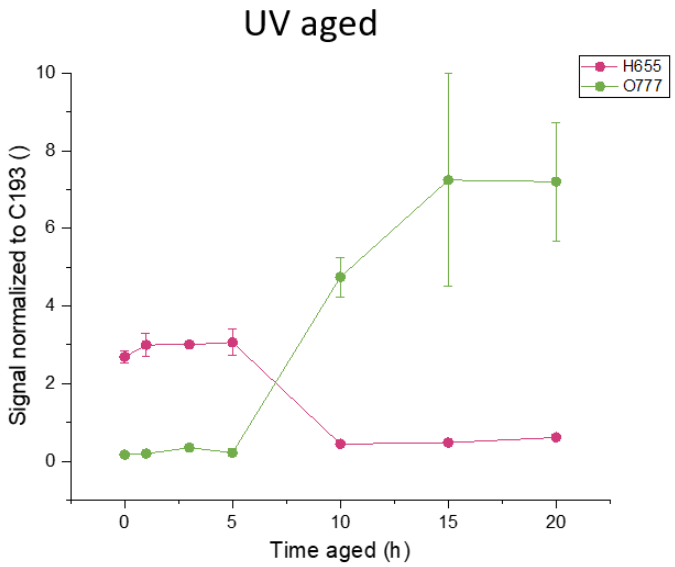

Figure 4.29: O at 777 nm detected with ICCD and H at 655 nm normalized to C at 193 nm and measured with LIBS broad band spectrometer from different UV irradiated PS samples

Figure 4.30 contains the HNO_3 and H_2O_2 treated PS samples. There was a drop in the H signal and an increase in the O signal to, but only in comparison to the unaged sample. the course is relatively constant between the aged samples. Only the sample treated with 80 Vol% HNO_3 shows a stronger increase in O, but there is also a higher standard deviation which should not be ignored.

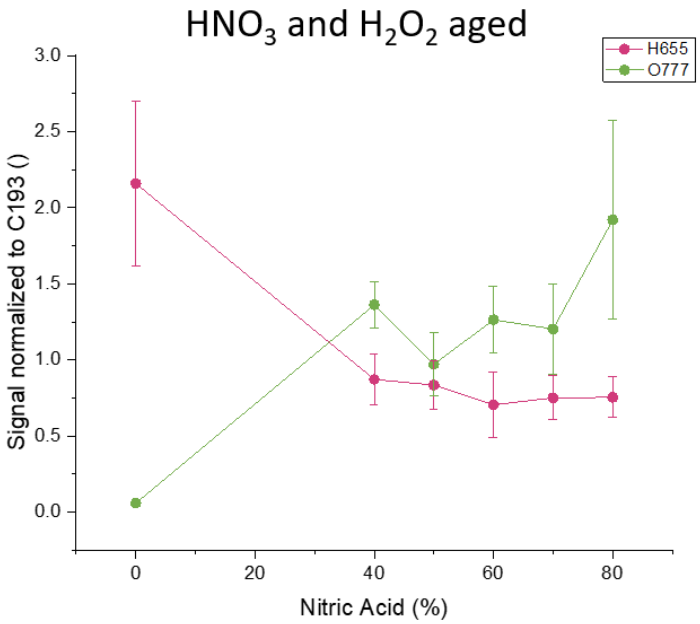

Figure 4.30: O at 777 nm detected with ICCD and H at 655 nm normalized to C at 193 nm and measured with LIBS broad band spectrometer from different with HNO_3 and H_2O_2 (5%) treated PS samples

The UV irradiated samples showed a stronger change in both signals, than the ones treated with oxidizing reagents.

4.1.7 He pycnometry

The results of the density measurements by He pycnometry are summarized in the following graphs. The influence on density at different aged PS samples is shown in Figure 4.31. A blue dashed line indicates the density of water at 20 °C. As already mentioned, different sink and swim behaviours of the particles were observed after the ageing procedure. So, the sample which was treated with UV irradiation and oxidizing reagents shows a decrease in density due to the ageing procedure and tends to swim in water. Because of the expanded particles and their small pores, the density measurement was not as reliable compared to the other measurements resulting in a higher standard deviation. The other aged samples had a comparable density close to the unaged native sample.

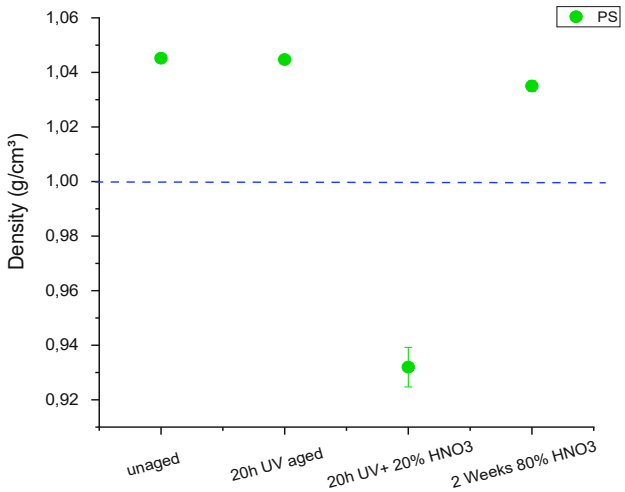

Figure 4.31: Results of He pycnometry of different aged PS samples (green) and density of water (blue dashed line)

Figure 4.32 contains the summary of density measurements of the four investigated polymers. Except PET none of the polymers show a clear trend in density change, so more measurements at different irradiation times are required. The density of PET seems to increase with further irradiation time but needs also further analysis at longer ageing times to probe this observation.

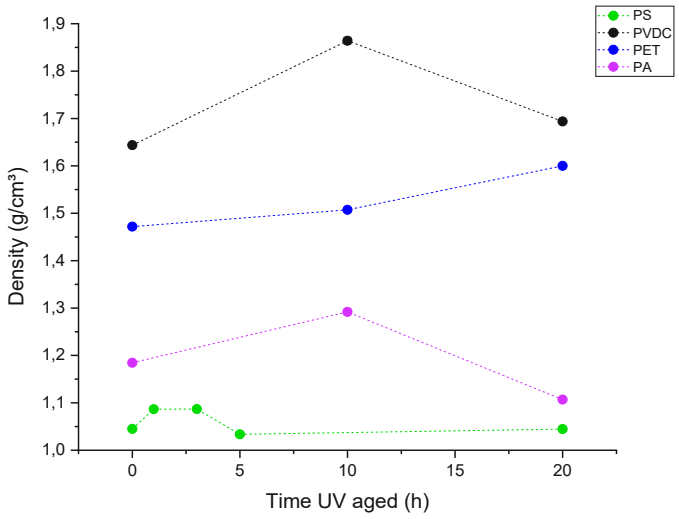

Figure 4.32: Results of He pycnometry of different UV irradiated polymer samples; PS (green); PVDC (black), PET (blue); PA (purple)

Generally, density measurements of porous particles are particularly difficult. Even though the standard deviation of the measurements is low. Due to the different flow velocities of the He in and out of the pores it comes to greater differences between the measurements, and it takes more time to reach the equilibrium.

4.2 Uptake and release of trace elements

In the following chapter the results of liquid sampling analysis with ICP-MS, solid sampling measurements for spatially resolved analysis with LA-ICP-MS and LIBS for the investigated polymers are discussed.

4.2.1 Liquid sampling with ICP-MS

4.2.1.1 Leaching of additives

In the following chapter the leaching of additives contained in the investigated polymers is discussed.

Figure 4.33 shows the release behaviour of the additives in the PS. To see changes due to the ageing procedure the measured additives Al, Ti and Zn are shown in comparison for the unaged native sample and the 20h UV aged sample. It is apparent that Zn as well as Al was washed. Ti content was not affected by the treatment.

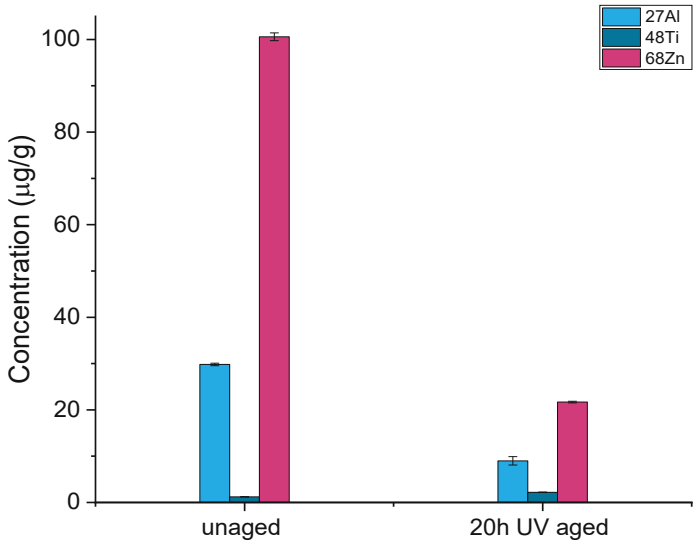

Figure 4.33: Liquid bulk analysis from unaged and UV irradiated unspiked PS samples

In contrast to the results for the material change, the bulk analysis of PA showed a difference before and after ageing. Figure 4.34 exhibits the outcome of this analysis for the additive release in native versus UV irradiated samples. All four detected elements show a decrease in content after the ageing procedure.

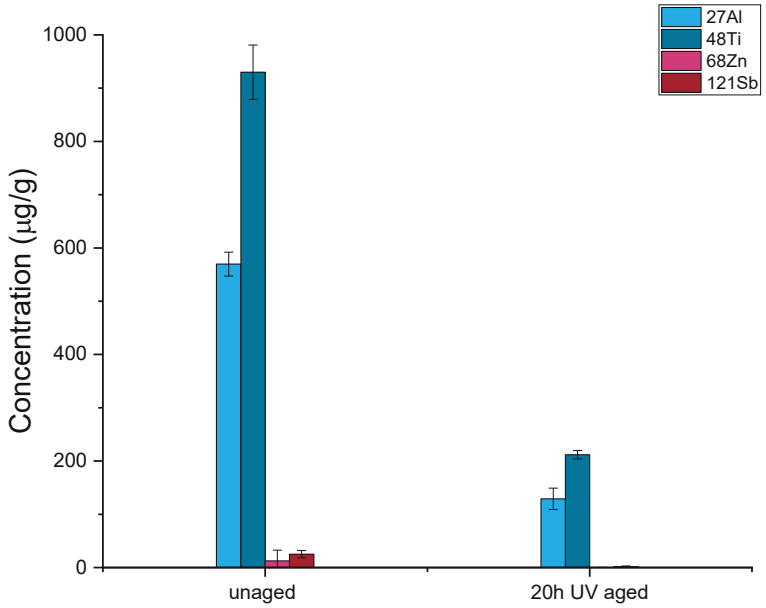

Figure 4.34: Liquid bulk analysis from unaged and UV irradiated unspiked PA samples

Figure 4.35 presents the results of the release of trace elements by analysis of the liquid bulk measurements of unaged and aged PET samples. The impact of the alteration is little compared to the native sample. The contained additives show a small decrease in concentration.

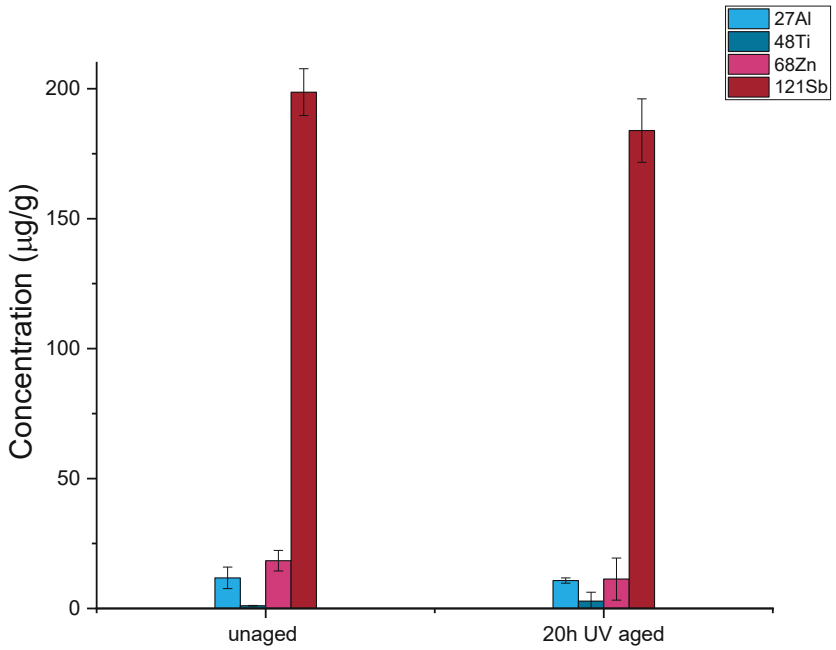

Figure 4.35: Liquid bulk analysis from unaged and UV irradiated unspiked PET samples

The results of the liquid bulk measurements from leaching of PVDC samples shown in Figure 4.36. PVDC clearly shows an uptake of Al. This was not expected, and may is a evidence for the inhomogeneous distribution in the particles and points the difference between the individual particles out. The other supposed elements are only in a small quantity included.

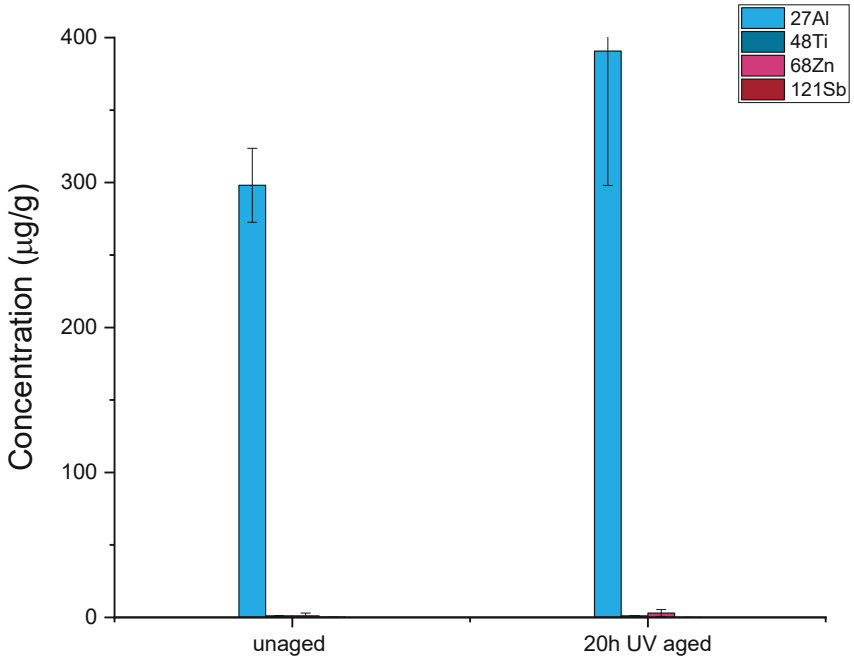

Figure 4.36: Liquid bulk analysis from unaged and UV irradiated unspiked PVDC samples

All polymers except PVDC show leaching of additives after ageing. The effect was different for the individual elements and each polymer. PS showed molecular changes after degradation and a strong leaching effect especially for Zn. Whereas PA showed only small molecular changes after degradation, but a strong leaching effect of every additive.

4.2.1.2 Adsorption of trace elements

The following chapter contains the results of the adsorption experiments of the investigated polymers.

Figure 4.37 shows changes in the elemental composition caused by exposure to artificial seawater spiked with various metals. The native samples do not contain any of the spiked elements as it was expected. The unaged spiked sample did show a small uptake of Pb and a higher uptake of Cd. The aged, spiked sample showed a much higher uptake of Pb than the unaged one whereas Cd showed similar behaviour. Therefore, its uptake is not depended on the ageing procedure. Results for other elements can be found in the appendix under Figure A. 1. For example, for Sb the uptake in PS was always under the LOD.

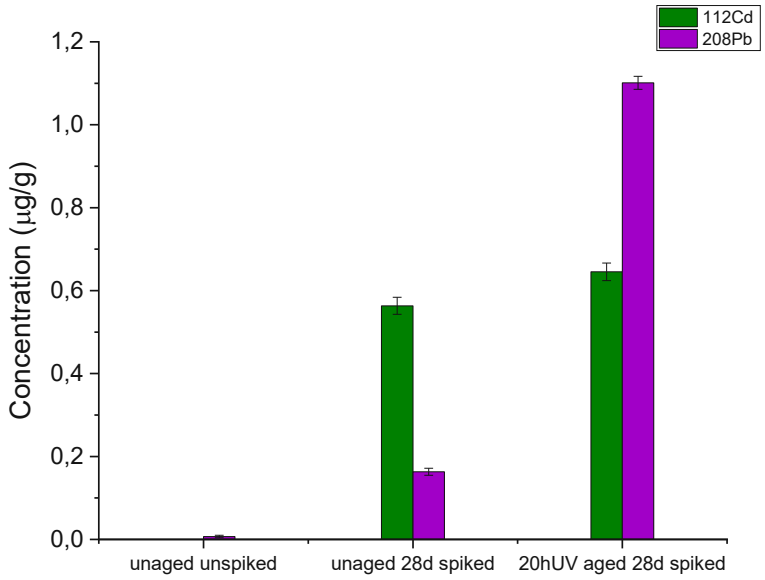

Figure 4.37: Liquid bulk analysis from unaged unspiked, unaged spiked and UV irradiated aged and spiked PS samples

Figure 4.38 contains the results for the uptake of trace elements in PA. It was revealed that Pb must be already contained in the native sample. This contradicts to the results of the survey run but may is a result of the different detection conditions. A second option is that the samples were contaminated during the handling. And the added Pb was decreasing during the spiking and ageing procedure. To anticipate, also the results of the depth profiles and images show a detectable Pb content in the native samples. The same is observed for Ni and Sb, which were decreasing slightly due to the treatment. The analytes Cd, Nd and Th were slightly increasing because of the treatment methods.

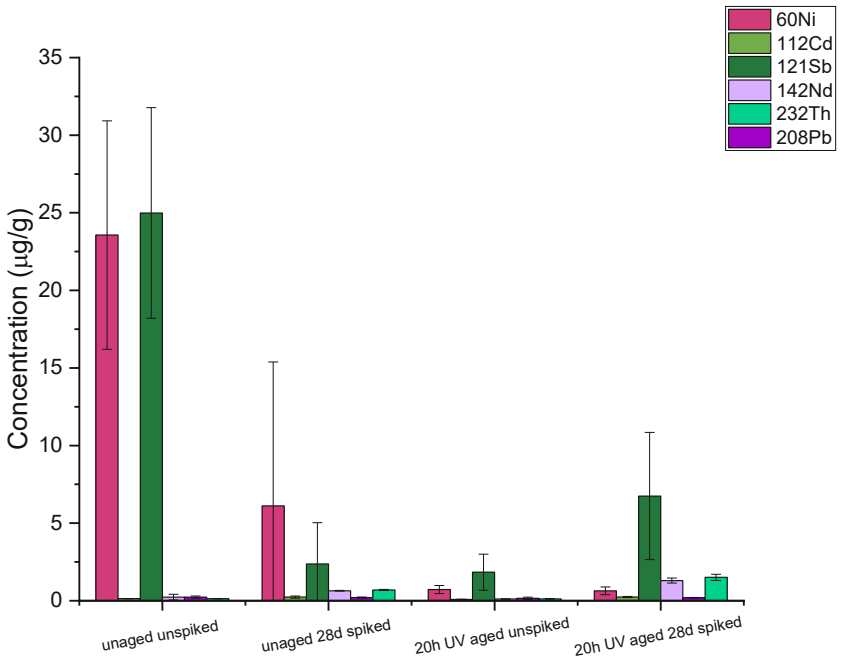

Figure 4.38: Liquid bulk analysis from unaged unspiked, unaged spiked and UV irradiated aged and spiked PA samples

Figure 4.39 presents the results of the uptake behaviour after treatment with UV radiation and artificial seawater. The native sample seems to contain Pb which was not expected. The remaining four added trace elements seem also to be contained in the native sample, but in a much smaller range. It is visible that the concentration of these elements is increasing due to the spiking and especially in combination with the ageing procedure. It is remarkable that the uptake behaviour is different for every added element. Th for example showed a higher uptake than the other elements.

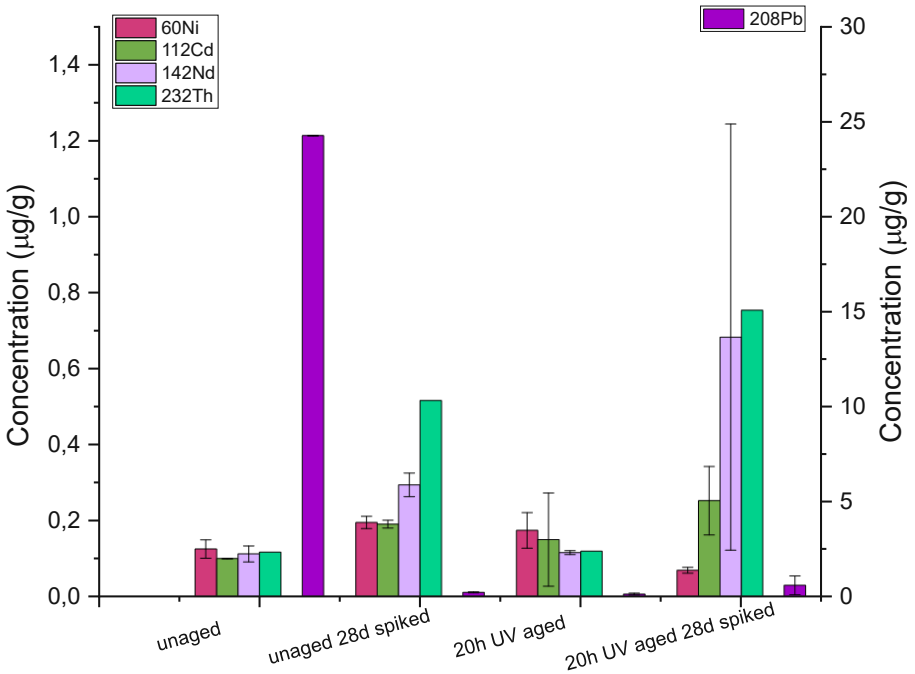

Figure 4.39: Liquid bulk analysis from unaged unspiked, unaged spiked and UV irradiated aged and spiked PET samples; left y-axis for Ni, Cd, Nd and Th; right y-axis for Pb

Figure 4.40 contributes the uptake of different trace elements in PVDC. It is clear to see that the uptake is dependent on the element itself. Thus, Cd showed the same uptake behaviour for the native and the aged samples. The same was for Th and Ni. For the selected elements the ageing procedure did not cause an increase in uptake of the trace elements.

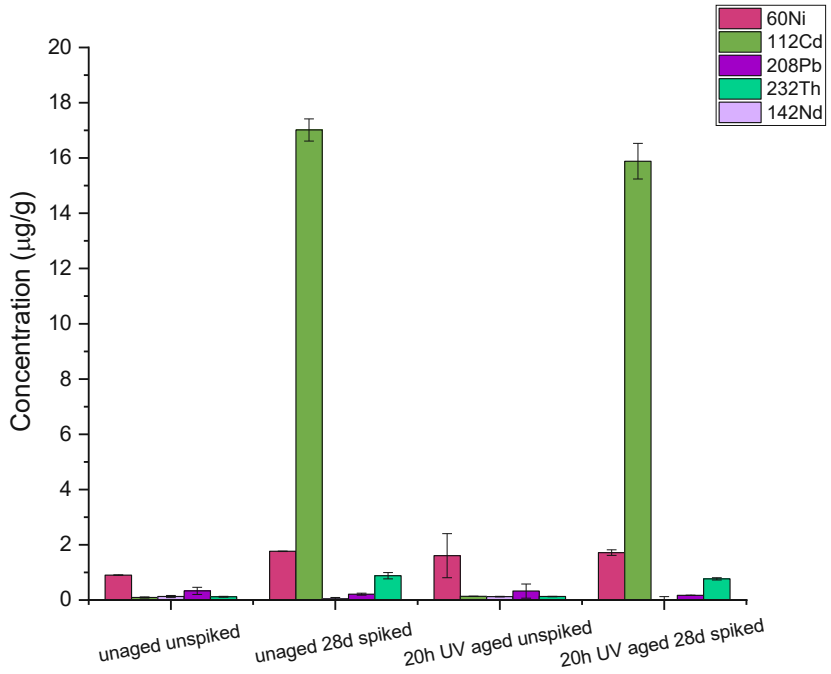

Figure 4.40: Liquid bulk analysis from unaged unspiked, unaged spiked and UV irradiated aged and spiked PVDC samples

An uptake due to ageing procedure was clearly to see for PS and PET. PA and PVDC did not show an uptake for the investigated elements.

4.2.2 Solid sampling with LA-ICP-MS – Imaging

In the following sections images of the four investigated polymers were discussed.

4.2.2.1 PS

The following images show cross sections from different treated PS samples embedded in acryl resin described in 3.2.3.2. At first the images were performed with samples embedded in epoxy resin. The long hardening time of 12 h enables the diffusion of the elements out of the particles into the resin, the images of these samples are found in the appendix Figure A. 2. Therefore, the experiment was repeated by using acryl resin which has a hardening time of 20 min which led to less diffusion of the trace elements. The resulting figures are discussed in the following part. The scale range for Zn/Pb is the same in all pictures. The other detected isotope distributions ^{27}Al and ^{121}Sb are found in the appendix in Figure A. 3.

Figure 4.41 shows the distribution of Zn and Pb in PS cross sections from unaged unspiked and spiked particles. Compared to the particles in epoxy resin which can be found in the appendix, less diffusion of the Zn in the embedding material happened. The circles in the pictures imply the particles contour. It is visible, that there is an enrichment in the outer regions of the particles ((a) and (b)). These seems a bit strange in accordance it is an additive. But it was proven later by depth profile analysis.
(c) confirms that there is no Pb neither in the native PS samples nor in the embedding material. It is evident that some of the Zn was washed out after the seawater treatment, and some Pb was taken up ((b) and (d)). Even though the acrylic resin has a hardening time of only 20 min it is obvious that some of the (trace) metals present in the particle diffused into the embedding material during hardening.

Therefore, the elemental distribution within the particles is difficult to assess but the results still strongly indicate uptake of Pb and release of Zn during the spiking procedure. The smaller dots outside of the bigger circles are from the resin, and do not have to be considered.

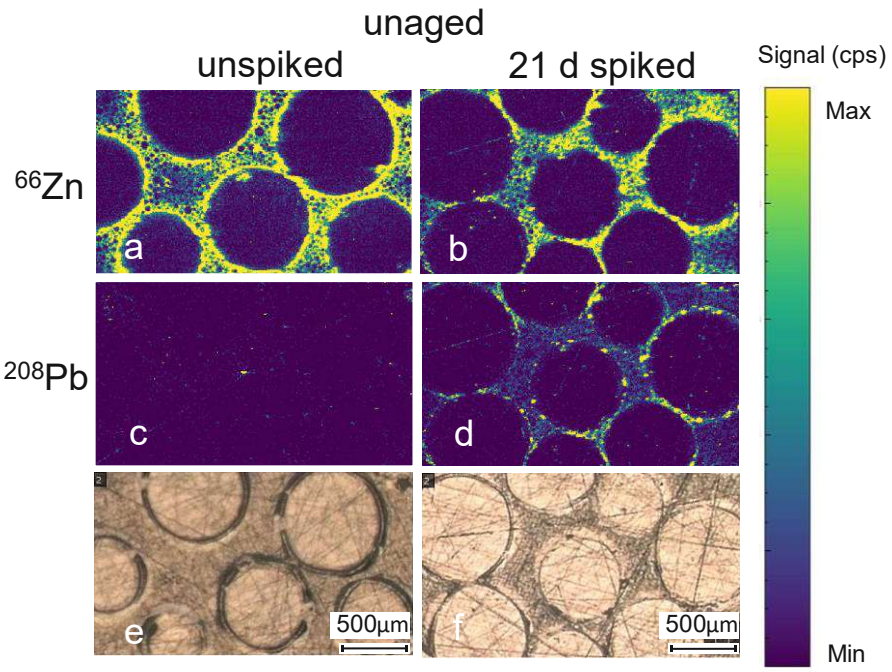

Figure 4.41: unaged unspiked and spiked PS particles embedded in acryl resin; (a) 66Zn distribution in unspiked PS (b) 66Zn distribution 21 d spiked PS (c) 208Pb distribution in unspiked PS (d) 208Pb distribution in 21 d spiked PS particles (e) microscope picture unspiked PS particles (f) microscope picture 21 d spiked PS particles

The following Figure 4.42 delineate the behaviour of 20 h UV irradiated PS samples. The UV treated samples are supposed to be contaminated with Pb, so the unspiked samples already contain Pb. However, the uptake was increased by the spiking procedure and even more because of the ageing.

Furthermore, the acryl resin seems to react with the UV aged samples, visible by the uneven contour of the particles, compared to the unaged samples and the in-epoxy resin embedded particles. The individual particles were also investigated with a microscope and there were no changes visible on the single particles. Therefore, these changes must come from the reaction with the acryl resin.

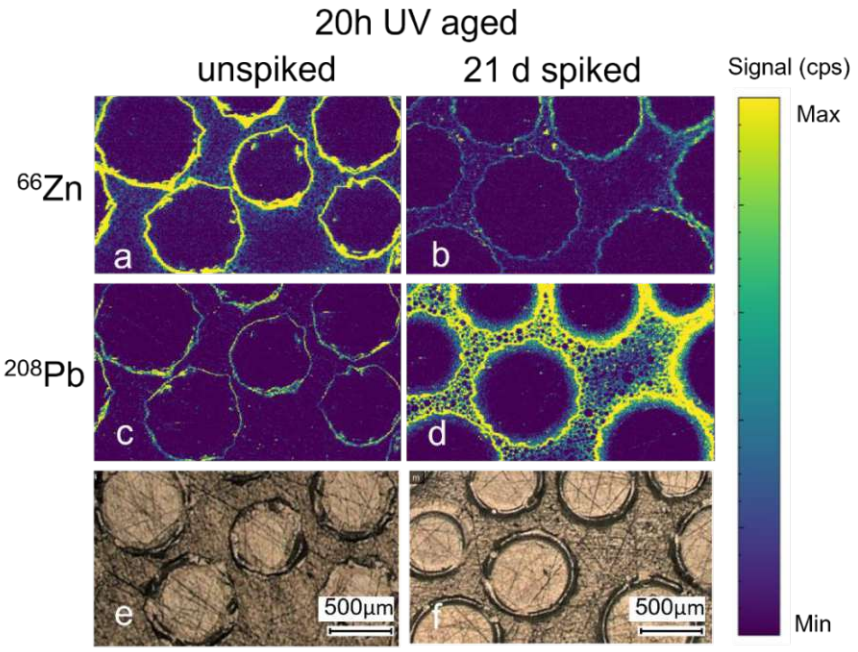

Figure 4.42: 20 h UV aged unspiked and spiked PS particles embedded in acryl resin; (a) 66Zn distribution in unspiked PS (b) 66Zn distribution 21 d spiked PS (c) 208Pb distribution in unspiked PS (d) 208Pb distribution in 21 d spiked PS particles (e) microscope picture unspiked PS particles (f) microscope picture 21 d spiked PS particles

The following picture shows PS samples treated for two weeks with 80% HNO_3 and 5% H_2O_2 (Figure 4.43). (a) and (c) show that there is no Zn left in the aged particles. Only the spiked and aged sample (d) contains some Pb. This means that the acid treatment leads to complete wash out of the additive Zn. In the appendix are also the images of Al and Sb found. Al was not washed out completely, although the concentration of Zn is much higher in the native samples. Also, this ageing treatment led to an increase in uptake of trace elements like Pb and Sb (Figure A. 3).

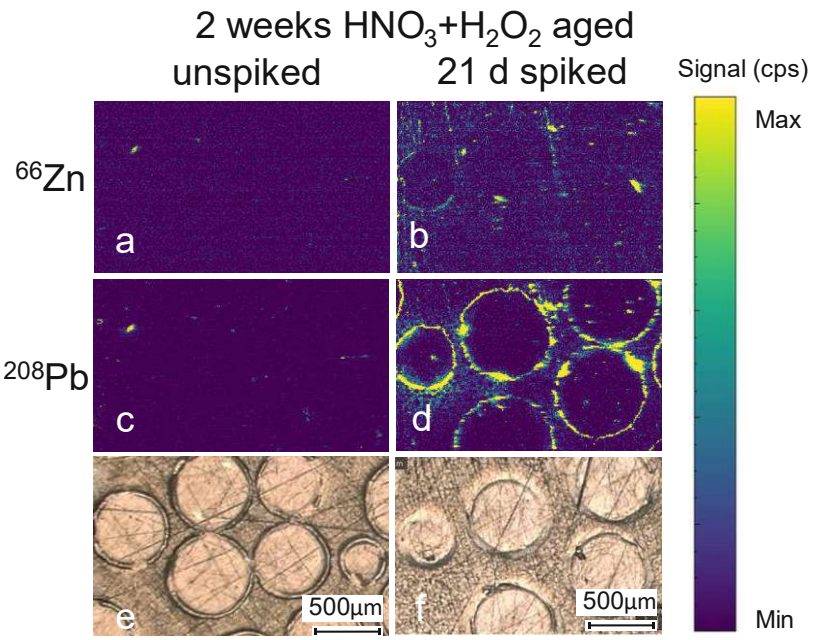

Figure 4.43: two weeks 80% HNO_3 and 5% H_2O_2 aged unspiked and spiked PS particles embedded in acryl resin; (a) 66Zn distribution in unspiked PS (b) 66Zn distribution 21 d spiked PS (c) 208Pb distribution in unspiked PS (d) 208Pb distribution in 21 d spiked PS particles (e) microscope picture unspiked PS particles (f) microscope picture 21 d spiked PS particles

Comparing Figure 4.41 (b), Figure 4.42 (b) and Figure 4.43 (b) it can be concluded that Zn is easier washed from the particles during the soaking procedure when the particles are previously aged and more after leaching in HNO_3 and H_2O_2 than after UV irradiation. Additionally, comparing Figure 4.41 (d) and Figure 4.42(d) a significantly increased uptake of Pb in aged samples was observed.

Figure 4.44 and Figure 4.45 illustrate the O, Zn and Pb distribution in PS particle cross sections embedded in acryl resin, investigated with LIBS and LA-ICP-MS as tandem. To avoid effects on the elemental distribution caused by sample preparation, preablation was carried out removing the surface layer. For qualitative evaluation the scale range for O/Zn/Pb was the same in both pictures discussed further.

Figure 4.44 is the unaged unspiked sample. The distribution of the analytes is illustrated as image stack, constructed with ImageLab. Because the alignment of the microscope picture with the measured data is not perfect, the circles built from the analytes is slightly displaced from the particle cross section. The lines on the microscope picture are from the ablation. O (yellow) is mostly found in the acrylic resin. The unaged unspiked sample contains a lot of Zn (blue) which is similar to the findings presented in the previous section. Also, the diffusion of the additive is well seen. As expected only minor amounts of Pb (red) were found in the particles, which are not visible in this scale range.

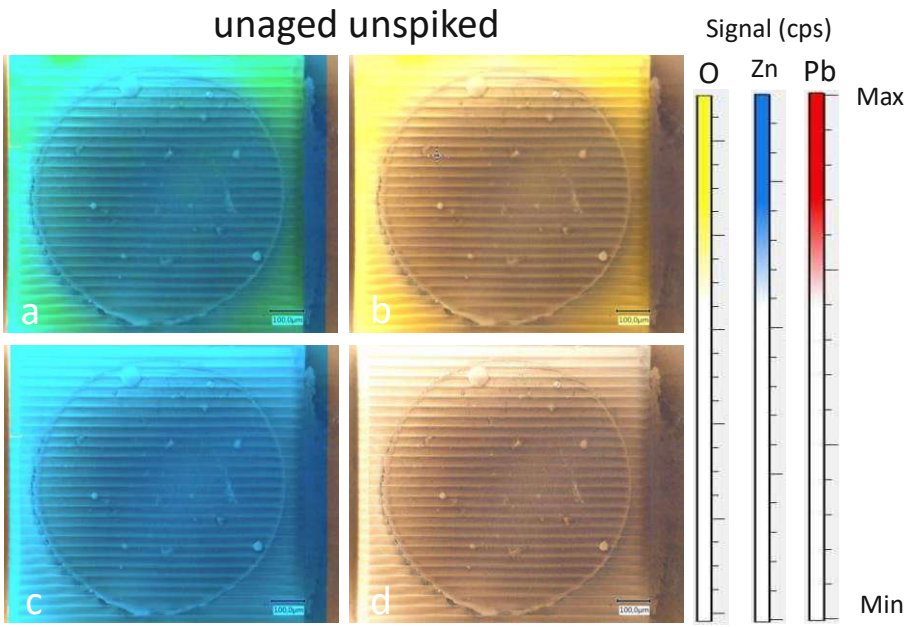

Figure 4.44: Image stacks of O, Zn and Pb on microscope picture of an unaged unspiked PS particle cross section and scales of O (yellow), Zn (blue), Pb (red) (a) Image stack with O, Zn and Pb (b) Image stack with O (c) Image stack with Zn (d) Image stack with Pb

Compared to the native sample, the 20 h UV irradiated and 21 d spiked sample (Figure 4.45) less Zn was left in the particle (c) and less diffusion took place in the embedding material. The O distribution seems to be nearly the same (b). The particle showed a remarkable Pb uptake (d).

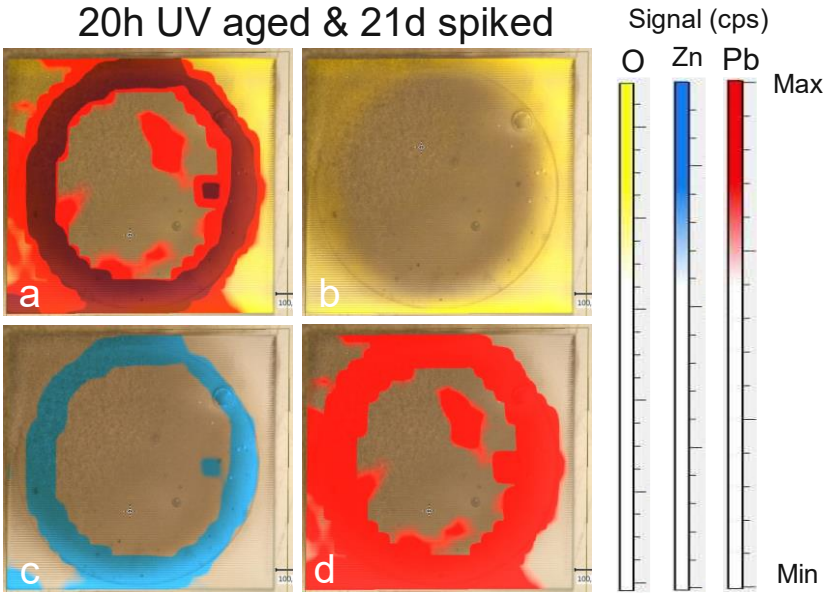

Figure 4.45: Image stacks of O, Zn and Pb on microscope picture of an 20 h UV aged 21 d spiked PS particle cross section and scales of O (yellow), Zn (blue), Pb (red) (a) Image stack with O, Zn and Pb (b) Image stack with O (c) Image stack with Zn (d) Image stack with Pb

The problem with tandem image measurements of O and trace elements simultaneously, was to find the right compromise between an adequate O signal and spatially resolution of the image. The poor sensitivity of LIBS compared with the MS systems leads to lack of signal intensity of O. The inner of the particles contained less O than the resin. To reach higher signals a greater beam diameter had to be chosen, this comes to bear the resolution. It follows that it is harder to tell where the particle ends and where the resin starts. This limits also the minimal possible size of particles that can be imaged. This is the reason why, the other samples with smaller particle size were not imaged in tandem mode.

4.2.2.2 PA

Imaging of the PA samples was particularly challenging. While polishing it was hard to determine, if the particles were already free from embedding material, because of the small size of 30 to 250 µm and the light colour. This procedure was done multiple times to get better results. This explains the poor resolution of the images (Figure 4.46 and Figure 4.47).

Images of the unaged unspiked and spiked PA samples are shown in Figure 4.46 (a) shows the distribution of Al in the native sample. Compared with the spiked sample in (b) is no clear difference visible. The images for Sb in the unspiked samples (c) fits with the results of the liquid measurements. According to the survey run, there shouldn't be any Sb in the native samples. However, the results of the images agree with the results from the bulk analysis of the native samples. Both, the unspiked and spiked sample contain Sb (c) and (d)). As already mentioned, it is hard to discern single particles on the images. This might come from remaining embedding material on the particles or the small particle size.

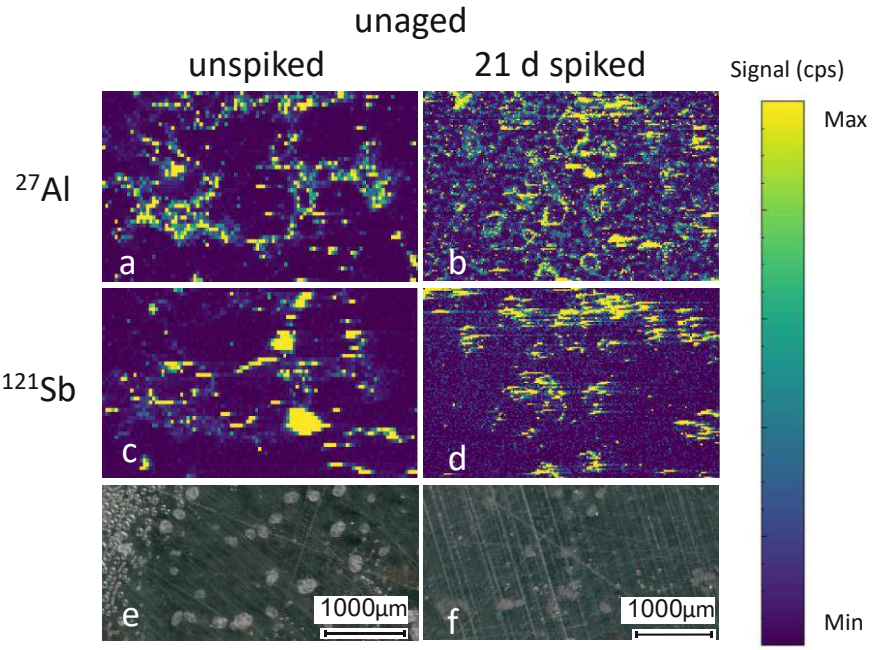

Figure 4.46: unaged unspiked and spiked PA particles embedded in acryl resin; (a) 27Al distribution in unspiked PA (b) 27Al distribution 21 d spiked PA (c) 121Sb distribution in unspiked PA (d) 121Sb distribution in 21 d spiked PA particles (e) microscope picture unspiked PA particles (f) microscope picture 21 d spiked PA particles

The aged unspiked and spiked PA samples (Figure 4.47 (a) and (b)) seem to contain a bit less Al in the native sample. Also, Sb seems to stay the same before and after the spiking procedure ((c) and (d)). Because of the results of liquid ICP-MS analysis, it is known that there were almost no changes in the polymer, so it was expected that also in the images, will be only a few changes.

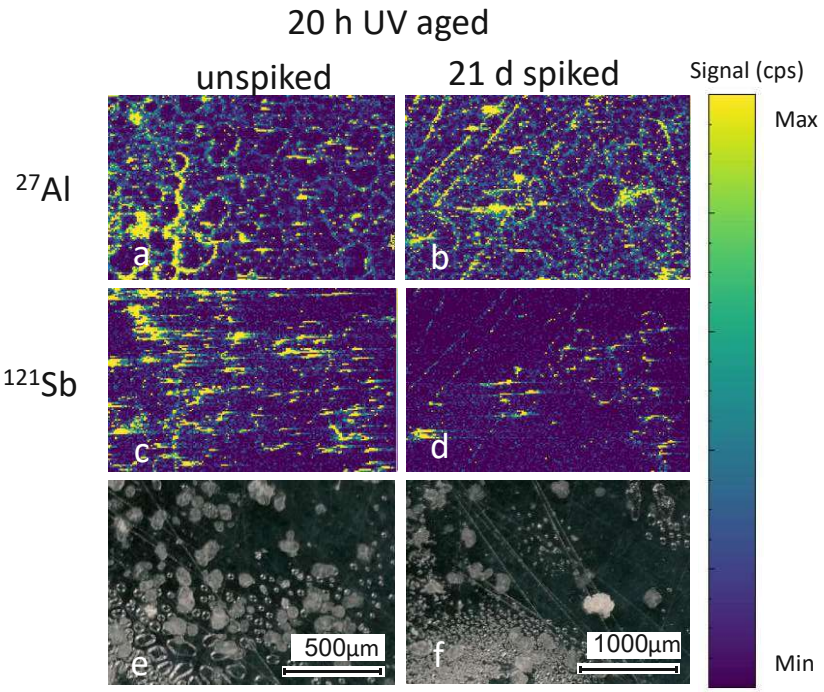

Figure 4.47: 20 h UV aged unspiked and spiked PA particles embedded in acryl resin; (a) 27Al distribution in unspiked PA (b) 27Al distribution 21 d spiked PA (c) 121Sb distribution in unspiked PA (d) 121Sb distribution in 21 d spiked PA particles (e) microscope picture unspiked PA particles (f) microscope picture 21 d spiked PA particles

In the appendix (Figure A. 4) the remaining investigated element images are found. Zn and Pb should be additives according to the survey run, and Cd was another spiked element. The remaining additives showed the same behaviour as Al. No uptake of Cd was observed.

4.2.2.3 PET

In the following part the results of the images of PET samples are discussed (Figure 4.48 and Figure 4.49). Sb acts as an additive in PET and is not washed out during the spiking process ((a) and (b)). Visible is also the homogenous distribution of the additive in the polymer cross section, in contrary to PS, where the additives are accumulated in the outer layers of the polymers. The unaged sample adsorbed only small amounts of Pb ((c) and (d). The particles are a bit larger than the PA particles and have an opaque look. Compared to the microscope pictures the images show less particles. This might come from the different height in the embedding material, so, the remaining particles are deeper than the particles on the images.

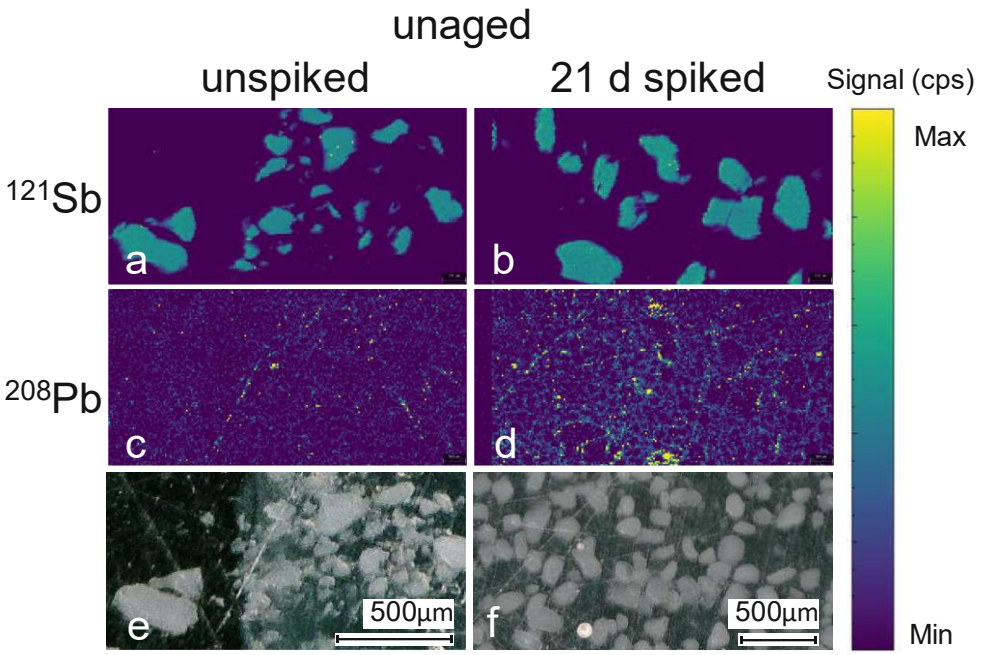

Figure 4.48: unaged unspiked and spiked PET particles embedded in acryl resin; (a) 121Sb distribution in unspiked PET (b) 121Sb distribution 21 d spiked PET (c) 208Pb distribution in unspiked PET (d) 208Pb distribution in 21 d spiked PET particles (e) microscope picture unspiked PET particles (f) microscope picture 21 d spiked PET particles

The aged unspiked and spiked PET particles are seen in Figure 4.49. In contrast to PS, PET also does not seem to lose additives during the ageing process ((a) and (b)). But it also shows a stronger uptake for Pb in the aged sample ((c) and (d)).

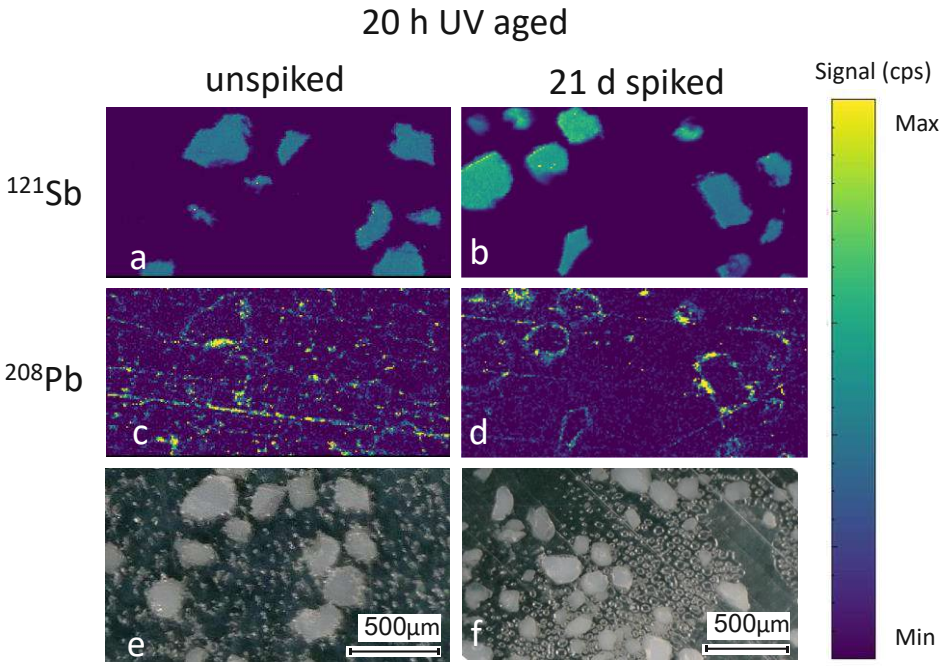

Figure 4.49: 20 h UV aged unspiked and spiked PET particles embedded in acryl resin; (a) 121Sb distribution in unspiked PET (b) 121Sb distribution 21 d spiked PET (c) 208Pb distribution in unspiked PET (d) 208Pb distribution in 21 d spiked PET particles (e) microscope picture unspiked PET particles (f) microscope picture 21 d spiked PET particles

Al was another additive contained in the polymer. Zn and Cd were both spiked. The images of these three elements are found in the appendix in Figure A. 5. Al is contained in much lower concentrations and did not show that much change. Only the aged and spiked sample containing a lot more Al, but this might come from contaminations. The PET samples generally have more deeper scratches from the polishing, which are also visible as lines in the images. The uptake for Zn and Cd in unaged and aged PET samples was not remarkable and proves the dependence from the element itself.

4.2.2.4 PVDC

The images of unaged unspiked and spiked particles are shown in Figure 4.50. (a) and (b) visualize an inhomogeneous distribution of the additive Al. This impression can also be caused by the uneven surface. (b) suggests that the spiking procedure does not influence the wash out of Al. The native sample did not show an uptake of Cd in the images (c) and (d). this contradicts the results of the bulk analyses, were PVDC samples unaged and aged, both showed a higher uptake of Cd independent from the ageing procedure.

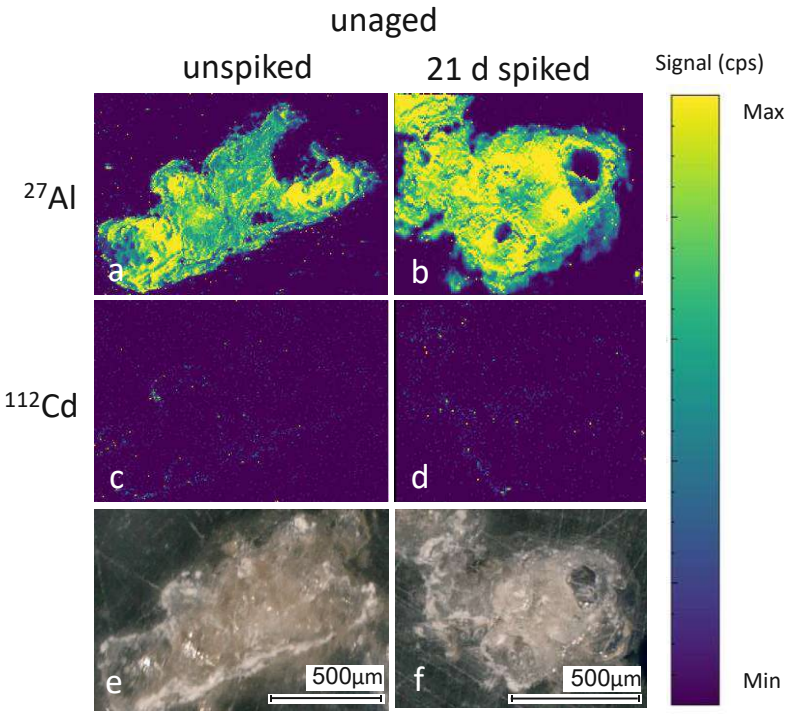

Figure 4.50: unaged unspiked and spiked PVDC particles embedded in acryl resin; (a) 27Al *distribution in unspiked PVDC (b)* 27Al *distribution 21 d spiked PVDC (c)* 112Cd *distribution in unspiked PVDC (d)* 112Cd *distribution in 21 d spiked* PVDC *particles (e) microscope picture unspiked* PVDC *particles (f) microscope picture 21 d spiked* PVDC *particles*

The aged unspiked and spiked PVDC samples are shown in Figure 4.51. The combination of the images with the microscope pictures reveal which parts of the polymers are still enclosed from embedding material and which are free. In the microscope pictures (e) and (f) the lighter areas are free from acryl resin and visible in the images. This differentiation was easier with aged PVDC because of the darker colour of the particles. The aged and spiked particle seems like it had lost some additive if (b) compared with (a). But this might come from the inhomogeneity in distribution and surface. The images of Cd for the aged PVDC particles contradict the results from the bulk analysis too. The uptake of Cd was not increasing due to the ageing procedure (c) and (d).

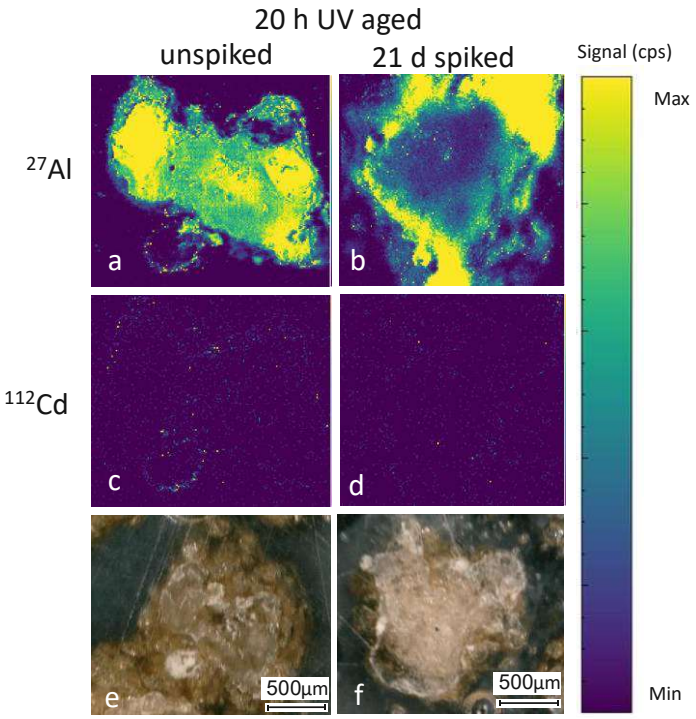

Figure 4.51: 20 h UV aged unspiked and spiked PVDC particles embedded in acryl resin; (a) 27Al *distribution in unspiked PVDC (b)* 27Al *distribution 21 d spiked PVDC (c)* 112Cd *distribution in unspiked PVDC (d)* 112Cd *distribution in 21 d spiked* PVDC *particles (e) microscope picture unspiked* PVDC *particles (f) microscope picture 21 d spiked* PVDC *particles*

The fact that the uptake of Cd was seen in the bulk analysis but not in the images is remarkable. A reason could be that the enrichment of the trace element only happened on the surface or respectively in a thin outer layer of the particles, which was removed due to the polishing.
The remaining detected elements are found in the appendix from in Figure A. 6. Pb and Zn were both already contained in the unaged unspiked particles, whereby these two elements should be contained according to the survey run. Sb was a second spiked element and shows the exact same behaviour as Cd.

4.2.3 Solid sampling with ICP-MS and LIBS Tandem – Depth profiles

4.2.3.1 PS

Figure 4.52 till Figure 4.54 show depth profiles of O signal at 777 nm detected with an ICCD Detector LIBS system and normalized Intensity of ^{68}Zn and ^{208}Pb to ^{13}C analysed with LA-ICP-MS from different treated PS samples. The measurements were performed as Tandem. Compared are unaged unspiked and spiked samples, UV irradiated unspiked and spiked samples and PS particles which were treated for two weeks with 80% HNO_3 and 5% H_2O_2. The depth of the layers was approximately determined with dektak (DektakXT, Bruker, Massachusetts, USA) measurements on the embedded particles. Therefore, a pattern with the same parameters as for depth profile analysis of single particles was ablated on the embedded samples and the crater depth was determined depth profile analysed.

The O signal (Figure 4.52) shows a clear difference in the UV aged samples compared to the unaged and acid aged samples. Both UV aged samples show a higher O content in the outer layers, which is decreasing the further inside it was measured till it reaches a constant level at about 1000 nm depth. The other PS samples have nearly the same O content from the edge to the inner side.

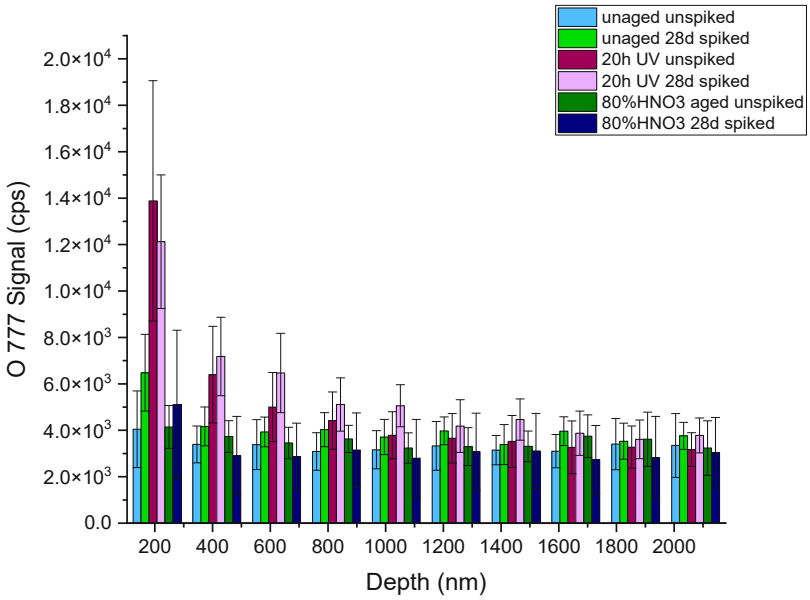

Figure 4.52: Depth profiles O at 777 nm LIBS from different treated PS samples

Considering the distribution of the Zn (Figure 4.53) in different layers it is obvious that it is washed out, because of the different used treatment methods. Only the unaged unspiked sample contains significant amounts of Zn which is enriched in the outer layers of the particles. This knowledge coincides with that of the recorded elemental maps.

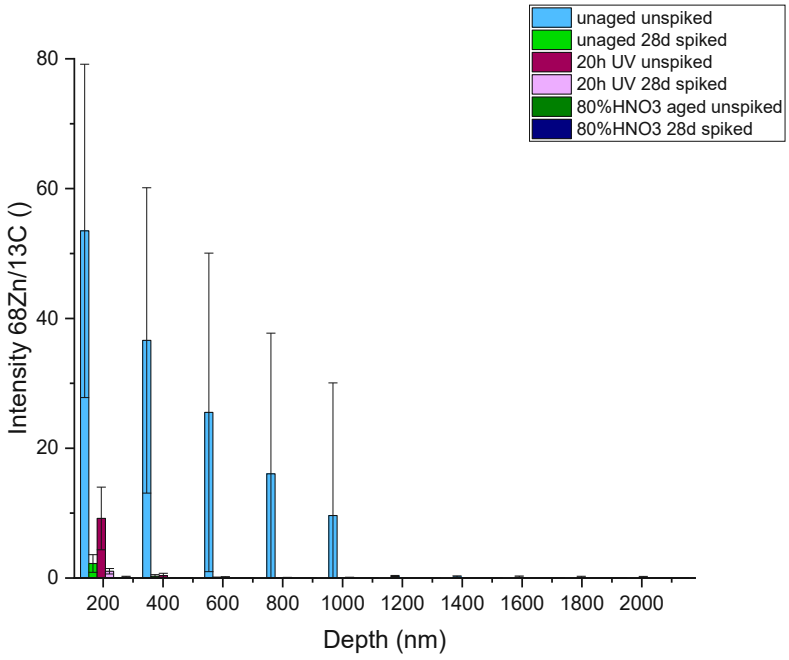

Figure 4.53: Depth profiles normalized 68Zn to 13C LA-ICP-MS from different treated PS samples

Figure 4.54 shows the distribution of Pb in the particles. As before Pb is concentrated in the outer layers and did not penetrate deep into the particles. The aged samples showed increased Pb uptake compared to the unaged sample. It is particularly striking that the UV-treated showed the largest uptake.

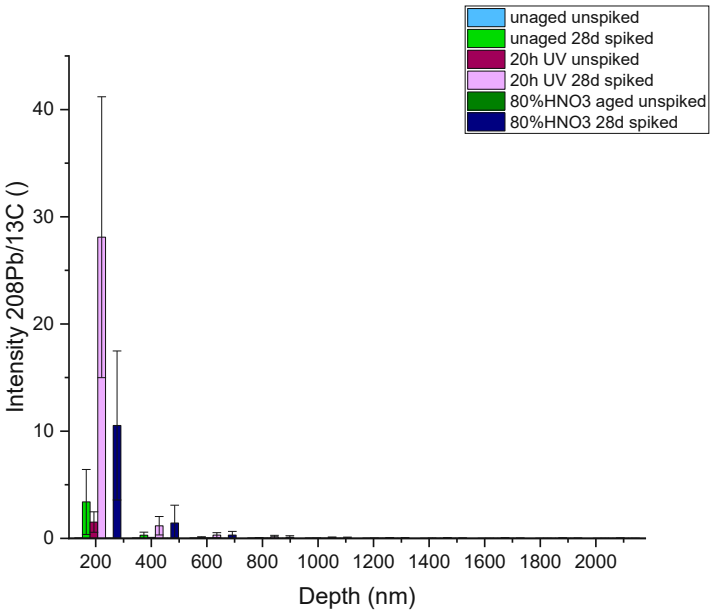

Figure 4.54: Depth profiles normalized 208Pb to 13C LA-ICP-MS from different treated PS samples

Noteworthy is also the huge standard deviation at the depth profile measurements. Standard deviation is calculated considering measurements of different individual particles. Therefore, it reflects the variation between particles. The particles all have different sizes and slightly different shapes, further focusing on the surface of the particle due to the spherical shape is not straight forward and may lead to the observed deviations.

4.2.3.2 PA

The following Figure 4.55 to Figure 4.60 show depth profiles of unaged unspiked and spiked samples and 20 h UV irradiated (aged) unspiked and spiked samples. Measured were O at 777 nm, Ca at 760 nm, K at 766 nm and 769 nm with LIBS. For K only the Results at 766 nm were discussed because of the higher intensity of the line. Simultaneous ^{27}Al, ^{68}Zn and ^{208}Pb were detected by using LA-ICP-MS as tandem. Al and Zn are contained as additives, while Pb was added with Ca and K during the spiking procedure in artificially seawater.

Figure 4.55 makes the O distribution in PA particles visible. The content seems to be nearly constant through the whole investigated depth for all 4 samples. Only the aged unspiked sample show a slightly decreased content of O, but this might depend on the measured particles and is not a significant change. This matches with the characterization after ageing procedure with IR and Raman spectroscopy.

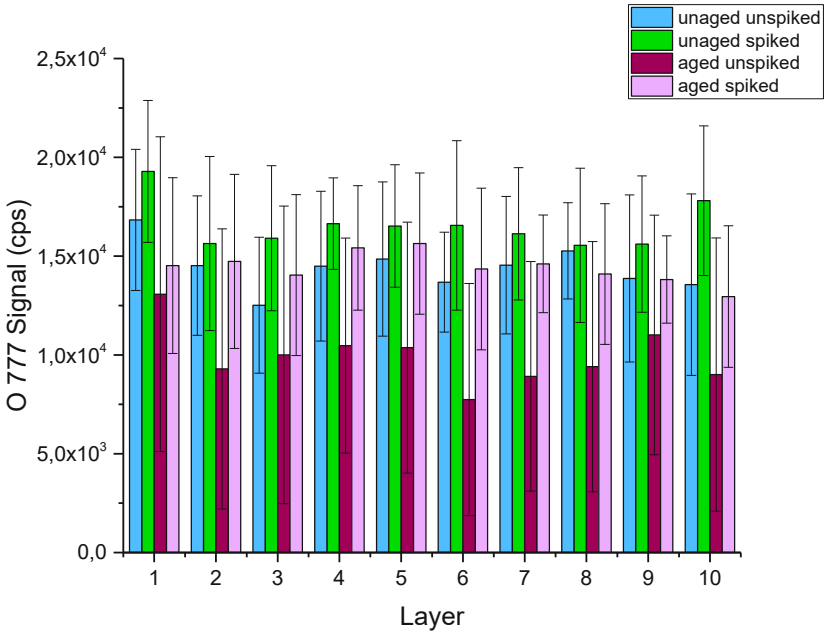

Figure 4.55: Depth profiles O at 777 nm LIBS from different treated PA samples

The Al distribution in PA is inhomogeneous. PA contains Al and a lot of other trace elements as additive/contamination. The graph in Figure 4.56 shows an enrichment in the outer layers of the particles. Further it shows an increase and homogenous distribution for the aged unspiked sample compared with the native sample. This is not plausible, because the particles were not spiked and especially not with Al. As well as the constant level of the Al concentration and the obtained standard deviation are nonsense. Half of the measured samples have a normalized intensity between 6 and 10 and the other half was below 1, which seems more realistic. Due to this interpretation a washing out of Al would be observed which matches also with the bulk analysis.

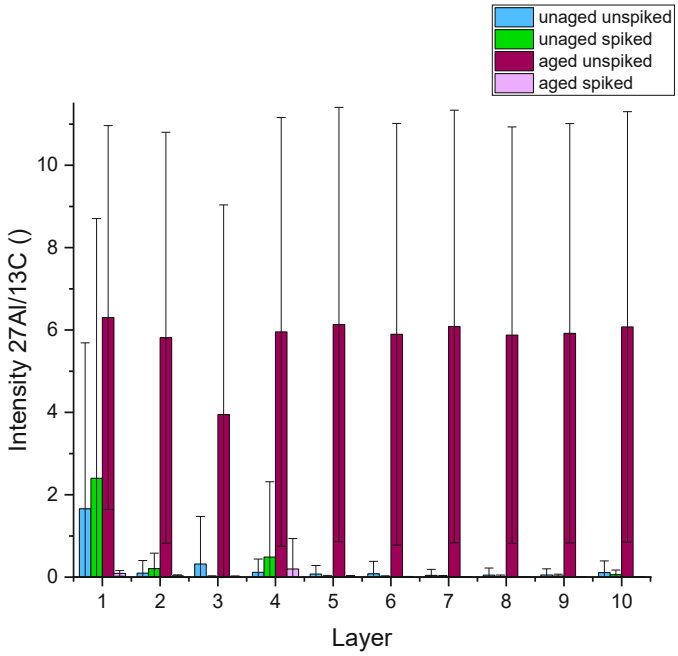

Figure 4.56: Depth profiles normalized 27Al to 13C LA-ICP-MS from different treated PA samples

In Figure 4.57 the distribution of Zn, contained as additive, seems also to be washed out during the treatment. Additionally, it was figured out, that Zn is only enriched in the outer layers.

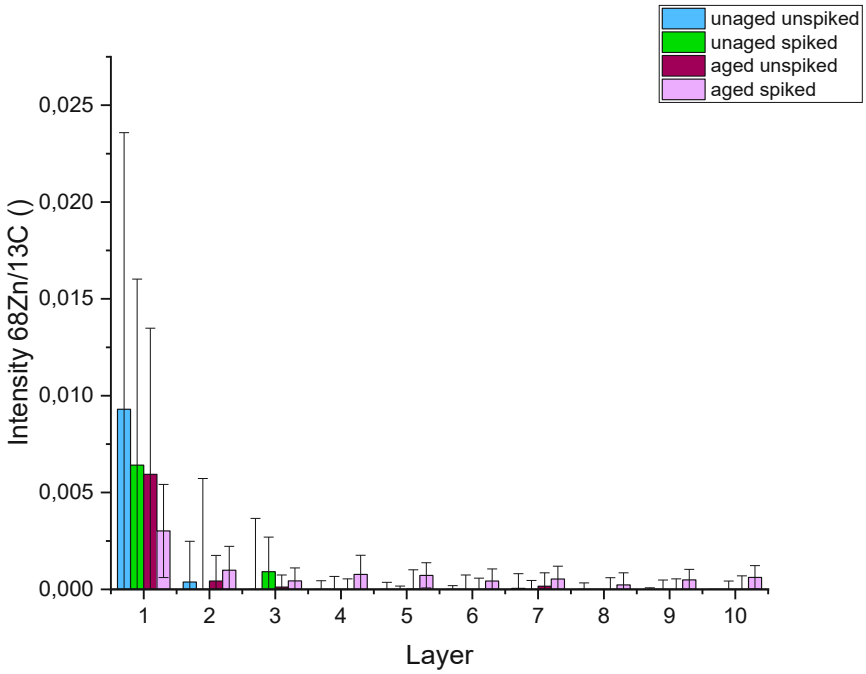

Figure 4.57: Depth profiles normalized 68Zn to 13C LA-ICP-MS from different treated PA samples

Pb seems to be already contained in the native particles (Figure 4.58). This contradicts the results from the survey run but was proven by the liquid measurements with ICP-MS. This samples might be contaminated or respectively it is a result of the measurement uncertainty.

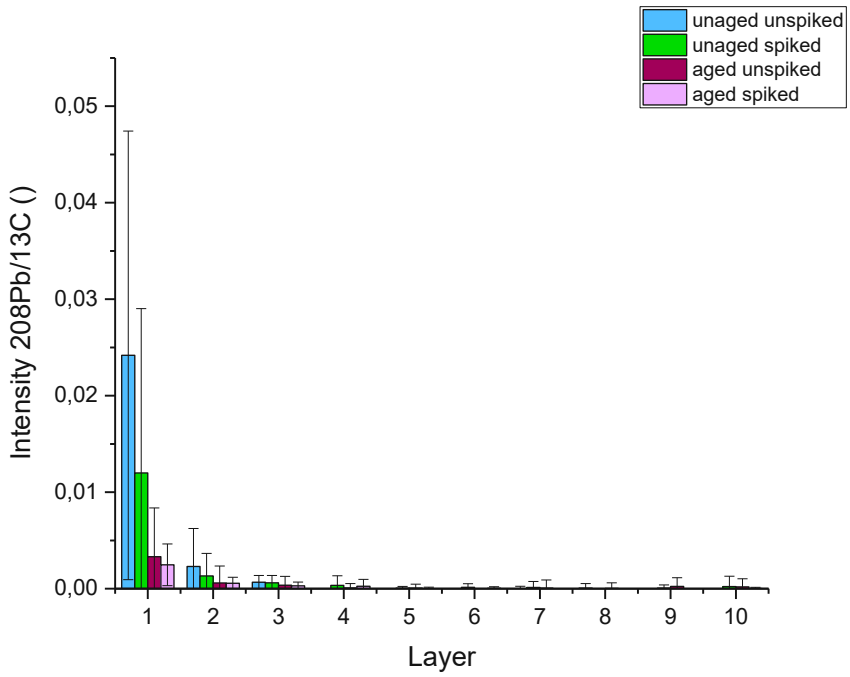

Figure 4.58: Depth profiles normalized 208Pb to 13C LA-ICP-MS from different treated PA samples

For PA also Ca at 760 nm was detected with LIBS. The results in Figure 4.59 show a similar behaviour like Al. The results of the aged unspiked samples were not reasonable and therefore, were removed from the graph.

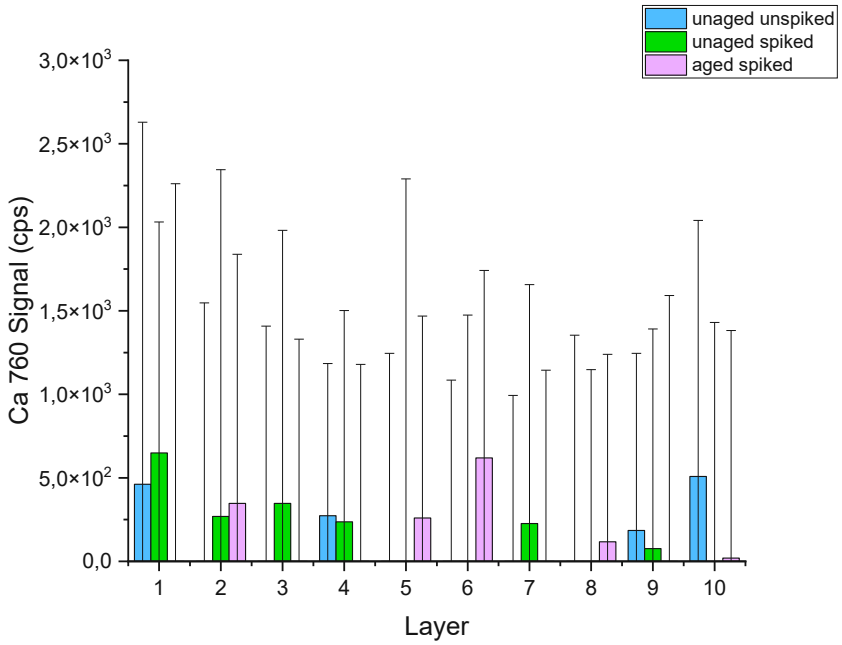

Figure 4.59: Depth profiles Ca at 760 nm LIBS from different treated PA samples

Also, the K signal shows a high standard deviation (Figure 4.60) and no clear trend for distribution through the layers.

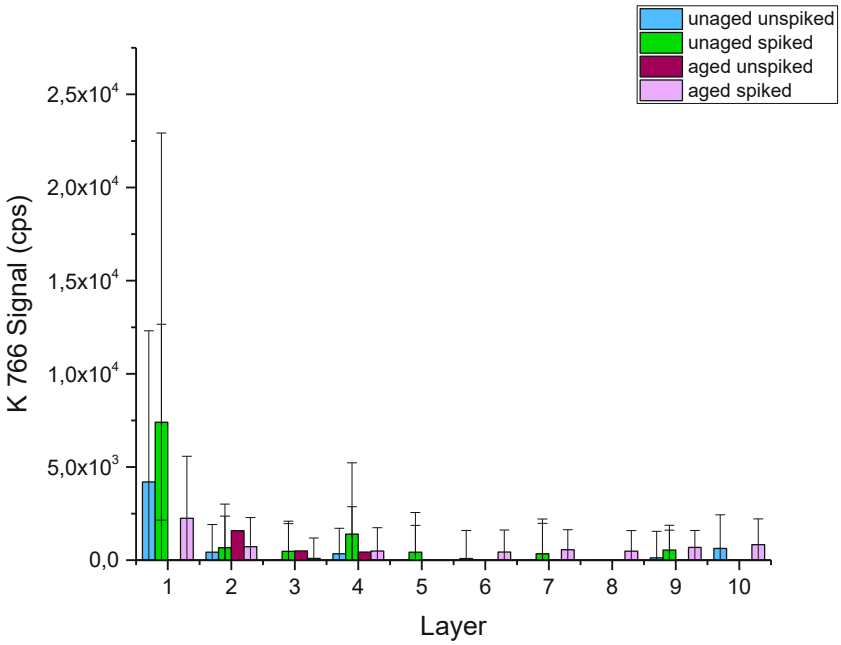

Figure 4.60: Depth profiles K at 766 nm LIBS from different treated PA samples

In summary the investigation of depth profiles of PA is not that easy and reliable due to the small particles (30-250 µm) and difficult focusing on the surface of the particles. This explains the high standard deviation of the measurements. Only the O and Zn signal seem to obtain reliable distribution profiles.

4.2.3.3 PET

The following Figure 4.61 to Figure 4.66 show depth profiles of unaged unspiked and spiked samples and 20 h UV irradiated (aged) unspiked and spiked samples. Measured were O at 777 nm, Ca at 760 nm, K at 766 nm and 769 nm with LIBS. For K only the results at 766 nm were discussed because of the higher intensity of the line. Simultaneously ^{27}Al, ^{121}Sb and ^{208}Pb were detected by LA-ICP-MS as tandem. Al and Sb are contained as additives, while Pb was added with Ca and K during the spiking procedure in artificially seawater.

The O distribution of different PET particles in Figure 4.61 shows a change in content due to ageing procedure. Both aged samples seem to have a higher signal for O. It must be recognized that the value for all sample types seem constant, so that there is no change in depth except the outermost layer.

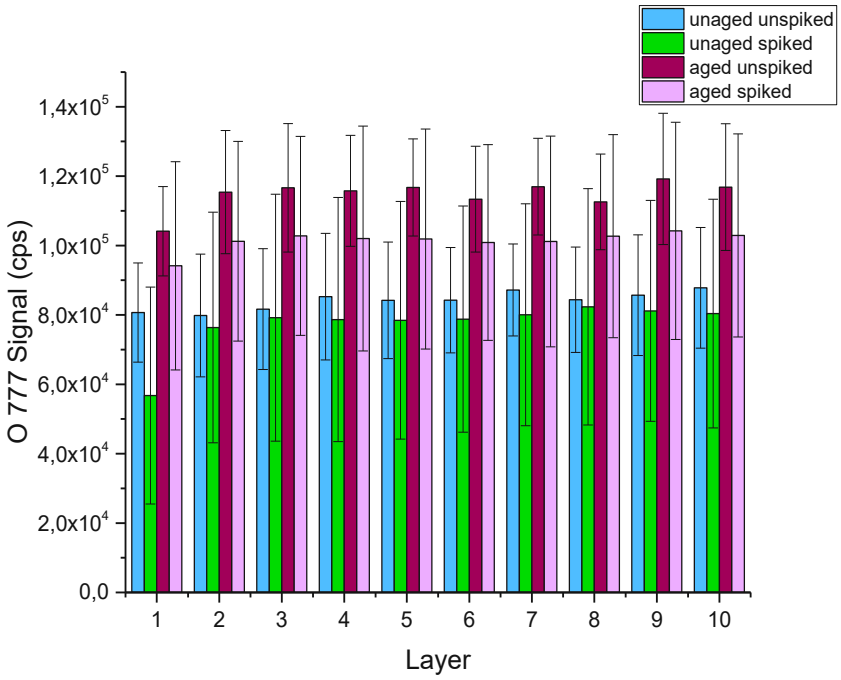

Figure 4.61: Depth profiles O at 777 nm LIBS from different treated PET samples

The graph in Figure 4.62 suggests a higher concentration of Al in the outer regions of the particles and a sightly wash out of the additive.

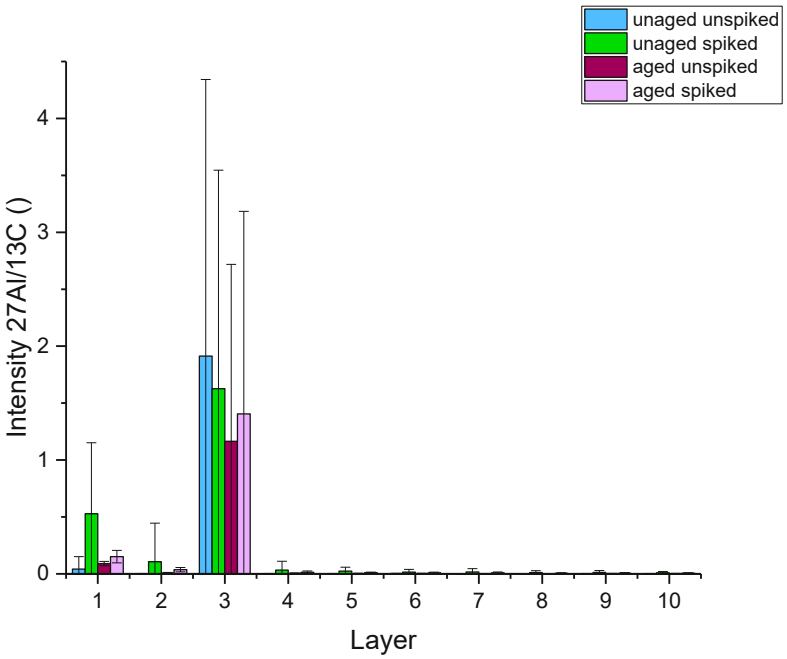

Figure 4.62: Depth profiles normalized 27Al to 13C LA-ICP-MS from different treated PET samples

Figure 4.63 makes two things visible. The first is the homogenous distribution of Sb in the hole polymer particle. The second is the wash out of this additive but only in the outermost layers.

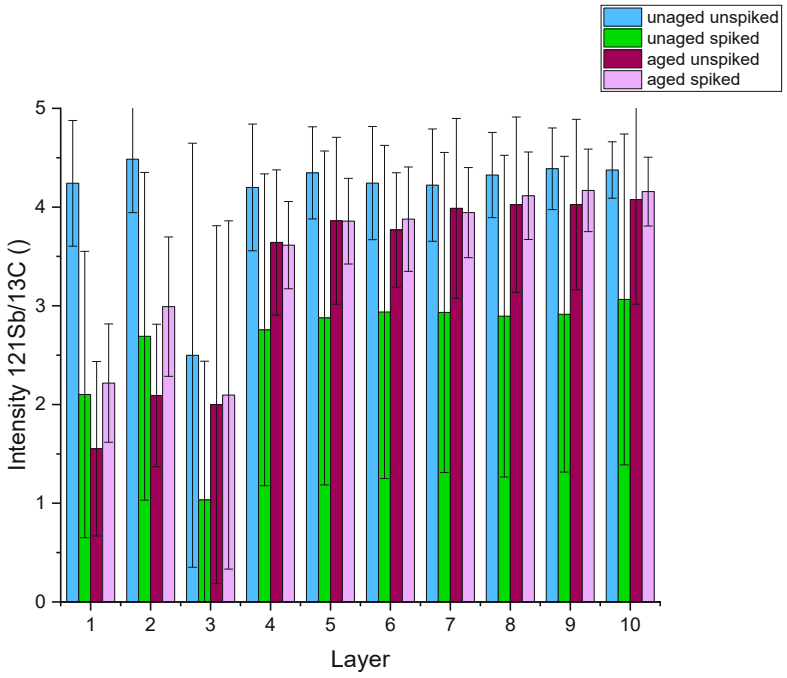

Figure 4.63: Depth profiles normalized 121Sb to 13C LA-ICP-MS from different treated PET samples

The uptake behaviour for Pb has changed during the ageing treatment. This is visible in Figure 4.64 which shows that no Pb is contained in the unspiked samples, while show an increase of Pb uptake according to the ageing procedure.

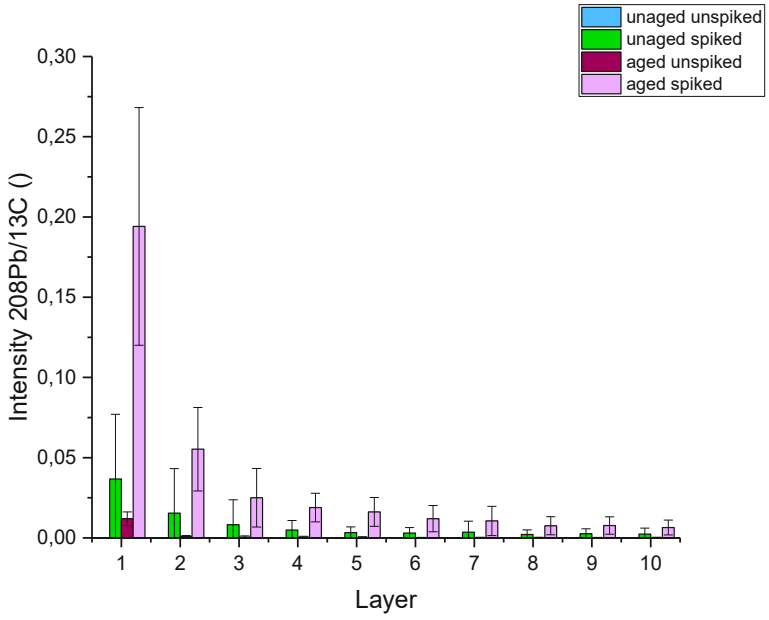

Figure 4.64: Depth profiles normalized 208Pb to 13C LA-ICP-MS from different treated PET samples

While the former discussed species suggest trends in uptake and release, the Ca content in PET does not (Figure 4.65).

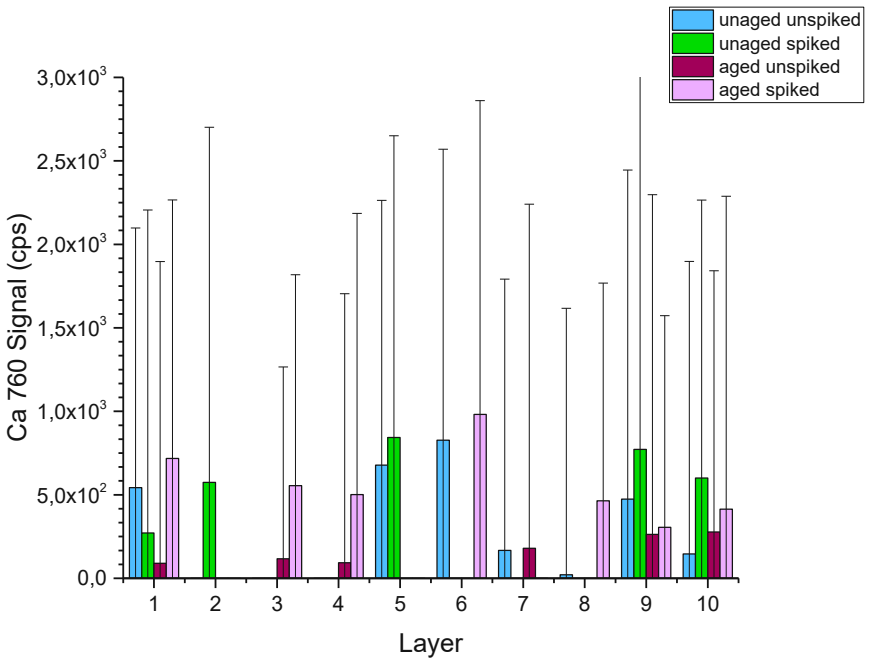

Figure 4.65: Depth profiles Ca at 760 nm LIBS from different treated PET samples

K which is seen in Figure 4.66 seems to diffuse deep into the polymer until it reaches a constant value especially for the unaged spiked sample.

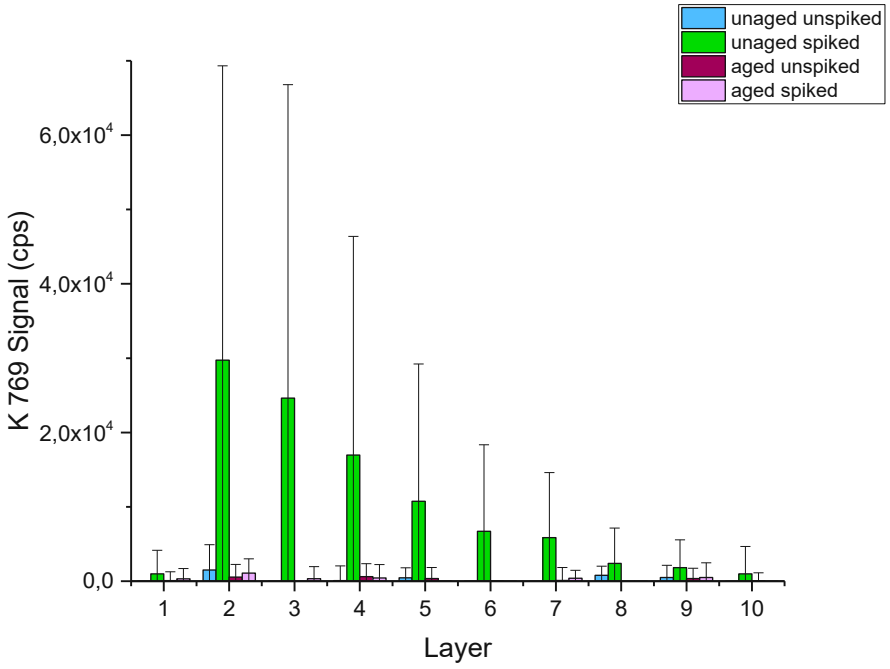

Figure 4.66: Depth profiles K at 769 nm LIBS from different treated PET samples

K and Ca were added in the artificial seawater so only the spiked samples should show a content of both elements. For Ca a band was used for investigation which was not one of the most intensives, so it is more effected by the signal to noise ratio. The intensity of Ca was an order of magnitude smaller than O and K.

4.2.3.4 PVDC

The following Figure 4.67 to Figure 4.72 show depth profiles of unaged unspiked and spiked samples and 20 h UV irradiated (aged) unspiked and spiked samples. Measured were O at 777 nm, Ca at about 760 nm, K at 766 nm and 769 nm with LIBS. For K only the results at 766 nm were discussed because of the higher intensity of the line. Simultaneous ^{27}Al, ^{68}Zn and ^{208}Pb were detected by using LA-ICP-MS as tandem. Al and Zn are contained as additives, while Pb was added with Ca and K during the spiking procedure in artificially seawater.

PVDC showed an increase in O content through the investigated depth of the particles according to the ageing procedure (Figure 4.67).

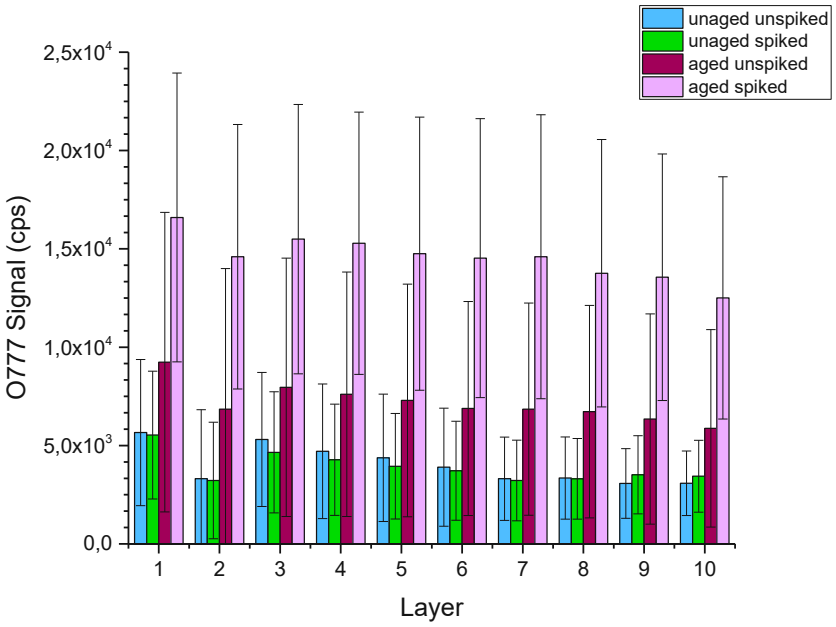

Figure 4.67: Depth profiles O at 777 nm LIBS from different treated PVDC samples

For the Al the graph in Figure 4.68 shows a difference between the unaged and aged samples. So, the Al which is distributed homogenous in the PVDC particle was washed out during the treatment especially during the ageing.

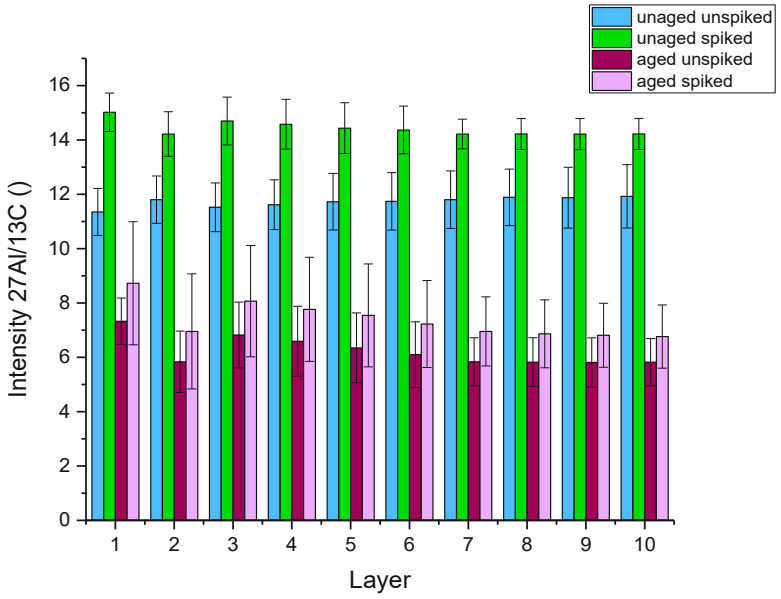

Figure 4.68: Depth profiles normalized 27Al to 13C LA-ICP-MS from different treated PVDC samples

Zn was only contained in low concentrations. Figure 4.69 shows a constant value and distribution for the native sample, whereas the spiked samples show a decrease with depth.

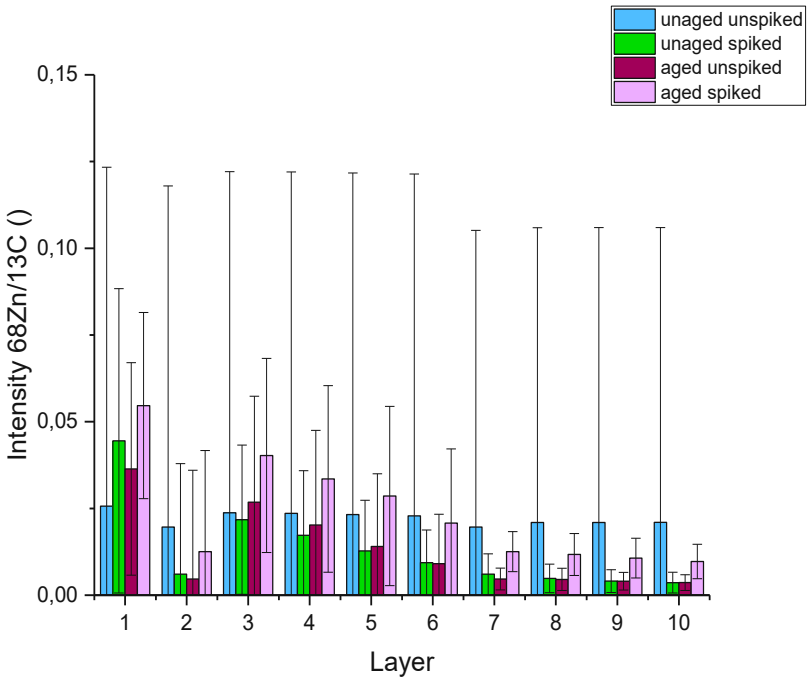

Figure 4.69: Depth profiles normalized 68Zn to 13C LA-ICP-MS from different treated PVDC samples

Figure 4.70 shows that the PVDC samples have an increase of Pb uptake due to the ageing procedure. The aged unspiked sample should not have such an increase, so it bight was contaminated.

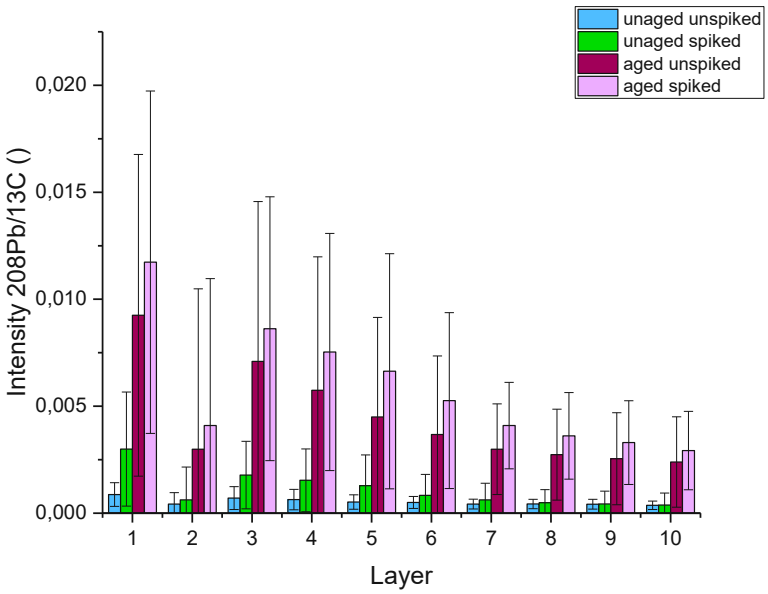

Figure 4.70: Depth profiles normalized 208Pb to 13C LA-ICP-MS from different treated PVDC samples

Ca seems to be higher in the unaged samples, so it might be already contained as additive. All samples show a nearly constant value through the depth (Figure 4.71). But the high standard deviation is noticeable.

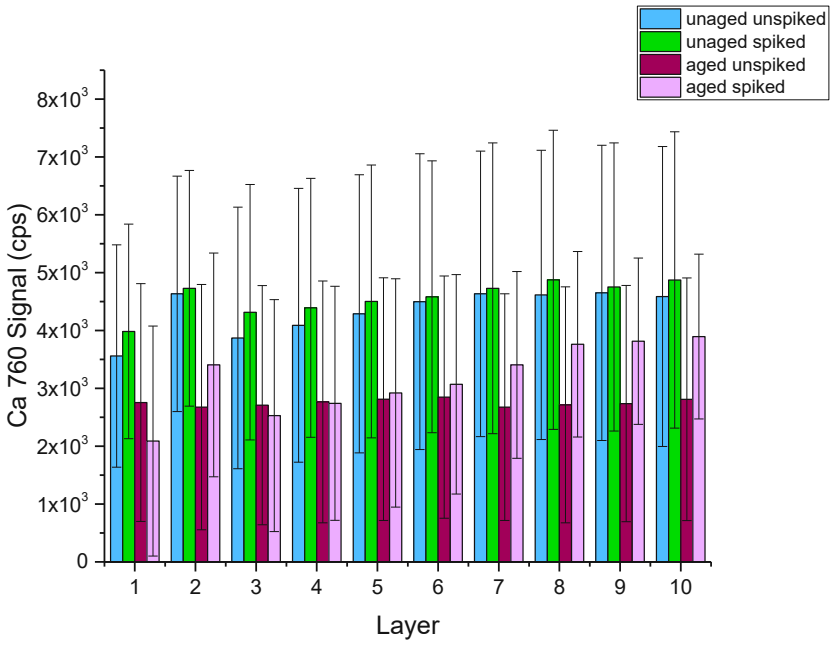

Figure 4.71: Depth profiles Ca at 760 nm LIBS from different treated PVDC samples

The K distribution (Figure 4.72) shows a trend by decreasing with the depth in the spiked polymers. So, K is kind of a marker how deep the seawater was penetrating in the particle. The aged unspiked sample shows the highest K content which could only come from contamination.

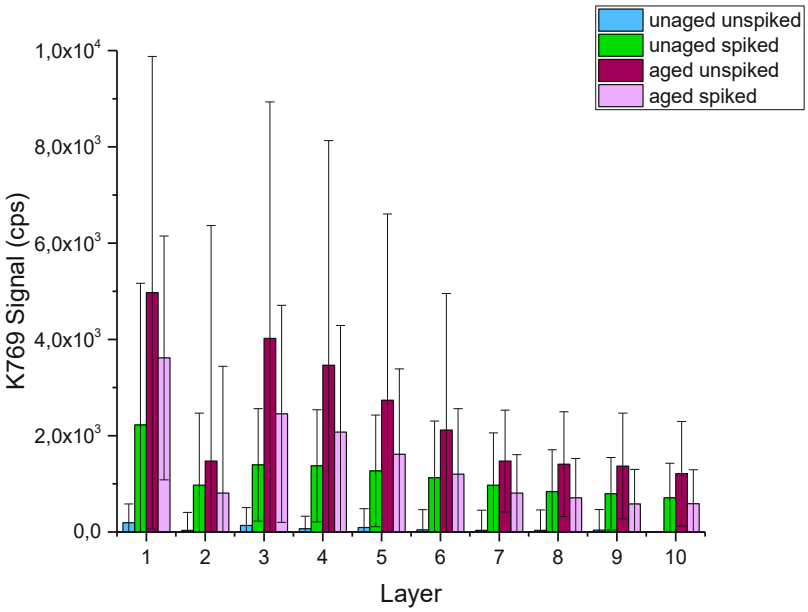

Figure 4.72: Depth profiles K at 766 nm LIBS from different treated PVDC samples

5 Conclusion

In this work, the effects of microplastics degradation and the concomitant release of inorganic additives and uptake of contaminations from the environment of microplastics was investigated with conventional techniques and LA-ICP-MS/LIBS to assess the distribution of prevailing elements.

The MP particles were artificially aged by exposure to UV light or treatment with oxidizing reagents. To evaluate the extent of degradation the polymers were characterized with several common methods. Molecular changes were observed with Raman and FT-IR spectroscopy. Light microscopy and He pycnometry were used to characterize the particles. Elemental changes were determined with LIBS, ICP-MS and LA-ICP-MS. LIBS was the method of choice for lighter elements like H, O, and C and ICP-MS/LA-ICP-MS for heavier trace elements like Zn, Pb or Cd.
ICP-MS was used to quantitatively determine the uptake and release of trace elements in bulk samples. Spatially resolved qualitative results were received using LA-ICP-MS and LIBS individually and in combination. For these methods the solid samples were measured directly. Polymer cross sections were scanned with LA-ICP-MS and LIBS to generate images of distribution. Depth profile analysis was carried out by using LIBS and LA-ICP-MS together analysing individual particles.

The principle working procedure was divided into three sample preparation steps and one measurement step, which were explained individually in the single chapters. For a better overview a flow chart is shown in Figure 5.1.

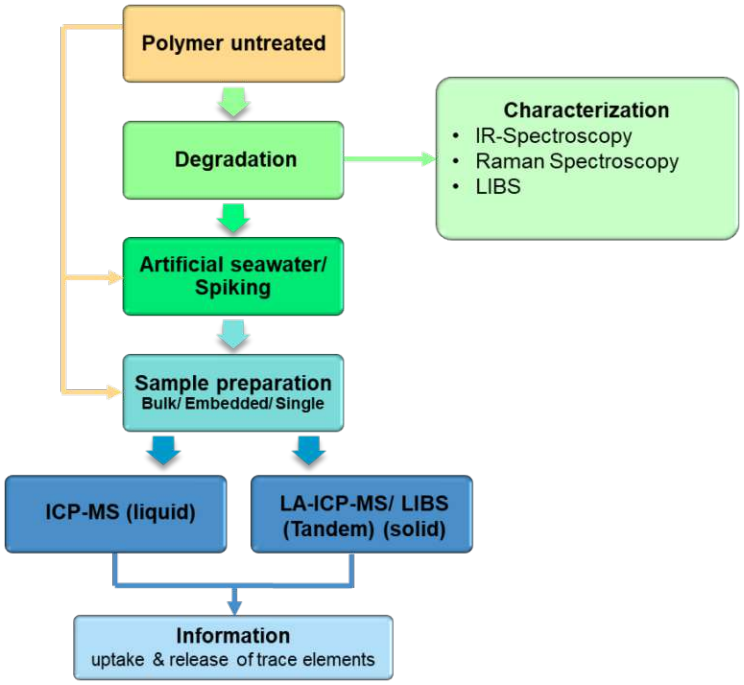

Figure 5.1: Scheme of the 4 process steps and the use of untreated polymer

The main conclusions of this project are that clearly some of the additives present in polymers are washed out when exposed to harsh environments, even more if the samples were aged. Moreover, the uptake of trace elements from artificial seawater was observed, some of the elements present in the artificial seawater were adsorbed on the polymer matrix. Both processes, uptake, and release, are dependent on the polymer type and the chemical element.

Polystyrene (PS) is the best examples for both processes and the bulk analysis fits good with the images and the depth profile measurements. For PS not only predictions of the amount of uptake and release could be made, but also, about the depth of the concerned analytes.
Polyamide (PA) has a half-life of several thousand years and is according to that relatively inert (Affolter, 2001). It is not surprising, that there was not that much change in the material because of the ageing treatments. But there were also changes in the additive content noticed caused by leaching during the treatments. The spatially resolved analysis of PA particles turned out to be difficult due to the small particle size. This highlights the importance of different complementary analysing methods. Further it promotes the meaningfulness of the results.
Polyethylene terephthalate (PET) showed less release of additives, but also less adsorption of trace elements. It introduces a homogenous distribution of the additives in the polymer matrix, which was visible in the images as well as in the depth profiles. Moreover, Sb leaching in the outer layers was visualized by depth profiles.
The macroscopic change and the results of the characterization after aging led to the conclusion that the UV irradiation has an influence on the Polyvinylidene chloride (PVDC) particles. The bulk analysis and imaging results were not that meaningful, but even more was the depth profile analysis. Not only the change distribution of O in the unaged and aged PVDC particles was visible, but also the release of Al as additive, which was not that easy to see, with the other methods. As well as the uptake of Pb and Zn.

The more different the polymers are, the more different is the behaviour during the treatments of them. In summary all three methods, the ICP-MS bulk analysis, the LA-ICP-MS imaging and the LIBS and LA-ICP-MS tandem depth profile analysis support each other to gain reliable results especially for this issue. By combination of these techniques not only quantitative information was received, but also information about the distribution on the inside of the MP particles. The behaviour in the regions close to the surface was particularly interesting, since accumulations or leaching were particularly easy to see here.
For future work the next step would be to quantify the observed elements detected by spatially resolved analysis. Therefore, solid standards must be made in-house adapted to the individual issue. Polymers must be dissolved and spiked with the corresponding elements. The dissolved polymers can then be returned in solid state by vaporizing the solvent. After measuring them a calibration curve will be carried out and can be used to evaluate the quantitative distribution in images and depth profiles.

This enables more information and can help to evaluate the danger from polymers in the environment. It is an important step in raising awareness of humanity's responsibility towards nature and the planet.

6 Literature

Affolter, S., 2001. *Langzeitverhalten von Thermoplasten ,* CH-9471 Buchs, Schweiz: Interstaatliche Hochschule für Technik NTB.

Ambrogie, V., Carfagna, C., Cerruti, P. & Marturano, V., 2017. 4 - Additives in Polymers. *Modification of Polymer Properties,* Issue William Andrew Applied Science Publishers, pp. Pages 87-108.

Bart, J. C. J., 2005. *Additives in Polymers: Industrial Analysis and Applications.* s.l.:John Wiley & Sons.

Becker, J. S., 2007. *Inorganic Mass Spectrometry Principles and Applications.* Jülich Germany: Wiley John Wiley & Sons Ltd, The Atrium, Southern Gate, Chichester.

Brunnbauer, L. et al., 2020. Spatially resolved polymer classification using laser induced breakdown spectroscopy (LIBS) and multivariate statistics. *Elsevier,* Talanta(Volume 209, 1 March 2020, 120572).

Brunnbauer, L. et al., 2020. Combined LA-ICP-MS/LIBS: powerful analytical tools for the investigation of polymer alteration after treatment under corrosive conditions. *nature,* Volume Article number: 12513.

Deutschland, U., 2017. *Umweltbundesamt DE.* [Online]
Available at: https://www.umweltbundesamt.de/service/uba-fragen/welche-abfallmengen-befinden-sich-in-den-meeren
[Accessed 10 06 2022].

Deutschland, W., 2021. *WWF.* [Online]
Available at: https://www.wwf.de/themen-projekte/plastik/unsere-ozeane-versinken-im-plastikmuell/plastikmuell-im-meer-die-wichtigsten-antworten

Elias, H.-G., 2001. *Makromoleküle Band 3 Industrielle Polymere und Synthesen.* 6. Auflage ISBN: 9783527626519 ed. s.l.:Wiley-VCH.

Frick, A. & Stern, C., 2017. *Einführung in die Kunststoffprüfung: Prüfmethoden und Anwendungen.* München: Carl Hanser Verlag.

GoodFellow, 2021. [Online]
Available at: https://www.goodfellow.com/de/de/displayitemdetails/p/st31-pd-000103/polystyrene-powder

Göpferich, A., 1994. *Mechanisms of polymer degradation and erosion,* Department of Pharmaceutical Technology, University of Erlangen-Nürnberg, Cauerstraße 4, 91058 Erlangen: Elsevier.

Guezenoc, J., Gallet-Budynek, A. & Bousquet, B., 2019. Critical review and advices on spectral-based normalization methods for LIBS quantitative analysis. *Elsevier,* Spectrochimica Acta Part B(Spectrochimica Acta Part B 160 (2019) 105688).

Günther, D. & Hattendorf, B., 2015. Solid sample analysis using laser ablation inductively coupled plasma mass spectrometry. *Elsevier,* Issue Trends in Analytical Chemistry, Vol. 24, No. 3, 2005.

Kester, D. R., Duedall, I. W., Connors, D. N. & Pytkowicz, R. M., 1967. *PREPARATION OF ARTIFICIAL SEAWATER.* Limnology and Oceanography; Volume 12, Issue 1; p.176-179; doi/10.4319/lo.1967.12.1.0176: ASLO.

Kooi, M., van Nes, E. H., Scheffer, M. & Koelmans, A. A., 2017. *Ups and Downs in the Ocean: Effects of Biofouling on Vertical Transport of Microplastics.* Aquatic Ecology and Water Quality Management Group,

Department of Environmental Sciences, Wageningen University & Research, P.O. Box 47, 6700 AA Wageningen, The Netherlands: Enviromental Science& Technology.

Linge, K. L. & Jarvis, K. E., 2009. Quadrupole ICP-MS: Introduction to Instrumentation, Measurement Techniques and Analytical Capabilities. *Geostandards and Geoanalytical Research*, 31 Jul.

Maier, R. D. & Schiller, M., 2016. *Handbuch Kunststoff Additive.* 4. Auflage ISBN: 978-3-446-22352-3 ed. s.l.:Hanser.

Marturano, V., Cerruti, P. & Ambrogi, V., 2017. Polymer additives. *Physical Science Reviews,* Issue https://doi.org/10.1515/psr-2016-0130.

Massos, A. & Turner, A., 2017. Cadmium, lead and bromine in beached microplastics. *Elsevier Enviromental Pollution,* Issue Volume 227, pp. Pages 139-145.

McCreery, R. L. & Winefordner, J., 2000. *Raman Spectroscopy for chemical Analysis.* The Ohio State University Columbus, Ohio: Wiley - Intersience A. John Wiley & Sons, Inc., Publication .

Miziolek, A. W., Palleschi, V. & Schechter, I., 2009. *Laser-induced breakdown spectroscopy (LIBS) : fundamentals and applications.* Cambridge: Cambridge University Press 2006.

Neves, D., Sobral, P., Ferreira, J. L. & Pereira, T., 2015. *Ingestion of microplastics by commercial fish off the portuguese coast.* Mare- Faculade de Ciencias e Tecnologia, Universidale Nova de Lisboa, Campus da Caparica, 2829-516 Caparica, Portugal): Elsevier.

Noda, I. et al., 2007. *Group Frequency Assignments for Major Infrared Bands Observed in Common Synthetic Polymers*. he Procter & Gamble Company, Beckett Ridge Technical Center, 8611 Beckett Road, West Chester, OH 4506: Springer, New York, NY Physical Properties of Polymers Handbook.

Pennsylvania State University, 2022. *mri.psu.edu.* [Online]
Available at: https://www.mri.psu.edu/materials-characterization-lab/characterization-techniques/density-helium-pycnometry#:~:text=Skeletal%20density%20is%20the%20ratio,the%20material%20(ASTM%20D3766).
[Accessed 22 04 2022].

Pereira, J. et al., 2011. Evaluation of sample preparation methods for polymerdigestion and trace elements determination by ICPMS and ICPOES. *Journal of Analytical Atomic Spectrometry,* Issue J. Anal. At. Spectrom., 2011,26, 1849-1857.

Pfaender, R., 2013. *Handbook of Polymer Synthesis, Characterization, and Processing.* 1.Edition ed. s.l.:John Wiley & Son.

Shimadzu, 2022. *Shimadzu.com.* [Online]
Available at: https://www.shimadzu.com/an/service-support/technical-support/analysis-basics/fundamental/core_principles.html
[Accessed 27 8 2022].

Shim, W. J., Hong, S. H. & Eo Eo, S., 2016. Identification methods in microplastic analysis:. *Royal Society of Chemistry,* Issue Cite this: Anal. Methods, 2017, 9, 1384.

Singh, J. P. & Thakur, S. N., 2007. *Laser-Induced Breakdown Spectroscopy.* https://doi.org/10.1016/B978-0-444-51734-0.X5001-7 ed. s.l.:Elsevier Science.

Thomas, R., 2013. *Oractical Guide to ICP-MS.* Boca Raton, FL 33487-2742: CRC Press Taylor & Francis Group.

Thompson, J. M., 2018. *Infrared Spectroscopy.* Singapore 038988: Pan Stanford Publishing Pte. Ltd..

Turner, A. & Holmes, L. A., 2014. Adsorption of trace metals by microplastic pellets in fresh water. *Environmental Chemistry 12(5) 600-610,* Issue https://doi.org/10.1071/EN14143.

Turner, A., Holmes, L., Thompson, R. C. & Fisher, A. S., 2020. Metals and marine microplastics: Adsorption from the environment versus addition during manufacture, exemplified with lead. *Elsevier Water Research,* Volume Volume173.

Wang, W., Ge, j. & Yu, X., 2020. *Bioavailabilty and toxicity of microplastics to fisch species: A review.* Jiangsu Key LAboratory for Food Quality and Saftes-State Key Laboratory Cultivation Base Ministry of Science and Technology, 50 Zhongling Street, Nanjing, 210014 China: Elsevier.

Wikipedia.org, 2021. *Wikipedia.* [Online]
Available at: https://en.wikipedia.org/wiki/Polyethylene_terephthalate

Wiley Information Services GmbH, 2021. *Chemgapedia.* [Online]
Available at:
http://www.chemgapedia.de/vsengine/vlu/vsc/de/ch/3/anc/masse/ms_massenanalysator_quadrup.vlu/Page/vsc/de/ch/3/anc/masse/2_massenspektrometer/2_4_massenanalysator/2_4_4_quadrupol/2_4_4_6_stabildiag/stabidiagr_m34ht0302.vscml.html

Yabagi, J. A. et al., 2017. The effect of gamma irradiation on chemical, morphology and optical properties of polystyrene nanosphere at various exposure time. *IOP Publishing,* Issue IOP Conf. Series: Materials Science and Engineering 298 (2017) 012004 doi:10.1088/1757-899X/298/1/012004, p. 11.

7 List of Tables

8 List of Figures

9 Appendix

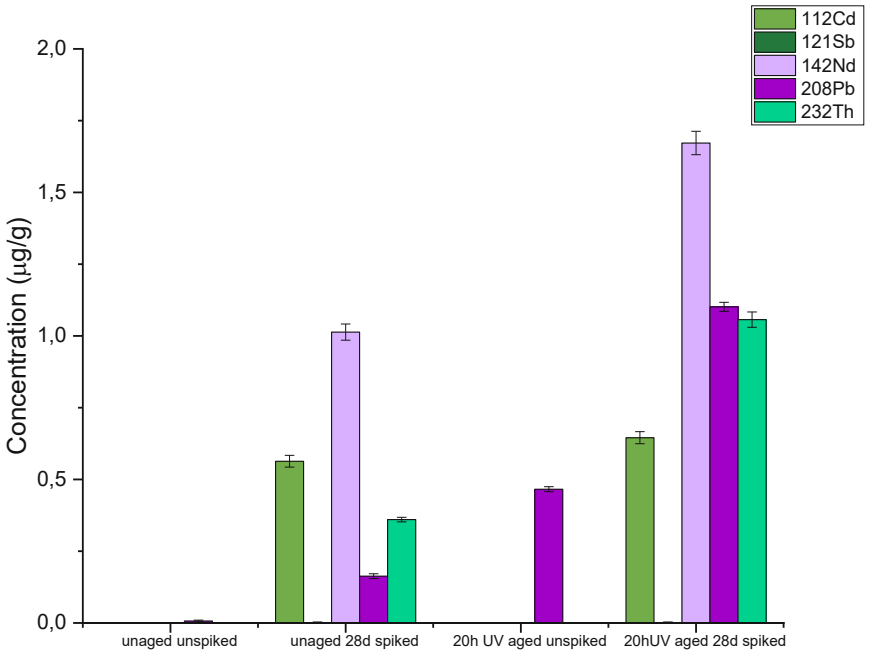

Figure A. 1: Liquid bulk measurements of unaged and aged unspiked and spiked PS samples with Cd, Sb, Nd, Pb and Th

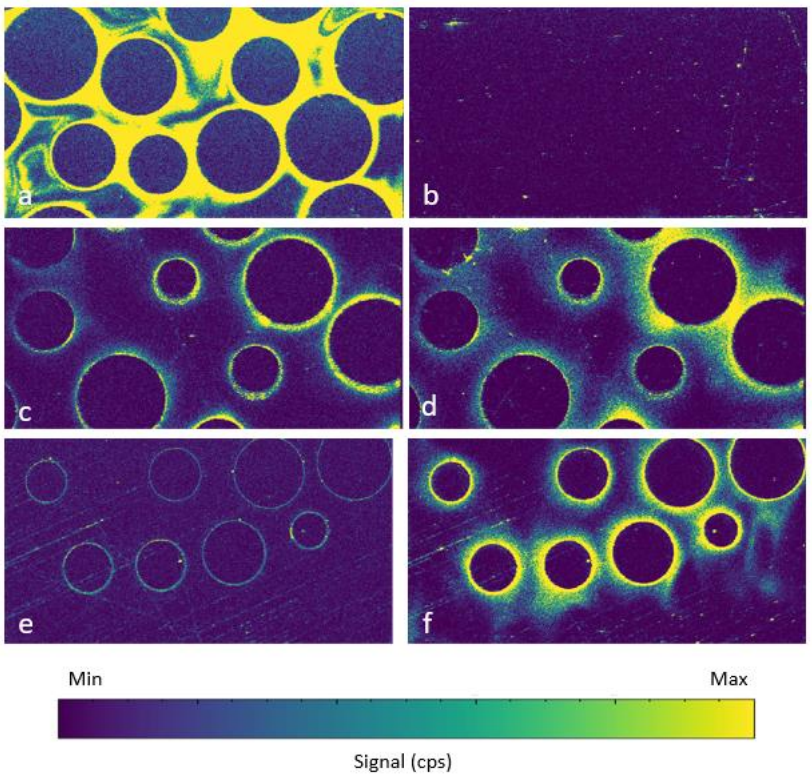

Figure A. 2: unaged and aged, unspiked and spiked PS particles embedded in epoxy resin (a) 66Zn distribution in unaged unspiked PS particles (b) 208Pb distribution in unaged unspiked PS particles (c) 66Zn distribution in unaged 28 d spiked PS particles (d) 208Pb distribution in unaged 28 d spiked particles (e) 66Zn distribution in 20 h UV aged 28 d spiked PS particles (f) 208Pb distribution in 20 h UV aged 28 d spiked PS particles

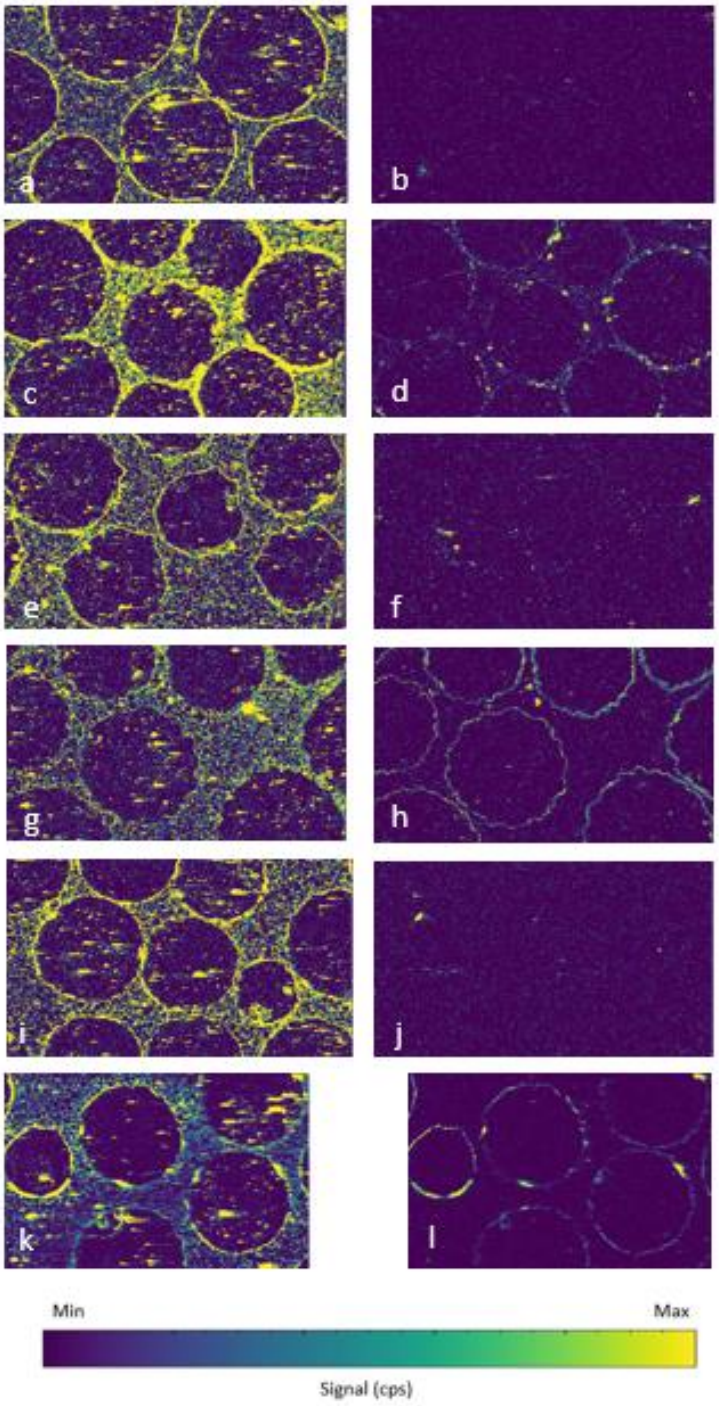

Figure A. 3: unaged and aged unspiked and spiked PS particles in acryl resin (a) 27Al distribution in unaged unspiked PS particles (b) 121Sb distribution in unaged unspiked PS particles (c) 27Al distribution in unaged 21 d spiked PS particles (d) 121Sb distribution in unaged 21 d spiked PS particles (e) 27Al distribution in 20 h UV aged unspiked PS particles (f) 121Sb distribution in 20 h UV aged unspiked PS particles (g) 27Al distribution in 20 h UV aged 21 d spiked PS particles (h) 121Sb distribution in 20 h UV aged 21 d spiked PS particles (i) 27Al distribution in two weeks 80% HNO_3 and 5% H_2O_2 aged unspiked PS particles (j) 121Sb distribution in two weeks 80% HNO_3 and 5% H_2O_2 aged unspiked PS particles (k) 27Al distribution in two weeks 80% HNO_3 and 5% H_2O_2 aged 21 d spiked PS particles (l) 121Sb distribution in two weeks 80% HNO_3 and 5% H_2O_2 aged 21 d spiked PS particles

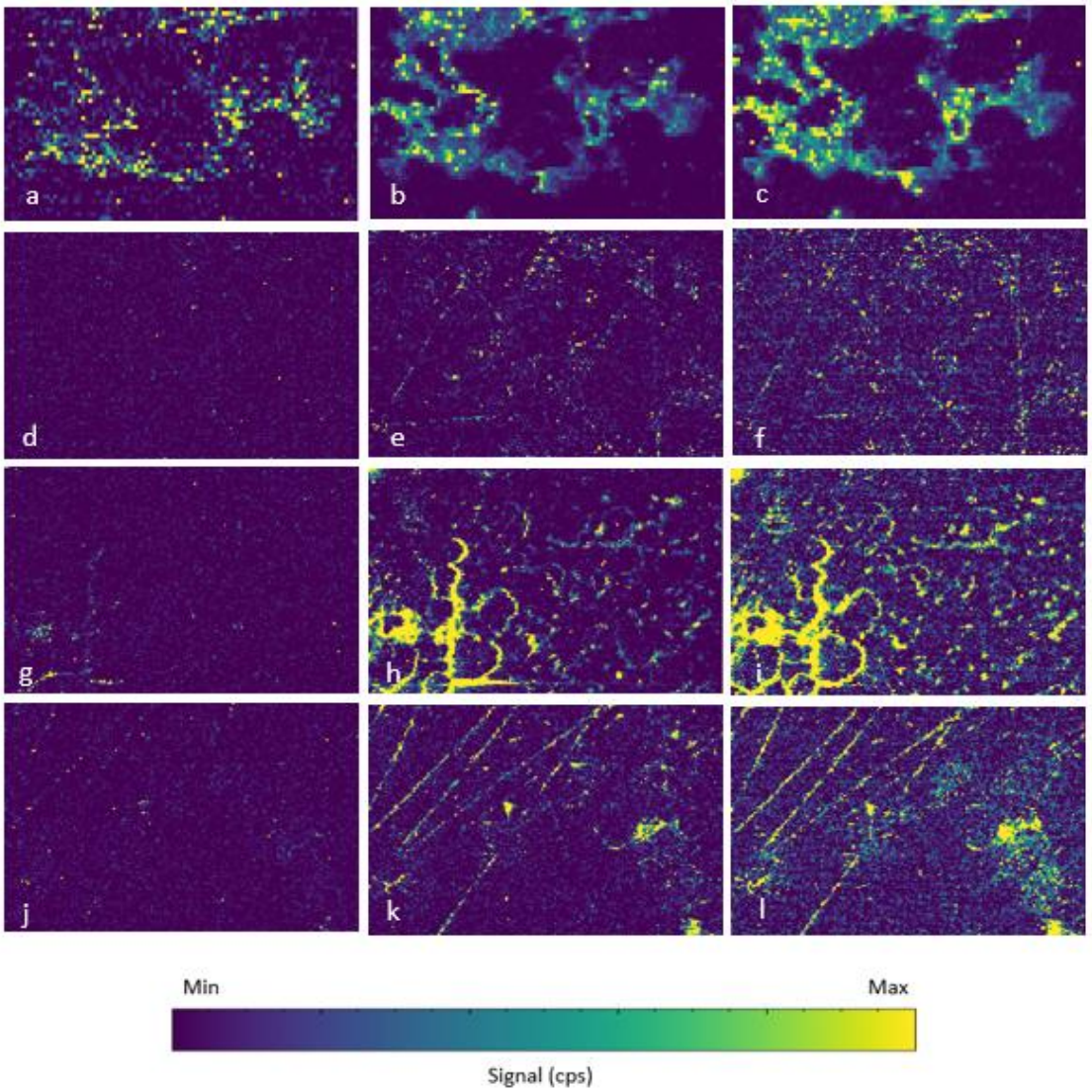

Figure A. 4: unaged, aged, unspiked and spiked PA particles embedded in acryl resin (a) 112Cd distribution in unaged unspiked PA particles (b) 208Pb distribution in unaged unspiked PA particles (c) 64Zn distribution in unaged unspiked PA particles (d) 112Cd distribution in unaged 21 d spiked PA particles (e) 208Pb distribution in unaged 21 d spiked PA particles (f) 64Zn distribution in unaged 21 d spiked PA particles (g) 112Cd distribution in 20 h UV aged unspiked PA particles (h) 208Pb distribution in 20 h UV aged unspiked PA particles (i) 64Zn distribution in 20 h UV aged unspiked PA particles (j) 112Cd distribution in 20 h UV aged 21 d spiked PA particles (k) 208Pb distribution in 20 h UV aged 21 d spiked PA particles (l) 64Zn distribution in 20 h UV aged 21 d spiked PA particles

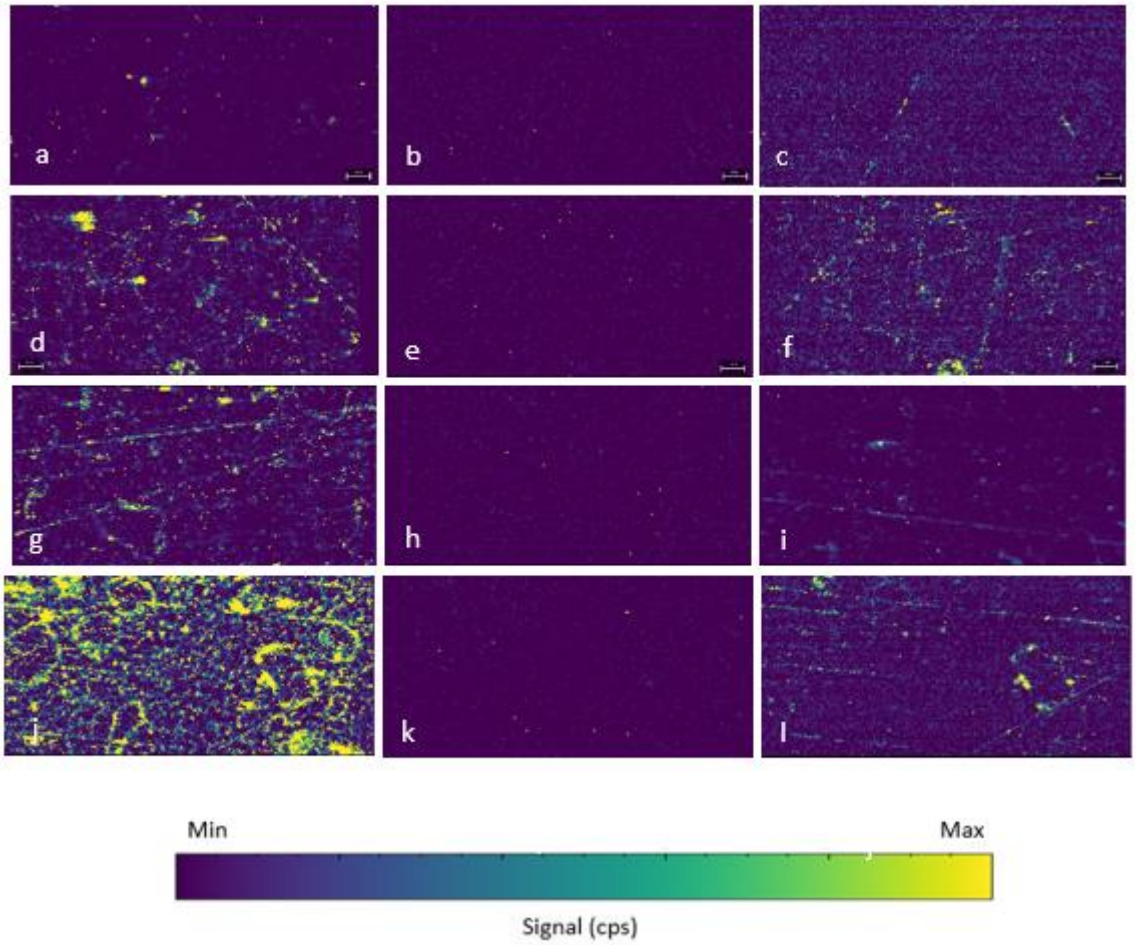

Figure A. 5: unaged, aged, unspiked and spiked PET particles embedded in acryl resin (a) 27Al distribution in unaged unspiked PET particles (b) 112Cd distribution in unaged unspiked PET particles (c) 64Zn distribution in unaged unspiked PET particles (d) 27Al distribution in unaged 21 d spiked PET particles (e) 112Cd distribution in unaged 21 d spiked PET particles (f) 64Zn distribution in unaged 21 d spiked PET particles (g) 27Al distribution in 20 h UV aged unspiked PET particles (h) 112Cd distribution in 20 h UV aged unspiked PET particles (i) 64Zn distribution in 20 h UV aged unspiked PET particles (j) 27Al distribution in 20 h UV aged 21 d spiked PET particles (k) 112Cd distribution in 20 h UV aged 21 d spiked PET particles (l) 64Zn distribution in 20 h UV aged 21 d spiked PET particles

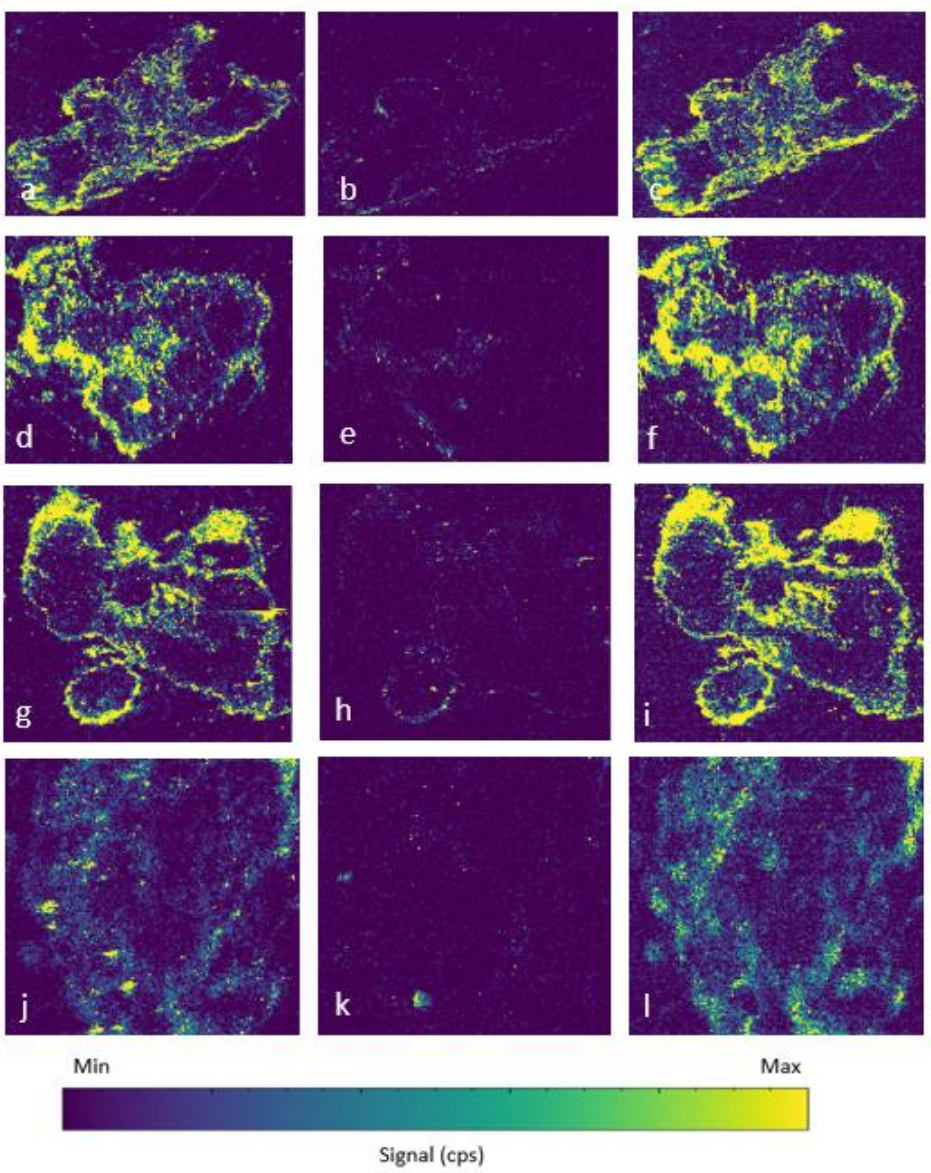

Figure A. 6: unaged, aged, unspiked and spiked PVDC particles embedded in acryl resin (a) 208Pb distribution in unaged unspiked PVDC particles (b) 121Sb distribution in unaged unspiked PVDC particles (c) 64Zn distribution in unaged unspiked PVDC particles (d) 208Pb distribution in unaged 21 d spiked PVDC particles (e) 121Sb distribution in unaged 21 d spiked PVDC particles (f) 64Zn distribution in unaged 21 d spiked PVDC particles (g) 208Pb distribution in 20 h UV aged unspiked PVDC particles (h) 121Sb distribution in 20 h UV aged unspiked PVDC particles (i) 64Zn distribution in 20 h UV aged unspiked PVDC particles (j) 208Pb distribution in 20 h UV aged 21 d spiked PVDC particles (k) 121Sb distribution in 20 h UV aged 21 d spiked PVDC particles (l) 64Zn distribution in 20 h UV aged 21 d spiked PVDC particles